THE DEVELOPMENT OF MICROFABRICATED MICROBIAL

FUEL CELL ARRAY AS A HIGH THROUGHPUT SCREENING

PLATFORM FOR ELECTROCHEMICALLY ACTIVE

MICROBES

A Dissertation

by

HUIJIE HOU

Submitted to the office of graduate studies of
Texas A&M University
in partial fulfillment of the requirements for the degree of

DOCTOR OF PHILOSOPHY

December 2011

Major Subject: Electrical Engineering

THE DEVELOPMENT OF MICROFABRICATED MICROBIAL FUEL CELL ARRAY AS A HIGH THROUGHPUT SCREENING PLATFORM FOR ELECTROCHEMICALLY ACTIVE MICROBES

A Dissertation

by

HUIJIE HOU

Submitted to the Office of Graduate Studies of
Texas A&M University
in partial fulfillment of the requirements for the degree of

DOCTOR OF PHILOSOPHY

Approved by:

Chair of Committee: Arum Han
Committee Members: Paul De Figueiredo
                      Xing Cheng
                      Chin B. Su
Head of Department: Costas N. Georghiades

December 2011

Major Subject: Electrical Engineering

ABSTRACT

The Development of Microfabricated Microbial Fuel Cell Array as a High Throughput

Screening Platform for Electrochemically Active Microbes. (December 2011)

Huijie Hou, B.E.; M.E., Zhejiang University, China

Chair of Advisory Committee: Dr. Arum Han

Microbial fuel cells (MFCs) are novel green technologies that convert chemical energy stored in biomass into electricity through microbial metabolisms. Both fossil fuel depletion and environmental concern have fostered significant interest in MFCs for both wastewater treatment and electricity generation. However, MFCs have not yet been used for practical applications due to their low power outputs and challenges associated with scale-up. High throughput screening devices for parallel studies are highly necessary to significantly improve and optimize MFC working conditions for future practical applications. Here in this research, microfabricated platforms of microbial fuel cell array as high throughput screening devices for MFC parallel studies have been developed. Their utilities were described with environmental sample screening to uncover electricigens with higher electrochemical activities. The first version of the MFC arrays is a batch-mode miniaturized 24-well MFC array using ferricyanide as catholyte. Several environmental species that showed higher electricity generation capabilities than *Shewanella oneidensis* MR-1 (SO) were uncovered using the developed MFC array, with one environmental electricigen, *Shewanella* sp. Hac353 (dq307734.1)

(7Ca), showing 2.3-fold higher power output than SO. The second MFC array platform developed is an air-cathode MFC array using oxygen in air as electron acceptor, which is sustainable compared to ferricyanide that depletes over time. Environmental electricigen screenings were also conducted, showing parallel comparison capabilities of the developed array. The third MFC array platform is a microfluidic-cathode MFC array that enables long-term operations of miniature MFC arrays with improved power generation abilities. The capability of the microfluidic-cathode MFC array to support long-term parallel analysis was demonstrated by characterizing power generation of SO and 7Ca, proving extended operation time and improved power outputs compared to batch-mode MFC array. The fourth MFC array platform enables both catholyte and anolyte replenishments for long-term characterization of various carbon substrate performances. Finally, the 24-well microfluidic MFC array was further scaled up to 96 wells, which greatly increased the throughput of MFC parallel studies. The developed MFC arrays as high throughput screening platforms are expected to greatly impact how current MFC studies are conducted and ultimately lead to significant improvement in MFC power output.

To my family, for their love and support

ACKNOWLEDGEMENTS

I would like to express my heartfelt gratitude to Professor Arum Han for mentoring me throughout my academic program. I am grateful that Dr. Han gave me such an interesting project to do and this dissertation could not have been written without him. He provided permissive managerial latitude to allow me to be a student, an independent thinker, an engineer and also a researcher.

I also would like to acknowledge Dr. Paul de Figueiredo for his guidance and valuable input throughout the research, I thank him for bringing excitement and fun into our discussions. I also want to make a special thank you to Dr. Lei Li for her guidance and friendship. I am very grateful to learn not only microbiology, but also a serious research attitude from her.

I thank all our group members in the NanoBio Systems lab for their support, help, and valuable recipes! Thank you all for giving me opinions from different angles. I would like to give special thanks to Jaewon Park for his initial lab training and wonderful and precious discussions over the years. I thank Sungmee Cho for the initial studies on the miniature microbial fuel cells and valuable data inputs, and I thank Younghak Cho for continuing the project during my travel and the wonderful work he has done. Thank you to Cemile Ümran Ceylan for her assistance on the development of the microfluidic-cathode MFC array.

"Thank you" is not enough for my family. My parents love me and support me no matter what I choose to do. My husband, my love and my best friend, always

supports and encourages me, no matter how things are going. My beloved daughter, you lighten my life with so many laughs. My parents-in-law, thank you for your support and love.

TABLE OF CONTENTS

LIST OF TABLES

LIST OF FIGURES

1. INTRODUCTION

1.1   Energy needs and renewable energy

Human population on the planet is over 6 billion and will exceed 9 billion in 2050[1]. Fossil fuels have support the civilization and industrial growth, and the need for fossil fuels has seen a twenty fold increase in the past century. According to BP's world energy review in 2011, overall energy consumption growth rate exceeded 5.6% in 2010, and coal's percentage of global energy consumption increased to 29.6%[2]. Considering the economic growth at current levels and the anticipated energy needs, the worldwide energy needs will be 27 TW by 2050 and 43 TW by 2100[1]. Although fossil fuels will not deplete in the next 100 years, the need for energy will exceed the production in 2015 to 2025 time frame[3].

In addition to shortage of fossil fuels for human needs in the near future, burning of fossil fuels is impacting the environment. Nitrogen oxides, sulfur dioxide, volatile organic compounds, and heavy metals generated by combusting fossil fuels and other energy needs contribute about 86.7% of greenhouse gas emissions[4]. Harvesting, processing and distributing fossil fuels also create environmental concerns, including hazards to aquatic organisms, air and water pollution.

Although fossil fuels are still the primary fuel sources that are used worldwide, renewable energy utilizing sunlight and it's direct and indirect impacts on earth

———————————

This dissertation follows the style of *Lab Chip*.

(photons, wind, falling water, heating effects, and biomass), tides, and geothermal heat to generate energy is being developed at an extraordinary speed for both environmental and energy needs[5]. Unlike fossil fuels that will deplete in the near future, such renewable energy resources are sustainable[6]. They have less environmental impact, and there are varieties of resources, many of which could be potentially available locally in urban areas. In 2009, about 8.2% of USA final energy consumption came from renewable energies[4]. As a renewable energy source, biomass is biological material derived from living or recently living organisms[7]. Great variety of biomass sources, such as wood, waste, animal manure, plants, make it become more of interest recently. However, traditional biomass technology based on combustion of carbon from biomass can produce air-pollution challenges, same as fossil fuels. Biomass sources from plants such as corns for ethanol generation directly compete with human food supply, hence makes its future not optimistic.

Both environmental challenges and energy crisis prompted the needs for developing whole new energy platforms that produce sufficient energy while at the same time reduces greenhouse gas emissions. Utilization of biomass in wastewater by electrochemically active microbes has generated great interest in bioenergy community for it remedies the above limitations of traditional biomass resources.

1.2   Microbial fuel cell (MFC) as a renewable energy

1.2.1   MFC development history

Microbial fuel cell is a device that can directly generate electricity from biomass using microbes. Potter firstly observed electrical current generated by bacteria in 1911[8]. The phenomenon did not attract much attention until the early 1990s, when fuel cell technologies started to become of more interest[9]. In the early days, mediators and electron shuttles were added into the culture to assist electron transfer since the outer layers of the majority of microbial species are composed of non-conductive lipid membrane (peptididoglycans and lipolysaccharides) that hinder the direct electron transfer to the anode. A real breakthrough in MFC technologies was made by Kim et al. when they demonstrated that mediators were not necessary for some microbial species in microbial fuel cells[10, 11]. Those microbes could form biofilm on the anode surface and transfer electrons directly through the microbial membrane, and were operationally stable and yielded a high Columbic efficiency[12]. Since the cost of mediators could be eliminated, mediator-less MFCs are of most interest in MFC technologies for electricity generation[13].

1.2.2   Applications of MFCs

1.2.2.1 Electricity generation

MFCs are capable of converting chemical energy stored in biomass compounds directly to electrical energy through microbial metabolism[14-16]. Because no intermediate product is generated, the Carnot cycle with a limited thermal efficiency is avoided and theoretically a high conversion efficiency can be achieved (>70%)[17]. Varieties of fuels such as sugar, fruit, dead insects, grass and weed could be used in MFCs to generate electricity, making MFCs extremely suitable for powering autonomous sensors for long-term operations in low accessibility regions[18-20], bioremediation devices[21, 22], and mobile robot/sensor platforms[23]. In addition, MFCs hold significant promise for supporting civilian and combat operations in hostile environment[23] and powering implantable medical devices with nutrients supplied by the human body if biocompatibility problems are thoroughly solved[24].

Electricity generation by MFCs holds great potential in solving energy crisis in the future. To date, the technology is still far from economical use because power generation by the MFCs is still too low to compete with other electricity generation technologies. Power densities ranging from 100 to 1000 W/m^3 in MFCs have been reported[25, 26], which is much lower than other fuel cell technologies such as methanol fuel cell[27].

1.2.2.2 Wastewater treatment

Wastewater contains organic compounds that can be utilized by MFCs. Organic molecules such as acetate, propionate, and butyrate can be thoroughly broken down to CO_2 and H_2O through microbial metabolism. Sulfate compounds, rich in waste streams from animal husbandry, mining, food processing, pharmaceutical industry, pulp and paper plants, affect the aquatic ecosystem by increasing acidity[28]. Gaseous sulfur-based compounds raise health risks and also create odors. Certain microbes have special abilities to remove sulfides from wastewater[29, 30]. Because microbes can feed on organic compounds in wastewater, growth of the electrochemically active microbes will be enhanced, thus providing very good operational stabilities for MFCs. It has been shown that up to 80% of the chemical oxygen demand (COD) could be removed by using MFC as a method for wastewater treatment[31, 32]. Columbic efficiency as high as 80% has been reported in MFCs[33].

As a novel wastewater treatment process, MFCs have generated great excitement due to their advantages over traditional wastewater treatment methods. Compared with other wastewater treatment processes, MFCs can generate electricity during the wastewater treatment process and can operate in a more stable condition with less excess sludge generation, which is expensive for disposal and is the major cost in wastewater treatment[34]. However, performance of MFCs has to be significantly enhanced before MFCs can be used in practice[34]. Scaling up MFC systems is another challenge[35].

1.2.2.3 Biogas generation

Hydrogen and methane have generated global interest as alternative sources of energy due to their potential for being employed as fuel sources for electricity generation and transportation fuel. In addition, these fuels have attractive characteristics such as ease of storage and transportation, and may also complement or even substitute for compressed natural gas. Currently, about half of the hydrogen production is derived from natural gas, produced mainly using other fossil fuels including oil and coal. Only 4% is generated from water using electricity derived from other resources[36, 37]. Alternatively, hydrogen can be generated through direct photolysis, photofermentation, and dark fermentation[38]. The first two methods require efficient solar energy capture technologies and the recovery rates are relatively low[39]. Fermentative biohydrogen production through bacterial anaerobic digestion is more of interest due to the higher production rate and simpler reaction digester configuration[39]. Organic matter from various waste resources such as animal manure and industrial or domestic wastewaters can be degraded to biogas while at the same time assisting waste treatment. For example, carbohydrates such as glucose have the potential of producing 12 mol of hydrogen from 1 mol of glucose theoretically. In practice, only 4 mol hydrogel/mol glucose is produced through a fermentation process if acetate is the only fermentation product[38]. Higher yield has been achieved using enzymes with a conversion efficiency of up to 96.7%[40]. However, the high cost of enzymes and their stability presently limits economic hydrogen production. Further degradation of fermentation products such as acetate requires significant external energy input, which is undesirable.

Another renewable biogas, biomethane, is generally converted through an anaerobic digestion process known as methanogenesis by converting organic substrates such as acetate, formate, and biohydrogen gas into CH_4[41]. This biomethanation process is widely harnessed for degrading organic waste while producing biomethane that is then used to power electrical generators for local energy needs[42]. However, methanogenesis is known to be only carried out by *Archaea*, and substrates that can be converted to methane are limited. Methane can also be produced electrochemically through carbon dioxide reduction, and has the added advantage of CO_2 capture, however is an energy intensive process.

Recently, it was demonstrated for the first time that electrochemically active microbes can be used to directly generate hydrogen gas through an electrolysis process in an MFC based technology, named microbial electrolysis cell (MEC)[43-50]. The configuration of microbial electrolysis cell is similar to a microbial fuel cell (MFC). Under normal MFC operating conditions, protons and electrons generated on the anode migrate into the cathode chamber through different paths and combine with oxygen to form water as a final product. However, when oxygen is eliminated from the cathode chamber and an external potential is applied to increase the cathode potential that can overcome the thermodynamic barrier, protons and electrons are combined at the cathode to form hydrogen[44]. Although MECs require energy for hydrogen production, the energy is less than 20% of the energy stored in hydrogen fuel. Hydrogen produced with MECs can be stored for later usage. Therefore MFC based MECs provides an alternative method for biohydrogen and biomethane generation.

1.2.2.4 Biosensors

MFCs can also be used as biosensors for pollutant analysis and *in situ* monitoring of wastewater[51, 52]. MFC type biological oxygen demand (BOD) sensors have excellent operational stability and good reproducibility. It can keep operating for over 5 years without extra maintenance[53]. The service life is longer than other types of BOD sensors. It has been demonstrated recently that MFCs can also be used as toxicity sensors[57] to detect the variation on the current produced by the cell when toxic compounds are present in the medium. Microbial fuel cells have also been used as microbial activity sensors, providing in situ monitoring of substrate concentration and microbial respiration rate[54, 55].

1.2.3   Future of MFCs

Despite the advantages of MFCs as renewable energy resource, they have been rarely used for practical applications. Few pilot scale MFC plants have been tested[56] and MFCs have been also used as wireless power sources for sensors in remote areas[18-20]. There are many limitations to overcome before MFCs can be applied to practical applications. Most importantly, low power density of current MFC devices is the main challenge. MFC designs, electrode materials, selection of microbial consortia and cultivation protocols are all contributing to the low efficiency. Second, the cost of MFCs is still high due to the usage of Pt as a catalyst on the cathode electrode in most applications. Other metals that could possibly replace Pt as catalysts have been studied[57], but still need further optimization. Third, scaling up MFCs is necessary especially for high power

generation and for large scale wastewater treatment plants[35]. Fourth, the naturally low catalytic rates of the microbes make the reaction rate low even at their optimized growth conditions, genetic engineering of microbes to further improve the catalytic rates is possible through thorough understanding of electron transfer mechanisms. Almost all current MFCs are at research stages with only few examples of pilot scale plants currently being tested, and significant improvement need to be made before MFCs can be applied to practical use.

2. MICROBIAL FUEL CELL

2.1 Principle of MFCs

2.1.1 Bioelectricity generation using microbial fuel cell

In microbial fuel cells (MFCs), microorganisms break down organic compounds in the anaerobic anode chamber to generate electricity. The illustration of a typical MFC system is shown in **Figure 2.1**. An MFC typically consists of two chambers: anode and cathode chambers, separated by a proton exchange membrane (PEM). The microbes ("electricigen", see section 2.1.1.1) are cultured in the anaerobic anode chamber, oxidizing organic matter and generating electrons and protons (equation 2.1). Electrons generated during the microbial oxidation procedure are delivered to the cathode through the external electrical circuit. In parallel, protons generated at the anode diffuse through the PEM and join the electrons released to the catholyte at the cathode chamber (equation 2.2). Electricity is generated by completing the circuit.

$$CH_3COO^- + 2H_2O \rightarrow 2CO_2 + 7H^+ + 8e^- \tag{2.1}$$

$$O_2 + 4e^- + 4H^+ \rightarrow 2H_2O \tag{2.2}$$
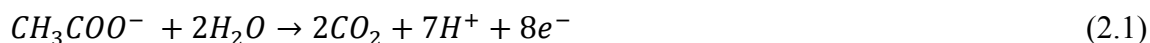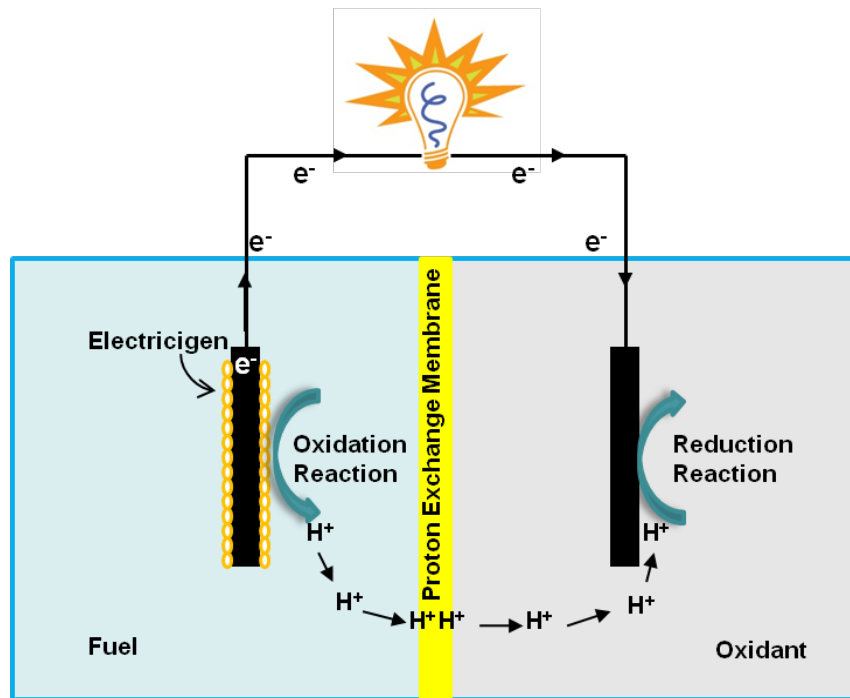
Figure 2.1 Schematic illustration of basic components of a microbial fuel cell (MFC).

2.1.1.1 Electricigens

Many microorganisms can contribute to electricity generation. However, only microorganisms that can completely oxidize organic compounds to carbon dioxide with direct electron transfer to electrodes offer the possibility of converting organic compounds to electricity in self-sustaining MFC systems. Those organisms are called "electricigens"[16].

To date, except sediment and wastewater treatment MFCs which use mixed microbial consortia for electricity generation[60, 61], most current researches on MFCs are focused on several already known pure microbial isolates[21, 58-61]. Mixture of different microbial species was shown to improve the electricity generation, and power density of 4.3 W/m^2 was achieved[62]. Electricigen functionalities are greatly dependent on efficiency and mechanism of electron transfer, cultivation protocol, substrate type and degree of anaerobiosis of the anode chamber.

2.1.2   Mechanisms of electron transfer in MFCs

Bacteria are so far known to have two electron transfer mechanisms from inside of their membranes to the outside electrode: under the assistance of mediators and through direct contact based electron transfer[15]. In the early days of MFC research, exogenous mediators were commonly used to increase the efficiency of electron transfer. Chemicals such as neutral red, nthraquinone-2,6-disulfonate (AQDS), thionin, potassium ferricyanide, methyl viologen and others were used to facilitate the shuttling of electrons from inside the cell to electrodes outside the cell[63]. It was later found that adding

exogenous mediators is not always essential. There are bacteria that can produce redox mediators themselves through the production of organic, reversibly reducible compounds and through the generation of oxidizable metabolites[64]. It was later discovered that some microbes are capable of direct electron transfer from inside of cell membrane to the surface of electrode through nanowires. Nanowires are conductive appendages founded in some bacteria species, and their conductivities were examined using conductive scanning tunneling microscopy (STM)[61, 65]. Nanowires found in one microbe could also assist other microbe species' electron transfer in a mixed microbial culture[60]. In addition to nanowires, it was also found that microbes could transfer electrons through direct cell surface contact with electrodes[59] or through biofilms formed on electrode surfaces[61, 66, 67].

2.1.3   Electron acceptors

Cathode reaction efficiency is greatly dependent on concentration and types of electron acceptor, proton diffusion efficiency, catalyst, and electrode material[68]. Oxygen is the most commonly used electron acceptor in MFCs. Two sources of oxygen are currently used in MFCs: oxygen dissolved in solution and oxygen directly from ambient air. For MFCs using oxygen dissolved in solution as electron acceptors, an extra power for an air-spurge system to continuously sparge air or pure oxygen into a water cathode is required[69-72]. MFCs using aqueous cathode with dissolved oxygen as electron acceptor can operate in a continuous mode with an oxygen pumping system. Although aqueous cathode with sparged air of pure oxygen was used as catholyte, power used in the air-

sparge system for now greatly exceeds the power that is generated by the MFC itself. This type is usually not used for power generation, but for MFC studies and wastewater treatment. While no oxygen sparging system is required when using oxygen directly from ambient air, power density is limited due to low oxygen permeability. Oxygen has advantages of low cost, high oxidation potential, and lack of chemical waste product (water is the product). However, oxygen can diffuse into the anode chamber, hence reducing the power generation efficiency.

Other than oxygen, ferricyanide is another commonly used electron acceptor[3, 62, 73]. It can greatly improve the power output due to the availability of electron acceptor at high concentrations. It has low overpotential when using carbon cathode, resulting in a cathode working potential close to its open circuit potential[74]. Use of ferricyanide in a conventional H-type reactor increased power by 50-80% compared to an air-sparged cathode. The use of ferricyanide is not always good. Although no air-sparging system is needed, the regeneration of the electrolyte is a problem in these systems, thus the use of ferricyanide is not sustainable in practice. Ferricyanide can also diffuse to the anode chamber by crossing PEM and thus influences the MFC performances.

In addition to ferricyanide, permanganate is also used as electron acceptor. Higher power than oxygen as electron acceptor was reported[75].

2.1.4 Anodes in MFCs

Selection of materials that are durable, conductive, biocompatible and easily fabricated as anodes of MFCs is an important strategy to improve their performances[76]. Graphite,

in the form of carbon cloth or graphite felt, has typically been the material of choice for
the construction of MFC anodes because of their stability in microbial cultures, high
electricity conductivity and large surface area[68]. Conductive elements such as
manganese, iron, quinines, and neutral red have been incorporated in graphite electrodes
to significantly increase power output[80, 81]. Modification of anodes with conductive
polymers such as polyaniline (PANI) and modified PANI (fluorinated PANI,
PANI/carbon nanotube composite, PANI/titanium dioxide composite) were also
demonstrated to produce higher current densities[77, 78], although the durability of these
modified electrode is of concern. Gold or modified gold has also been recently used as
anode materials to support electron transfer in MFCs[77-80].

2.1.5 Proton exchange membrane (PEM)

Proton exchange membrane (PEM) is commonly used in MFCs to separate the cathode
and anode chambers except sediment MFCs and some single chamber MFCs. PEM
facilitates proton transfer from anode chamber to cathode chamber while at the same
time keeps the anode chamber anaerobic. Nafion^{TM} is the mostly commonly used PEM
in MFCs. However, biofouling caused by ammonium that is rich in substrates could be
an issue[64]. Ultrex^{TM} cation exchange membrane was also used[62]. The problem of using
PEM is that it contributes to the most part of the internal resistance of MFC because of
the low efficiency of proton migration, contributing to low power generation efficiency.
Oxygen, ferricyanide used in the cathode, other ions and organic matter used in the
substrate can also migrate from the cathode chamber to the anode chamber and vice

versa, thus further reduce the power generation efficiency. Membrane-less MFCs without PEMs were shown to reduce the internal resistance[81-83]. A single chamber MFC with and without PEM were compared[31], showing power density increase from 262 to 494 W/m^2 by removing PEM. However, removing PEM is not an option for two chamber MFCs.

2.1.6   Cathodes in MFCs

Platinum coated carbon or graphite is most commonly used as cathode in MFCs. Pt is used as catalyst on cathode to increase the reduction rate. However, Pt is expensive and the long-term stability of adherence to the cathode surface also needs to be considered. Other inexpensive materials such as porphyrines, phthalocyanines and Co have been investigated as alternative catalysts in MFCs, and their oxygen reduction activities were also examined[84, 85]. In addition to metal catalyst, microbes have also been used as catalyst in the cathode side. It has been shown that power densities could be in the same range as Pt catalyst cathodes and operation period could also be elongated[22].

2.2　MFC architectures

2.2.1　Two chamber MFCs

The most commonly used and least expensive two-chamber MFC architecture is an H-type MFC. The H-type architecture usually consists of two bottles connected through a PEM (Nafion^{TM} or Ultex^{TM}) (**Figure 2.2** and **Figure 2.3A**). H-type MFCs are easy to use and good for basic MFC research. However, they typically produce low power densities due to the limited areas of anodes, cathodes, and membranes[72, 86]. The internal resistance is usually high in these systems due to PEM separating the two chambers and the distance between the anode and cathode. In addition to H-type MFCs, miniature two chamber MFC systems of various configurations in tubular shape and cylinder shape have also been developed to facilitate different MFC research (see section 2.2.3.1). Aqueous solutions with dissolved oxygen or ferricyanide are electron acceptors most commonly used in two-chamber MFC systems.
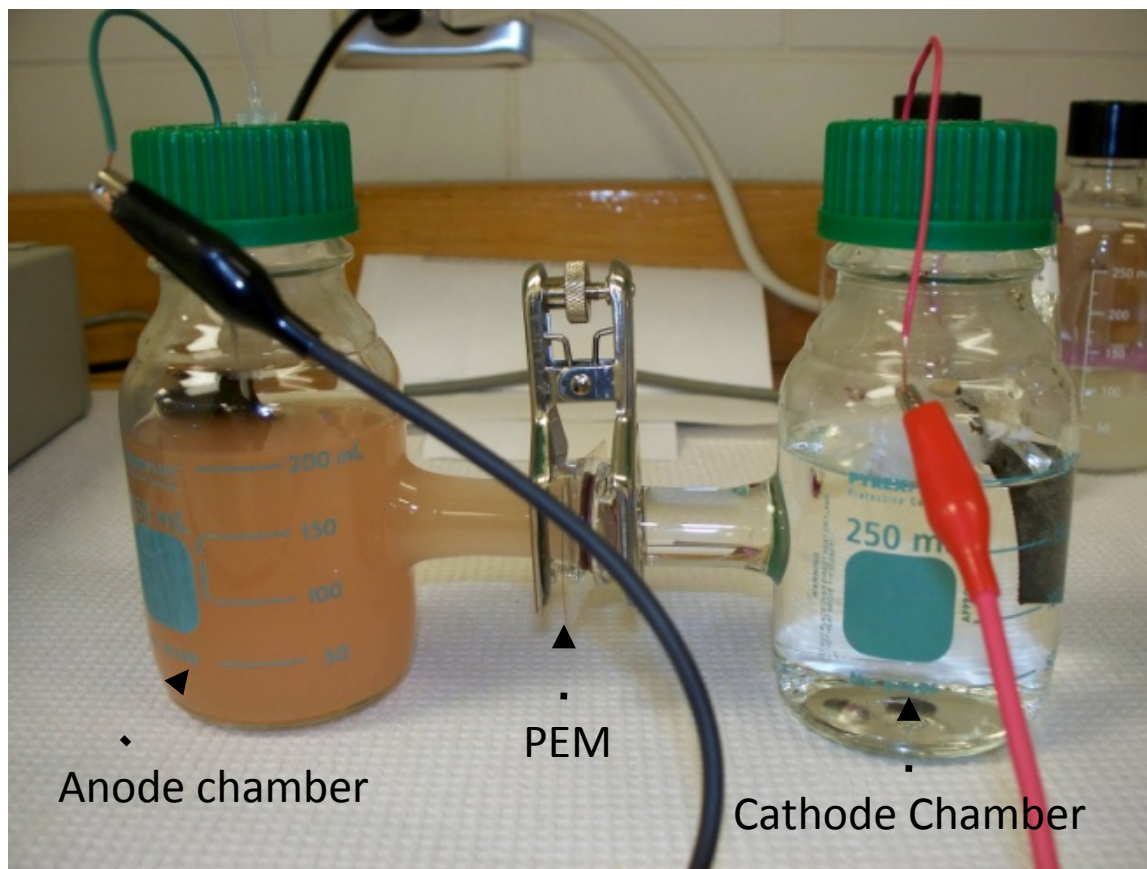
Figure 2.2 Conventional H-type MFC, which comprised of an anode chamber, a cathode chamber and a PEM separating the two chambers.

2.2.2 Single chamber MFCs (SCMFCs)

2.2.2.1 Air-cathode MFCs

Different from two-chamber MFCs, which use aqueous electron acceptors with cathode immersed in the cathode chambers, air-cathode MFCs uses oxygen in ambient air as electron acceptor (**Figure 2.3B&C**). Cathodes are exposed to the air directly in these systems with cathode chambers being removed. In this configuration, anode and cathode are housed in one chamber[87]. A carbon/Pt layer was fused with PEM to form an air-porous cathode. Air-cathode SCMFCs have continuous oxygen supply from the air, and can be operated with and without a proton exchange membrane[31, 88]. However, issues such as anode solution dry-out over time still need to be solved.

2.2.2.2 Sediment MFCs

When a microbial fuel cell is operated in a natural water source (river, lake, sea, etc.), electrons can be derived from microbial reactions on the anode buried under sediment. The type of MFC is so called sediment microbial fuel cell (SMFC)[19]. The mixed consortia in the sediment oxidize the organic matter in the sediment to derive electrons. Cathode made of graphite or stainless steel immersed in water above the anode reduces oxygen. Sediment MFC is another type of SCMFCs that is extremely suitable for operation in low accessibility regions as power sources for remote control systems[19, 20, 76].

A

B

C

e⁻ ... H⁺ H⁺ e⁻ H₂O

Substrate Aerobic

e⁻ ... H⁺ e⁻ H⁺ H₂O

Substrate Air

e⁻ ... H⁺ e⁻ H⁺ H₂O

Substrate Air

PEM   Cathode   Anode
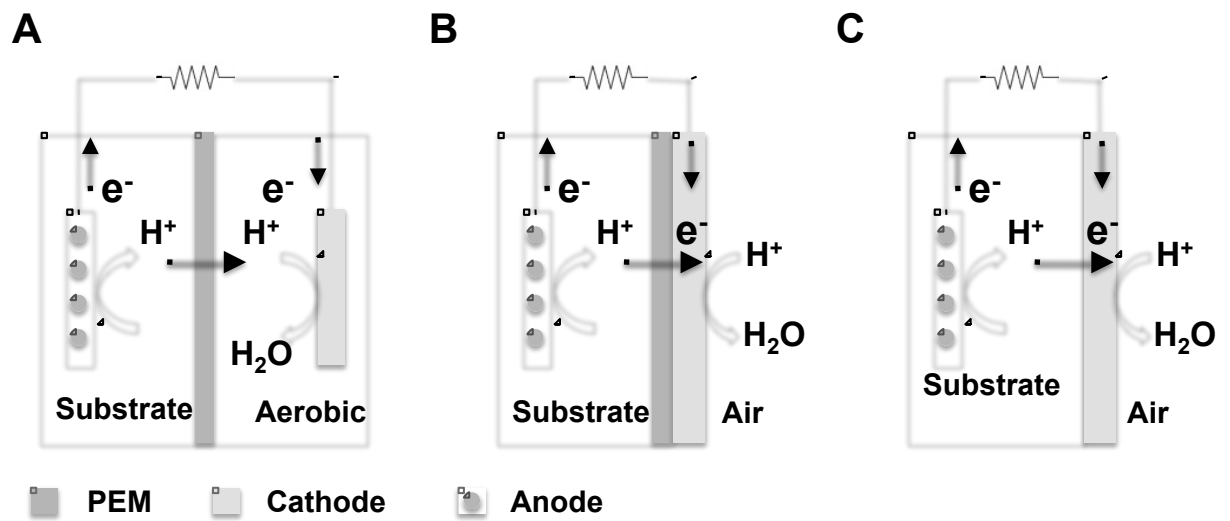
Figure 2.3 Illustrations of A: a typical two chamber MFC system, B: an air-cathode MFC system with PEM and C: an air-cathode MFC system without PEM.

2.2.3 MFC architecture variations

2.2.3.1 Tubular reactors

Tubular reactors are usually used for wastewater treatment. They are usually built with inlets and outlets for continuous wastewater run to work in a continuous mode[89, 90]. Tubular reactors can be single or two chamber MFCs with either oxygen[91, 92] or chemical catholytes such as ferricyanide[93-95] as electron acceptors.

2.2.3.2 Stacked MFCs

A single MFC produces low voltage. However it is possible to increase voltage by stacking MFCs together in series. Stacked MFCs have been investigated in a few studies and the sum of the individual cell voltages is usually higher than the final voltage due to the loss caused by connection. A 6-cell stacked MFC with ferricyanide as catholyte was constructed[58] and power output of 59 W/m^3 in parallel and 51 W/m^3 in series has been achieved. Coulombic efficiency was 78% when operated in parallel. A bipolar-plate type stacked MFC produced 1300 mW/m^2 with ferricyanide as catholyte and 230 mW/m^2 with pure oxygen[96]. However, stacking MFCs together may be a difficult way to increase voltage[97]. Variations of the output in individual cells could cause voltage reversal and damage some of the cells. Moreover, biological systems are not as stable as chemical cells. More work is needed to improve the stability and feasibility of the stacked MFCs.

2.2.3.3 Miniature MFCs

Miniature MFCs including mL-scale and μL-scale setups have been described recently for their ease of assembly, less reagent consumption, and flexibility of design for different functionalities[98]. High power mL-scale mini-MFC, in the forms of two-chamber designs using ferricyanide and air cathode that generate 100-1010 W/m^3 power output has been reported[99, 100]. Although power generation is low compared to MFCs with larger volume (>100s mL), miniaturized MFCs offer great opportunities for on-chip power sources and biosensors[101]. Miniature MFCs also function as flexible tools to understand the extracellular electron transfer process with excellent microenvironment control, and has the possibility of integrating microfluidics into the systems to achieve versatile functionality for fundamental MFC studies[102].

2.3   Power generation characterization of MFCs

2.3.1   Voltage

Voltage that an MFC can generate is around 0.3-0.7 V. It is a function of load resistance and current (equation 2.3, where E is the cell potential and R_{load} is the load resistance).

$$E = I \cdot R_{load} \tag{2.3}$$

It is decreasing with the decrease of the load resistance. The maximum voltage produced by an MFC is when the load resistance is infinite, meaning zero current, and is called

open circuit voltage (OCV). It is difficult to predict the voltage produced by an MFC, because the biological system is far more complicated than the chemical fuel cell, even when using pure microbial culture in MFCs. The limit of the maximum voltage that can be generated is based on thermodynamic relationships for the electron donor and acceptors[3].

2.3.2 Power

Power generation of an MFC is calculated from voltage and current across a loading resistance (equation 2.4). Current is usually calculated from the voltage across the load resistance, as shown in equation 2.3. Power output can be normalized by surface area (equation 2.5, in which, A_{anode} is the projected area of anode) or by volume of microbial culture (equation 2.6, in which, V_{anode} is the volume of anode microbe culture). When calculating based on normalized area, if the anode is suspended in culture media, A_{anode} is double the size of the projected area, and when only one side of the electrode is exposed, A_{anode} is the same as the projected area. The most useful parameter is the maximum power an MFC can produce. Maximum power can be predicted with equation 2.7 based on OCV and internal resistance measurement.

$$P = I_{load} \cdot V_{load} \tag{2.4}$$

$$P = \frac{I_{load} \cdot E_{load}}{A_{anode}} = \frac{E^2}{A_{anode} \cdot R_{load}} \tag{2.5}$$

$$P = \frac{I_{load} \cdot E_{load}}{V_{anode}} = \frac{E^2}{V_{anode} \cdot R_{load}} \tag{2.6}$$

$$P = \frac{OCV^2 R_{load}}{(R_{int} + R_{load})^2} \tag{2.7}$$

2.3.3 Polarization curve

Polarization curve is a plot of voltage over current, measured by connecting different load resistances and measuring the voltage and current through the load resistors. The plot is used to characterize resistance distribution and various losses of an MFC system. There are three characteristic regions on a polarization curve[103]. The region of charge transfer overpotentials occurs at low current region, and is derived from the slowness of the reactions taking place on the surface of the electrode. The ohmic overpotentials occur at the intermediate current and are caused by the ohmic resistance in the electrolyte. The mass transport overpotentials are prevalent at relatively high current level if the reactants cannot be supplied to the electrode reaction zone required to sustain the generation of current.

$$E = E_b - R_{int} I \tag{2.8}$$

The internal resistance is one of the most important factors that are limiting the performance of MFCs. It can be calculated based on the linearized ohmic losses region in the polarization curve by equation 2.8, where E_b is the linear extrapolation open circuit voltage. The internal resistance calculated in this method is the total resistance including ohmic resistance, and is influenced by the activation loss and concentration loss.

3. TWENTY-FOUR WELL BATCH-MODE MFC ARRAY

3.1 The needs for MFC architecture with parallel study capability

3.1.1 Limitations of current MFCs

MFCs have generated great excitement in the bioenergy community because of their potentials of powering diverse technologies. However, MFC technologies are still in its infancy and significant improvements in efficiency and cost are needed before MFCs can be applied to commercial use. There are several factors that are contributing to the low power generation in MFCs: Performance of anodes, including efficiencies of microbes, anode material, culture media used, and microbial cultivation protocols; low proton exchange efficiency of PEMs used in most MFC systems; catholyte types and concentrations used in the cathode side; and architectures of MFCs. In terms of cost, noble metals used in the cathode side as catalysts to increase the efficiency of MFCs and the use of PEM are the main factors that make MFCs expensive.

3.1.2 Motivations of the development of an MFC array

Important strategies for enhancing MFC performance include engineering optimized microbes (and microbial communities) for use in these devices[104] and improving cultivation practices for these organisms[105, 106]. To date, detailed description of individual microbe performance in MFCs has been limited to a surprisingly small

number of organisms[107]. MFCs that are fed by sediment and wastewater nutrient sources and that exploit mixed microbial consortia for electricity generation have been described[62, 108]. However, with the conventional H-type MFCs, characterization of the electrochemical activities of the microbial species in these consortia has not been possible because these conventional MFCs are not suitable for parallel analyses due to their bulkiness. To address this issue, MFC systems that support parallel, low cost, and reproducible analysis of the electrochemical activities of diverse microbes are required. High throughput microarrays, including DNA microarrays, protein microarrays, and cell arrays, are powerful platforms for screening and analyzing diverse biological phenomena[109]. Various MFC platforms, including miniature MFC devices that enable parallel comparison of electricity generation in MFCs, are emerging[110, 111]. However, state of the art microfabrication and highly integrated parallel measurement approaches[112, 113] have not yet been exploited to construct an MFC array with highly consistent architecture and performance.

To overcome such limitations, a compact and user-friendly MFC array device capable of examining and comparing the electricity generation ability of environmental microbes in parallel was developed. The MFC array consists of 24 integrated cathode and anode pairs as well as 24 cathode and anode chambers, which function as 24 independent miniature MFCs. Importantly, the array was fabricated using advanced microfabrication approaches that can be scaled-up to fabricate massively parallel systems.

3.2 Experimental methods

3.2.1 MFC array design

Figure 3.1 shows the schematic illustration of the MFC array. The 24-well device was composed of layered functional compartments in which microbe culture wells were embedded. Each microliter-scale microbe culture well was combined with individually addressable anode and cathode electrodes and functioned as an independent miniature MFC. The layers included anode electrodes, anaerobic microbe culture chambers (anode wells), a proton exchange membrane (PEM), cathode chambers, and cathode electrodes.

3.2.2 MFC array microfabrication

The electrode microfabrication procedure is shown in **Figure 3.2A.** Glass substrates (50 mm × 75 mm) were cleaned in "piranha" solution (H_2O_2 : H_2SO_4 = 1 : 3 v/v) for 30 min, followed by thoroughly washing with de-ionized (DI) water and blow-drying with N_2. Titanium (thickness: 200 Å, deposition rate: 2 Å/sec) and gold (thickness: 1200 Å, deposition rate: 3 Å/sec) were deposited on cleaned glass slides using electron beam evaporation. Photoresist (Shipley S-1818, Rohm and Haas, Inc., Philadelphia, PA) was spin-coated on metal coated glass slides at 4000 rpm, baked at 100°C oven for 10 min, then exposed to UV light through a photolithography mask for 18 sec using a mask aligner (MA6, SUSS Microtech, Germany) at an intensity of 8.5 mW/cm^2 (wavelength = 320 nm), and then developed in a photoresist developer (MF^{TM} 319, Rohm and Haas, Inc., Philadelphia, PA) for 20 sec. The exposed part of the Au and Ti layers were then
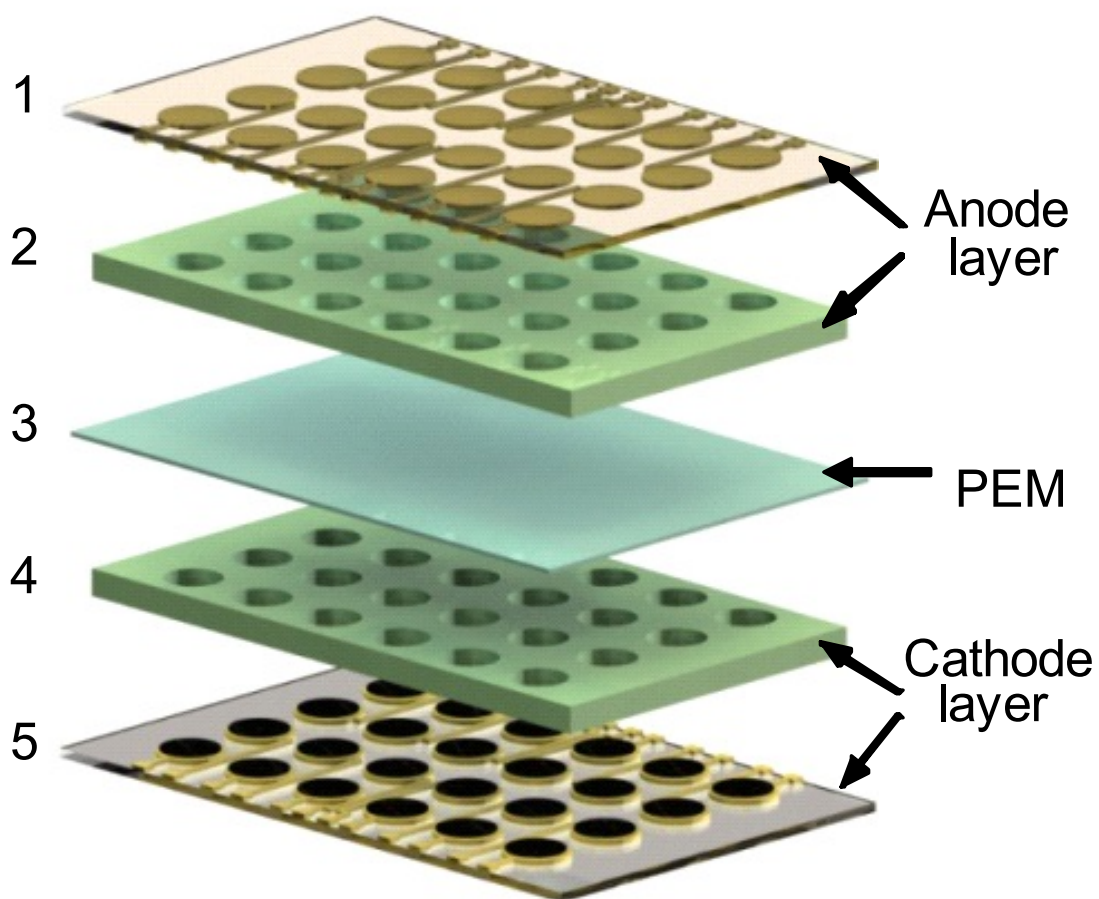
Figure 3.1 Schematic illustrations of a 24-well microbial fuel cell (MFC) array. The MFC array is composed of an anode layer (1: anode electrode layer, 2: anode well layer), a proton exchange membrane (3: PEM), and a cathode layer (4: cathode well layer, 5: cathode electrode layer).
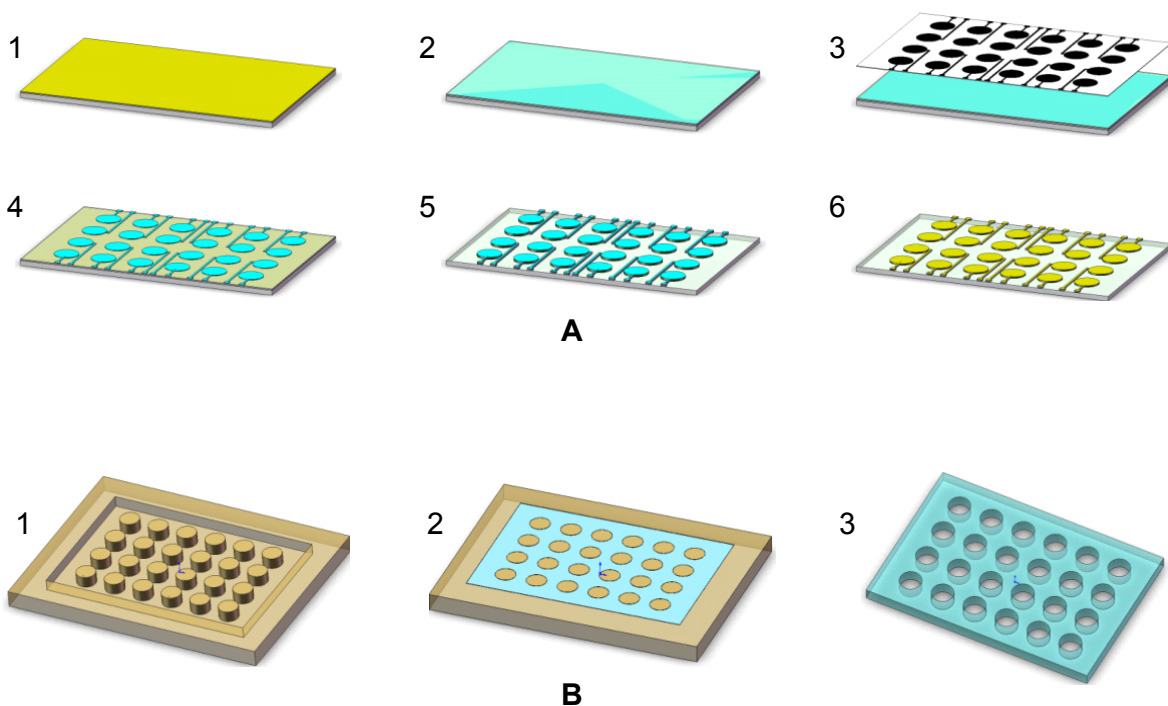
Figure 3.2 Fabrication steps of the MFC array. **A:** Electrode layer (both cathode and anode) fabrication steps. 1. Titanium/Au deposition; 2. Photoresist (PR) spin coating; 3. UV exposure of PR through a lithography mask; 4. PR developing; 5. Au and Ti etching; 6. PR removing. **B:** PDMS layer fabrication steps via softlithography for cathode and anode well layers. 1. Acrylic master mold fabrication using a rapid prototyping tool; 2. PDMS mixing and pouring onto the acrylic master mold; 3. PDMS curing and peeling off.

removed in Au etchant (Type TFA, Transene Company Inc., Danvers, MA) and Ti etchant (HF : H_2O = 1 : 300 v/v). Finally, the photoresist was removed with acetone and cleaned with isopropanol and DI water. The fabricated cathode and anode electrode substrates had 24 individually addressable electrodes, each having an 8 mm diameter disk pattern. Wires were then soldered to all contact pads to provide electrical interconnects between the MFC arrays and the voltage measurement setup.

An acrylic master mold having 4×6 arrays of pillars (diameter: 7 mm, height: 4 mm) was fabricated with a rapid prototyping machine (MDX-40, Roland Inc., Los Angeles, CA). PDMS precursor solution (Sylgard 184, Dow Corning, Auburn, MI) prepared by mixing base and curing agent at 10 : 1 ratio (v/v) was poured onto the acrylic master mold. After curing for 30 min at 85°C, the resulting polymerized PDMS slab was peeled off, creating an inverse replica of the acrylic master mold (**Figure 3.2B**). The cathode layer was prepared by aligning and permanently bonding a PDMS well layer onto a patterned electrode layer. Platinum loaded carbon cloth (10%, A1STD ECC, BASF Fuel Cell, Inc., Somerset, NJ) was cut to the size of a well (diameter: 7 mm) and bonded on top of the Au electrode pads in the cathode electrode layer using silver paste (Structure probe, Inc., West Chester, PA)

The PEM (Nafion 117[TM], Ion-Power, Inc., New Castle, DE) was pretreated by immersion in 5% H_2O_2 for 1 hour at 80°C, rinsed and boiled in DI water for 1 hour at 80°C, and then boiled in 0.5 M H_2SO_4 for 1 hour at 80°C. After rinsing with DI water followed by another 1 hour boiling in DI water at 80°C, the membrane was stored in DI water until use.

3.2.3 Assembly of the MFC array system

Individual parts of the 24-well MFC array system are shown in **Figure 3.3A**. The cathode layer consisted of a PDMS well layer permanently bonded on an electrode layer. Pt loaded carbon cloth was cut to the size of the well (diameter: 7 mm) and bonded on top of the Au electrode pads. The anode layer consisted of three layers: two PDMS layers fabricated as described above and an acrylic layer (8 mm thick) having 4 x 6 arrays of through-holes (7 mm diameter) fabricated by a rapid prototyping machine. The two PDMS layers were placed on both sides of the acrylic layer. The rigid acrylic layer served as a support layer that could be clamped tightly in the subsequent assembly step. The cathode layer, activated proton exchange membrane, and the anode layer were then assembled together. Top and bottom acrylic support frames that could be used to tightly clamp all layers together in between were cut out using a rapid prototyping machine. The sequence of images (**Figure 3.3A-E**) shows how all parts of a 24-well MFC array system was assembled. First, each cathode well was filled with 170 μl of cathode solution (100 mM ferricyanide in PBS) (**Figure 3.3B**) followed by placing the PEM and the anode well layer on top. The acrylic part of the anode well layer was then screwed together with the bottom acrylic frame. Microbe containing solution (650 μl) was pipetted into each anode well (**Figure 3.3C**). Finally, the anode electrode layer was flipped over and then the top acrylic frame was screwed with the bottom acrylic frame (**Figure 3.3D**). The assembled device (**Figure 3.3A-D**) with acrylic supporting frames was coupled to a load resistor circuit board and a digital multimeter through a computer controlled switch box module and a data acquisition system (**Figure 3.3E**).
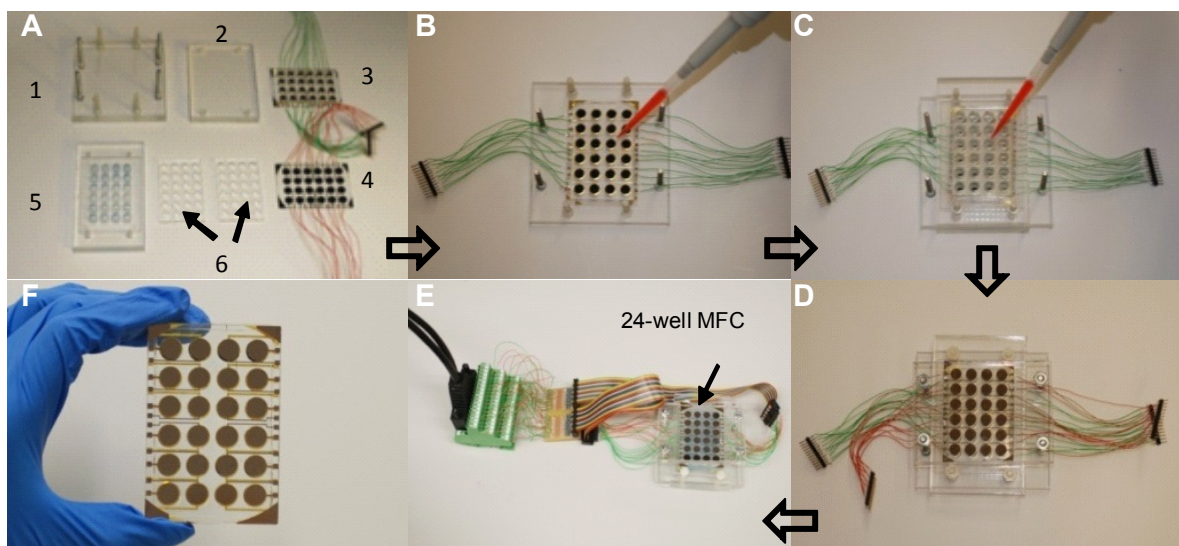
Figure 3.3 Assembly procedures of a 24-well MFC array. **A-D:** MFC array assembly. **A:** Individual layers of an MFC array: acrylic support frames (1 & 2), cathode layer (3), anode electrode substrate (4), anode well layer (5 sandwiched by 6). **B:** Assembly of the acrylic frame (1) with the cathode layer (3), followed by cathode solution loading. **C:** Anode well layer and PEM assembly followed by microbe loading. **D:** A fully assembled MFC array with an anode electrode layer (4) and acrylic frame (2) capping the anode wells. **E:** A fully assembled MFC array connected to load resistors and a data acquisition system. F: An MFC array device with no acrylic frame.

3.2.4   Data acquisition system and MFC array characterization

Two characterization methods were used to evaluate electricity generation from each of the 24 MFC wells. First, twenty-four 1 MΩ fixed load resistors were connected to each of the MFC wells and voltage across these resistors were recorded. Load resistance of 1 MΩ was selected for MFC characterization because power output of *S. oneidensis* MR-1 at this resistance was close to maximum and the fabricated MFC array showed a steady state current output much faster than using resistors with lower resistances. A switch box module having an integrated digital multimeter (PXI-2575, PXI-4065, National Instruments, Austin, TX) and controlled through LabView^{TM} (National Instruments, Austin, TX) was used to continuously measure voltages across the 24 load resistors that were connected individually to the 24-well MFC array (**Figure 3.4**). The measured voltages were converted to current densities (mA/m^2, electrode area: 0.385 cm^2) using Ohm's law, and power densities were calculated using P = VI/A (V: voltage, I: current, A: electrode area).

Full characterization of an MFC requires a current density versus power density plot, which can be obtained by measuring voltages across load resistors of different resistance values. For this characterization, twenty-four 100 KΩ variable resistors (652-3296Y-1-104LF, Mouser Electronics, Mansfield, TX) were connected in series with twenty-four 2 MΩ variable resistors (652-3296Y-1-205LF, Mouser Electronics, Mansfield, TX) in pairs on a circuit board, connected correspondingly to the 24 miniature MFC wells (**Figure 3.4A**). For environmental screening of microbes using the MFC array, both the primary screening and the secondary confirmation screening started
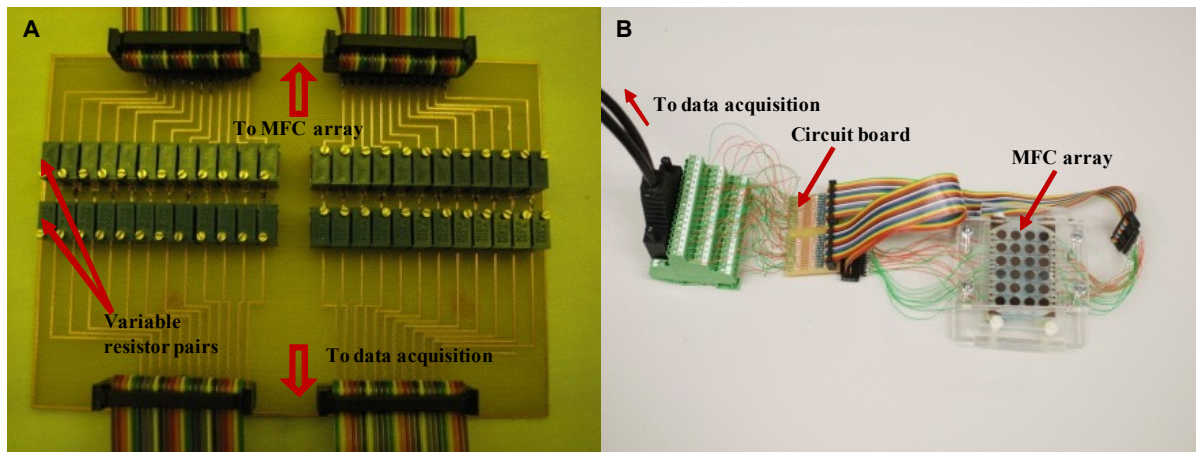
Figure 3.4 MFC array data acquisition system. **A:** Circuit board consisting of variable resistors for load resistance adjustment. **B:** An MFC array connected to the data acquisition system.

1000 min after loading microbes into the MFC array connected to 1 MΩ load resistors. One, 10, 20, 50, 100, 200, 500, 1,000, and 2,000 KΩ loading resistors were used and voltages across these resistors were continuously recorded (**Figure 3.4B**).

3.2.5   Conventional H-type MFC validation

The conventional MFC setup is comprised of two sterile glass containers (250 ml) with rubber gasketed glass bridges (**Figure 2.2**). The PEM was clamped between the two glass bridges. Each container had a cap with a 1 mm diameter opening through which wires were fed to make electrical contact with the anode and cathode. The anode opening was then sealed with a tape during experiments. The cathode cap remained open to allow oxygen exchange.

Gold substrate and carbon cloth were used as the anode materials. Gold was deposited on a clean 50 mm by 75 mm glass slide (Corning, NY) using an electron-beam evaporator to a thickness of 80 nm (deposition rate 5 Å/sec). The gold-coated glass slide was then cut to 2.5 cm by 3 cm size substrates (surface area: 7.5 cm^2), followed by rinsing with acetone, isopropyl alcohol, and deionized (DI) water.

When using carbon electrodes, carbon cloth without waterproofing (B1A, BASF Fuel Cell, Inc., NJ) was used as the anode material. The carbon electrode size was 2.5 × 3 cm (surface area: 7.5 cm^2). Wires attaching the electrodes were connected to a multimeter and a resistor board. For cathode, carbon cloth loaded with platinum (A1STD, 0.5 mg/cm^2 loading with 10% Pt, BASF Fuel Cell, Inc., NJ) was used. The

carbon cathode size was 2.5 × 3 cm, same as the carbon anode. All electrodes were sterilized in 70% ethanol for 10 min before use.

To evaluate electricity generation from this H-type MFC, open circuit voltage (OCV) and current density versus power density plots were obtained. OCV of the MFC was measured using a potentiostat with data acquisition capability (EC Epsilon, BASi, Inc., IN).

To characterize the power output, the MFC was connected to a resistance selector (Ohm-Ranger, Ohmite Mfg. Co., IL). For power curve generation, 0, 0.1, 0.5, 1, 2.5, 5, 10, 40, 100 and 500 KΩ loading resistors were used and current recorded with a digital multimeter (34410A, Agilent Technologies, Inc., WA) connected to a data acquisition setup (GPIB computer interface and LabView^{TM} software, National Instruments, Inc., TX). Current was first recorded for 16 h without load resistor to stabilize the MFC, and then recorded with varying load resistors. Current was measured for at least 20 min. Power was calculated using Ohm's Law ($P = I^2R$).

3.2.6 Microbe cultivation protocols

All bacterial cells were stored at -80°C in tryptic soy broth (TSB, pancreatic digest of casein 1.7%, enzymatic digest of soybean meal 0.3%, glucose 0.25%, NaCl 0.5%, K_2HPO_4 0.25%, pH 7.3) supplemented with 15% glycerol. Cells were streaked onto a TSB agar plate from storage. One of the resultant single colonies was inoculated into 5 ml of TSB medium, and then shaken at 150 rpm for 48 h at 30˚C. To perform MFC

array screening, the optical densities (OD_{600}) for *Shewanella oneidensis* MR-1 obtained

from American Type Culture Collection (ATCC, Manassas, VA) and the environmental

isolates were measured and adjusted to 0.8 before loading into the anode wells of the

MFC array, and 100 mM ferricyanide in phosphate buffered saline (PBS, 0.8% NaCl,

0.02% KCl, 0.144% Na_2HPO_4, 0.024% KH_2PO_4, pH 7.4) was used as the cathode

solution. For confirmation using the conventional MFC, 5 ml of the actively growing

overnight cultures (OD_{600} = 0.7) were inoculated into 500 ml of TSB and incubated for

48 h (OD_{600} = 1.5) at 30°C and then loaded into the anode chamber, and 100 mM

ferricyanide in 100 mM sodium phosphate buffer (pH 7.0) was used as the cathode

solution.

3.2.7   Microscopy

Biofilm formation was observed both under a fluorescent microscope (Eclipse LV100D,

Nikon Inc. NY) and a scanning electron microscope (SEM, JEOL JSM-6400). For

fluorescent microscopy, anodes with microbes were fixed in 4% paraformaldehyde for

30 min at room temperature, rinsed with PBS (pH 7.4), stained with 5 μg/ml DAPI (4',

6-diamidino-2-phenylindole) for 5 min, and followed by a final wash in PBS (pH 7.4)

for 5 min before microscopy. Bright field microscope images were taken with an

Olympus BX51 fluorescent microscope (Olympus America, NY) equipped with an

Olympus DP70 camera.

For SEM, electrodes were fixed in sodium phosphate buffer (0.05 M, pH 6.8)

with 3% glutaraldehyde for 90 min, and rinsed thoroughly in 0.05 M sodium phosphate

buffer (pH 6.8) for 90 min. Next, electrodes were placed in 2% osmium tetroxide (in 0.05 M phosphate buffer, pH 6.8) for 2 hr and then dehydrated in ethanol, followed by drying in a critical point drier.

Environmental SEM (ESEM E-3) images were taken after gently soaking microbe-attached electrode in 2% NaCl solution for 5 min to remove those loosely attached microbes. Excess solution was adsorbed from the side of the electrode using paper towel.

3.3   Performance of MFC arrays

3.3.1   Au working as an anode material

Graphite anode electrode is the most commonly used anode material in MFC. Graphite has the advantage of being stable in microbial culture, having high electrical conductivity, large surface area and low cost. However graphite is not suitable for microfabricated MFC array systems[80]. The surfaces of graphite electrodes are non-uniform and difficult to pattern in small-scale devices. The non-uniformity thwarts efforts to compare performances between individual miniaturized MFCs. Compared with graphite, gold is highly conductive, can be vapor deposited, and is compatible with a wide range of conventional microfabrication modalities[99]. Thus, gold is a very attractive anode candidate for the development of an MFC screening platform.

The selection of an appropriate anode material would be critical to the successful development of an MFC array, and therefore performances of a commonly used anode

material, carbon cloth was compared to gold in a conventional MFC device (**Figure 3.5**). The model facultative anaerobe *S. oneidensis* MR-1 was used for these experiments because this organism had previously proven useful for the development of MFC applications[114]. MFC power output was monitored for 5 h after bacteria were introduced into the MFC. The carbon electrode supported maximal power density was 33.01 ± 3.21 mW/m^2 at a current density of 92.55 ± 4.44 mA/m^2 compared with the gold electrode, which with maximal power density was 3.77 ± 0.02 mW/m^2 at a current density of 16.47 ± 0.04 mA/m^2. However, a higher standard deviation was observed (10% deviation) in the carbon anode configuration than the one with gold anode (3.1%), which demonstrated that MFC with gold anode displayed greater reproducibility. The OCV of MFCs containing gold and carbon cloth anodes was 514 ± 12 mV (mean $\pm$ SE, $n = 3$) and 538 ± 51 mV (mean $\pm$ SE, $n = 4$), respectively. These results indicated that the OCV of the MFC with the gold anode was comparable to the corresponding OCV with the carbon cloth anode. However, OCV measurements with the carbon cloth anode displayed greater variance (2.33% deviation vs. 9.48% deviation).
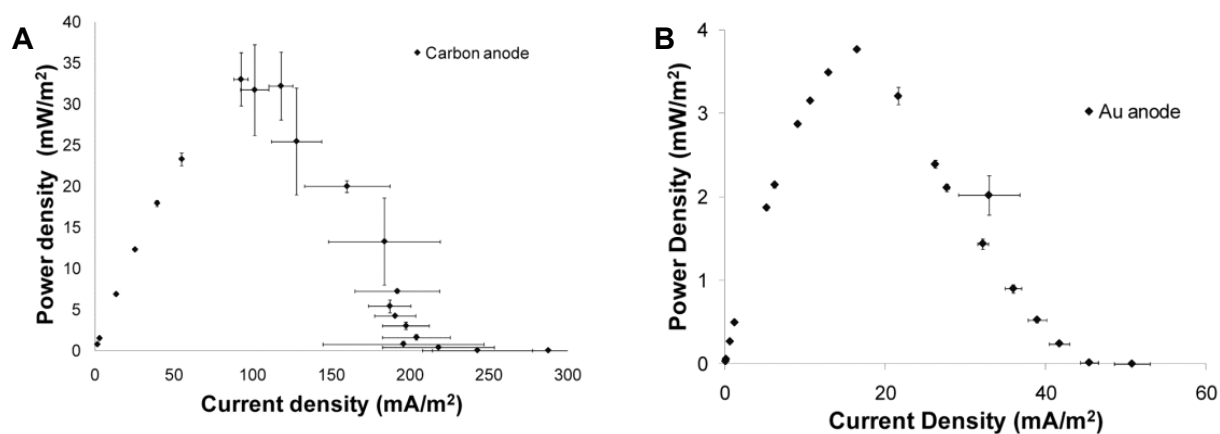
Figure 3.5 Au working as anode of MFC. A: Power density vs. current density from an MFC with carbon cloth anode ($n = 3$). **B:** Power density vs. current density from an MFC with gold anode ($n = 3$).

3.3.2   Biofilm formation on anodes

Biofilms, when established on the anode of MFCs, enhance MFC performance when some microbial systems (including *S. oneidensis* MR-1) are employed. The enhanced performance has been suggested to result from the enhanced ability of biofilms to exploit close physical contacts between microbial membranes and the anode surface for electron transfer [61]. Two types of anode materials, carbon cloth and Au were tested. Carbon cloth is a broadly used anode material in MFC system (section 2.1.4). Biofilm formation on carbon cloth was first examined with ESEM (**Figure 3.6**). Thick biofilm formed on the carbon fibers of the cloth can be clearly seen. To investigate whether biofilms form on the surface of gold electrodes as well, light and fluorescence microscopy images of Au anode were taken 1 hour and 5 hours post-inoculation (PI) (**Figure 3.7**). Within one-hour PI, microbes started attaching to the gold electrode surface (**Figure 3.7A**). Five hours later, an attached *S. oneidensis* biofilm was observed (**Figure 3.7B**). Scanning electron micrographs of the electrode surface confirmed microbial attachment (**Figure 3.7C, D**). These results clearly showed that gold electrode supports *S. oneidensis* biofilm formation.
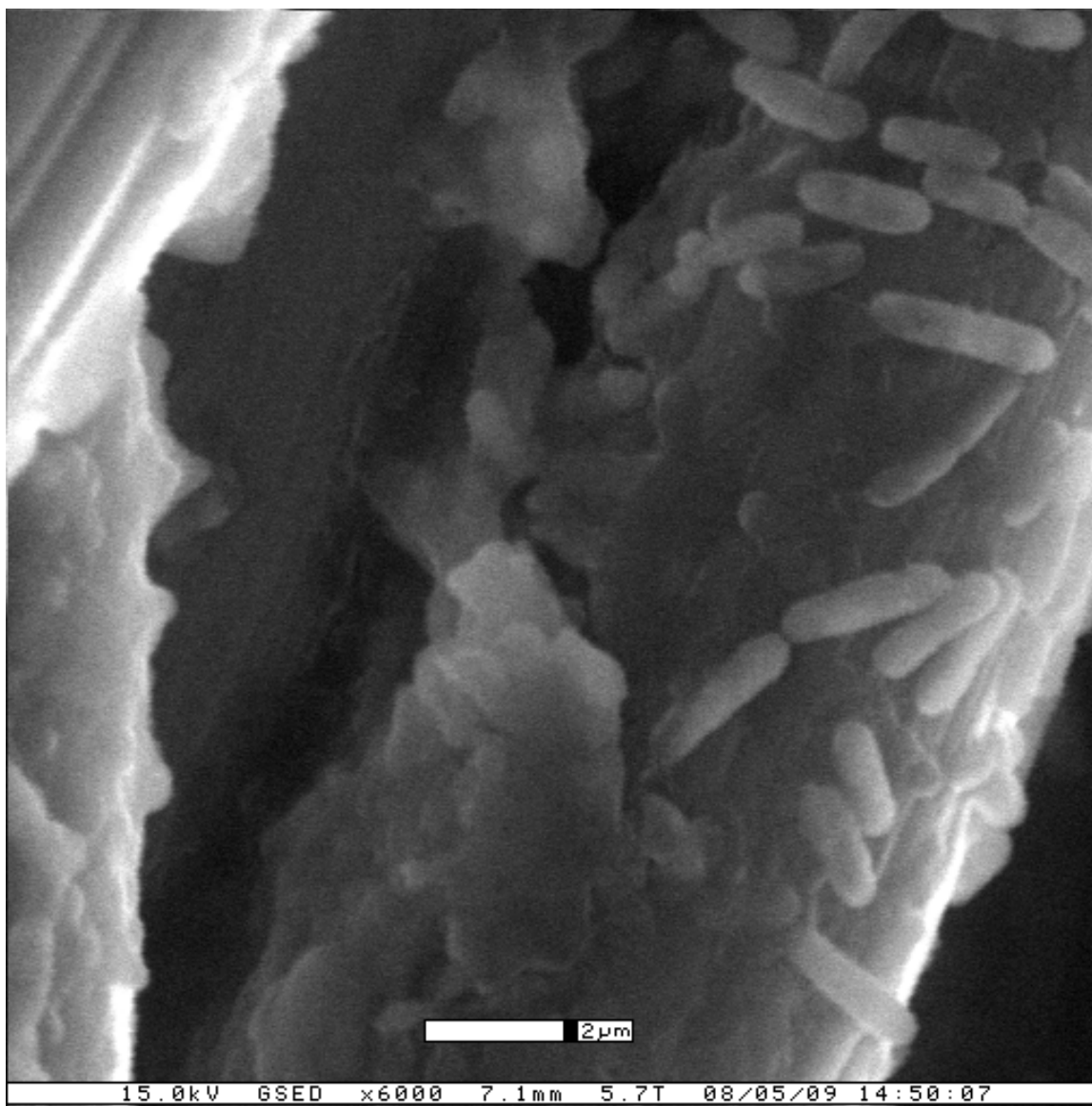
Figure 3.6 ESEM image of biofilm formed by *S. oneidensis* MR-1 on carbon cloth anode after 6 hours in an open circuit configuration (Scale bar: 2 μm).
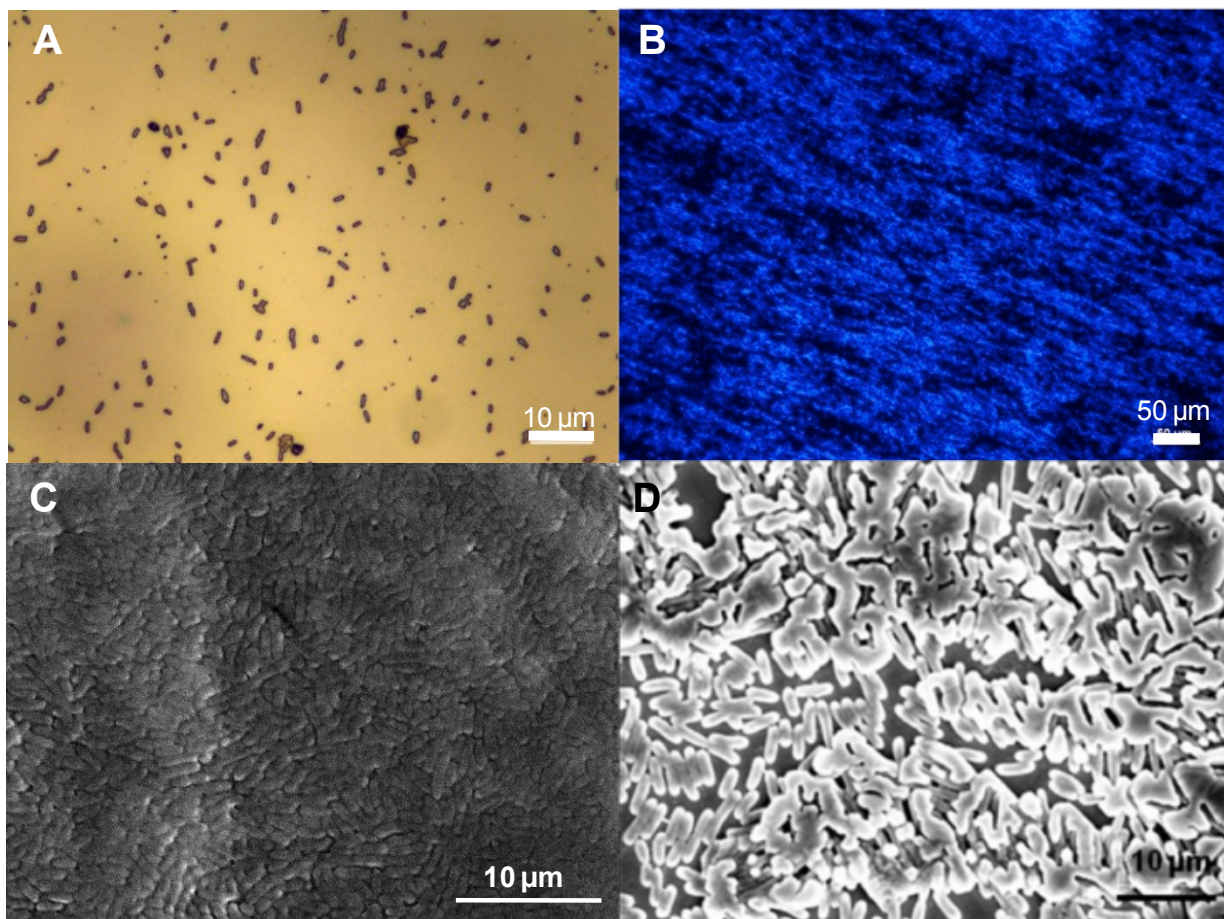
Figure 3.7 Microscopy images of Au electrode: A: After 1 hour of usage (light microscope). **B:** After 5 hours of usage (fluorescent microscopy, DAPI staining). Microbes attached to the gold electrode could be clearly observed. **C & D:** Scanning electron micrographs of microbes attached to the surface of the gold electrode after 5 hours in an MFC.

3.3.3 Repeatability characterization of the MFC array

Due to the good performance of gold as an anode material, it was used as the anode material in the subsequent MFC array development. Performance and reproducibility of the MFC array were initially assessed by loading *S. oneidensis* MR-1 into the device and then measuring the power output. The current densities for negative control (un-inoculated medium) and *S. oneidensis* MR-1 chambers were 0.40 ± 0.01 mA/m^2 (mean $\pm$ SE, $n = 4$) and 1.80 ± 0.24 mA/m^2 (mean $\pm$ SE, $n = 4$), respectively (**Figure 3.8A**). Therefore the MFC array reproducibly measured the electrochemical activities of this microbial system (less than 14% of variance).

To increase the current output of the MFC array, 100 mM ferricyanide was used as the catholyte to provide higher concentration of electron acceptors in the cathode solution. Under this condition, *S. oneidensis* MR-1 produced a current density of 5.54 ± 0.43 mA/m^2 (mean $\pm$ SE, $n = 5$) 100 minutes after loading microbes into the device (**Figure 3.8B**). Over time, the current density gradually dropped, but remained higher than that of the negative control for more than 1000 min. The electricity generation profiles of spatially distinct MFC array wells measured at multiple time points during 15 hours of operation differed by less than 8%, demonstrating that individual wells of the MFC array displayed comparable performance characteristics.

Performances of the same microbial culture were also compared using different batches of MFC arrays. Two arrays with the same configuration were tested with the same microbial culture (OD_{600} = 0.8) and showed current densities of 3.01 ± 0.18 mA/m^2 and 2.86 ± 0.10 mA/m^2 with an average of 2.94 ± 0.16 mA/m^2 (mean ± SE, n = 8) (**Figure 3.8C**). Thus the MFC arrays showed chip-to-chip variances of less than 5.4%. Performances of the same chip with microbial cultures of the same concentration (OD_{600} = 0.8) prepared on different days were also examined (**Figure 3.8D**). The current densities on 2 different days were 3.17 ± 0.20 mA/m^2 and 2.94 ± 0.16 mA/m^2 with an average of 3.05 ± 0.18 mA/m^2 (mean ± SE, n = 16), showing a 5.9% variance. These series of test results showed that the described MFC array demonstrated minimum variations not only among each of the 24 wells, but also from batch to batch, with excellent repeatability.
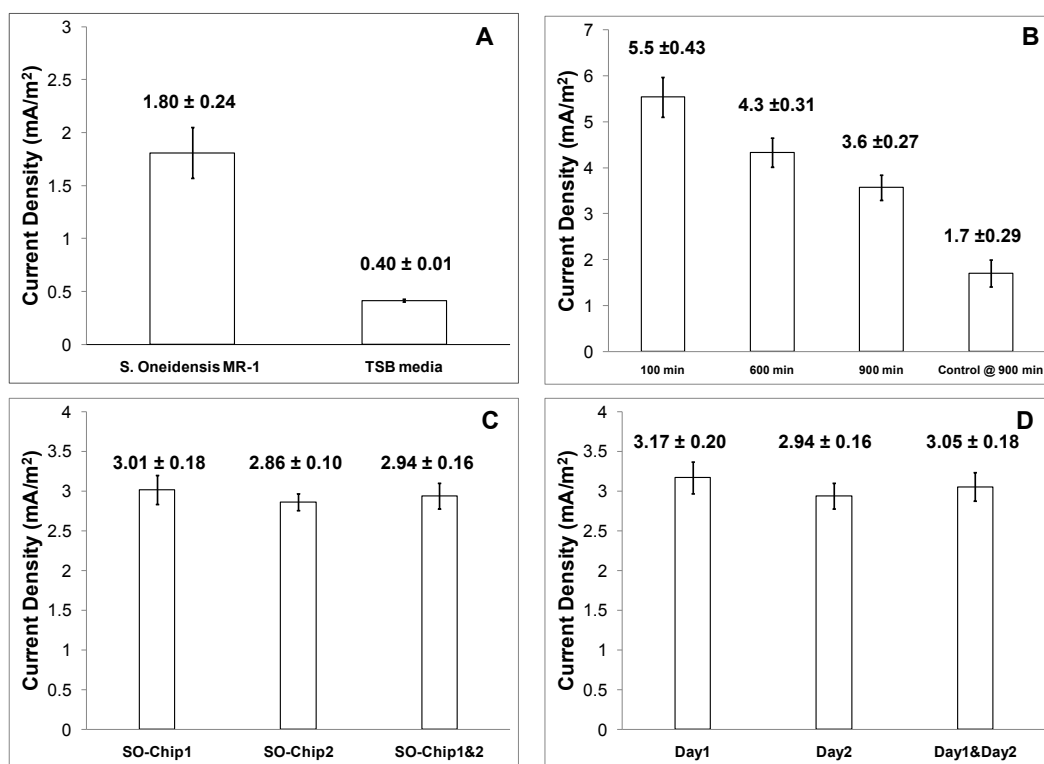
Figure 3.8 Characterization of current generated by _S. oneidensis_ MR-1 in an MFC array. **A:** Current densities generated by _S. oneidensis_ MR-1 with PBS as the cathode solution at 350 min ($n = 4$). TSB medium was used as the negative control ($n = 4$). **B:** Repeatability of current densities generated by _S. oneidensis_ MR-1 with ferricyanide (100 mM) as the cathode solution at different times after loading ($n = 5$). TSB medium was used as the negative control ($n = 5$). **C:** Chip-to-chip repeatability of current densities generated by _S. oneidensis_ MR-1 with ferricyanide (100 mM) as the cathode solution at 1000 min ($n = 4$ for each chip). **D:** Batch-to-batch repeatability of current densities generated by _S. oneidensis_ MR-1 with ferricyanide (100 mM) as the cathode solution at 1000 min ($n = 8$ for each day). Means and standard errors were indicated above the bars (mean ± SE).

3.4 MFC array as a High-throughput screening (HTS) platform for environmental microbe screening

3.4.1 Screening procedure

Encouraged by the performance and reproducibility of the MFC array, whether the device could be employed to quickly screen environmental microbes for individual isolates that display enhanced electrochemical activities was examined. A schematic representation of the overall screening process is illustrated in **Figure 3.9A**. First, environmental bacteria used for screening were isolated from eight different samples (soil and water) obtained from Lake Somerville (N30°30′09″ and E96°64′28″), Brazos River (N30°55′84″ and E96°42′24″; N30°62′64″ and E96°55′13″) and Lake Finheather (N30°64′93″ and E96°37′54″) around College Station, Texas. A prescreening was performed to pick out electrochemically active microbes from the environment samples. After isolate identification using 16S rDNA sequencing, a primary screening with MFC array was performed to select microbes generating highest power. The selected microbes were then loaded again onto the MFC array with more repeats for confirmation. Finally, an H-type MFC was used to validate the findings with the microfabricated MFC array. *S. oneidensis* MR-1 was used as a reference strain through this study.
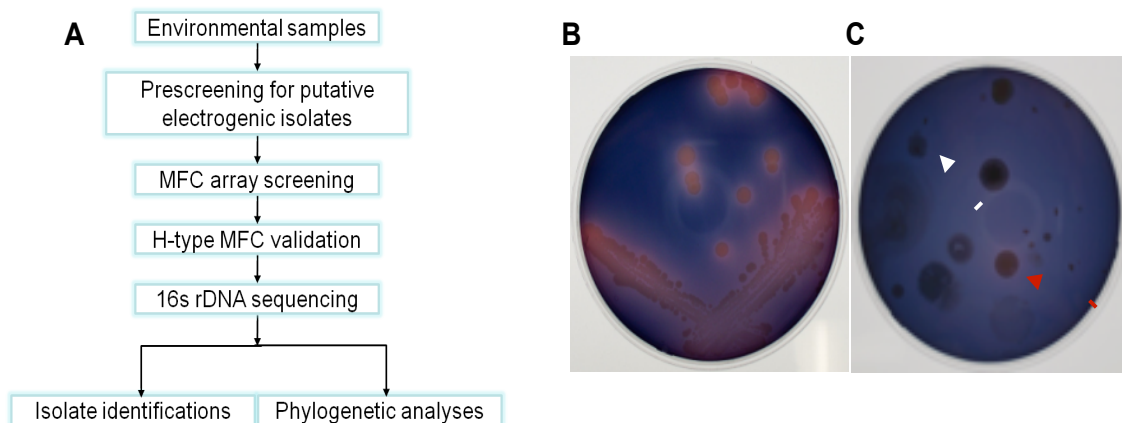
Figure 3.9 Screening procedures and prescreening results of electrochemically active environmental microbes. **A:** A schematic representation of the screening process for the environmental microbes with enhanced electricity generation capacities. B&C Electrochemically active microbes cause discoloration of an azo dye, reactive black 5 in the nutrient agar screening plate; **B:** *S. oneidensis* MR-1 was used as the control; **C:** A representative plate with a putative microbe isolate indicated by the red arrow and a non-putative microbe isolate indicated by the white arrow.

3.4.2 Isolation and pre-screening of environmental microbes

A pre-screening for electrochemically active microbes was performed. Each environmental soil sample was weighted in a 50 mL tube. To make sample suspension, 50 mL of sterile double distilled water were added in each tube and the tube was vortexed for 1 min. Microbial richness in each sample was determined by serial dilutions. Water samples were used for direct dilution. Specifically, 100 μl of each dilution was plated on nutrient agar with 100 μg/mL cycloheximide to eliminate fungal contaminations, and the plates were incubated for 3 days at 30°C under anaerobic conditions. The diluted samples that resulted in 50-100 microbial colonies per plate were then used for plating on nutrient agar containing 100 μM Reaction Black 5 (Sigma-Aldrich, St. Louis, MO), an azo dye that resulted in dark blue color of the media. The discoloration of the dye indicated reduction capability of the microbes. A total of 13 isolates were selected for MFC array screening. After 3 days of incubation, a total of 26 colonies formed discoloration halos out of about 1500 colonies plated for each of the eight environmental samples.

3.4.3 16S rDNA amplification and phylogenetic analyses for environmental isolates

Colony PCRs were performed using different environmental isolates as the templates. To amplify the 16S rDNA, primers 11F (GTTTGATCCTGGCTCAG) and 1492R (TACCTTGTTACGACTT) were used. The PCR thermal cycling program was as following: 94°C for 5 min, 35 cycles of 1 min at 94°C, 45 sec at 48°C and 2 min at

72°C, followed by a final extension for 10 min at 72°C. The PCR products were then purified with the QIAquick PCR Purification Kit (Qiagen, Valencia, CA) and sequenced with primers 11F and 1492R.

The16S rDNA sequences amplified from the environment isolates was BLAST searched against the GenBank database. The 16S rDNA sequences of the top hit for each isolate were then used for alignment and phylogenetic tree generation for all the environmental isolates. A matrix of pairwise genetic distances by the maximum-parsimony algorithm and the neighbor-joining method was used to generate phylogenetic trees using the ClustalX software (version 2.0).

3.4.4   MFC screening result

Up to 12,000 microbes derived from environmental (water and soil) samples were pre-screened on solid medium containing Reaction Black 5 (**Figure 3.9B,C**)[115]. 16S rDNA sequencing analysis of 26 hits obtained from the pre-screening plates revealed that the majority of the isolates ($n = 10$) were members of the *Bacilli* and γ-proteobacteria classes (**Table 3.1** and **Figure 3.10**). The MFC array was then exploited to characterize the electrochemical activities of 13 isolates. One isolate, 7Ca, reproducibly showed 266% higher power output than the *S. oneidensis* MR-1 reference strain in both the primary screening (**Figure 3.11A,** $n = 2$) as well as in the secondary confirmation test that had more replicates in the MFC arrays (**Figure 3.11B,** $n = 8$) (Polarization curve is shown in **Figure 3.14**). Phylogenetic analysis demonstrated that 7Ca was most closely related to *Shewanella putrefaciens* IR-1 (98% sequence similarity) and *Shewanella* sp. MR-7 (98%

Table 3.1 Identities of environmental isolates obtained from pre-screening.

Isolate	Top Hit (Genbank Number)	Identity %
1B	*Bacillus* sp. RC33 (FJ263036.1)	100
1C	*Bacillus* sp. W1-17 (FJ560473.1)	100
1D	*Bacillus niacini* strain YM1C7 (EU221338.1)	97.93
2A[#]	*Enterobacter* sp. CTSP29 (EU855207.1)	99
2B	*Bacillus* sp. SX51 (DQ227355.1)	
2C, 3B, 4A, 5A, 5B	*Bacillus thuringiensis* serovar tenebrionis (EU429671.1)	100
3A	Bacterium 3A13 (DQ298760.1)	99
3C	*Arthrobacter* sp. FB24 (EU147009.1)	100
3E, 3F	*Bacillus* sp. A1 (2008) (FJ535468.1)	100
5C	*Bacillus* sp. BM1-4 (FJ528077.1)	100
6A, 6C*	*Pseudomonas putida* strain J312 (EF203210.1)	98.50
6B*, #	*Stenotrophomonas maltophilia* strain CMG3098 (EU048328.1)	98.99
6E*	*Pseudomonas plecoglossicida* strain S19 (DQ095907.1)	98.52
6F*	*Pseudomonas* sp. lm10 (EU240462.1)	98.72
6G*	*Pseudomonas* sp. GNE25 (AM397659.1)	95
7A*, #	*Aeromonas* sp. LD151 (AM913921.1)	97.34
7Ca*	*Shewanella* sp. Hac353 (DQ307734.1)	99
7Cb	*Bacillus pumilus* strain TPR18 (EU373436.1)	99
8A*, #	*Paenibacillus* sp. oral clone CA007 (AF385540.1)	92
8B*,#	*Aeromonas hydrophila* strain IB343 (EU770277.1)	99
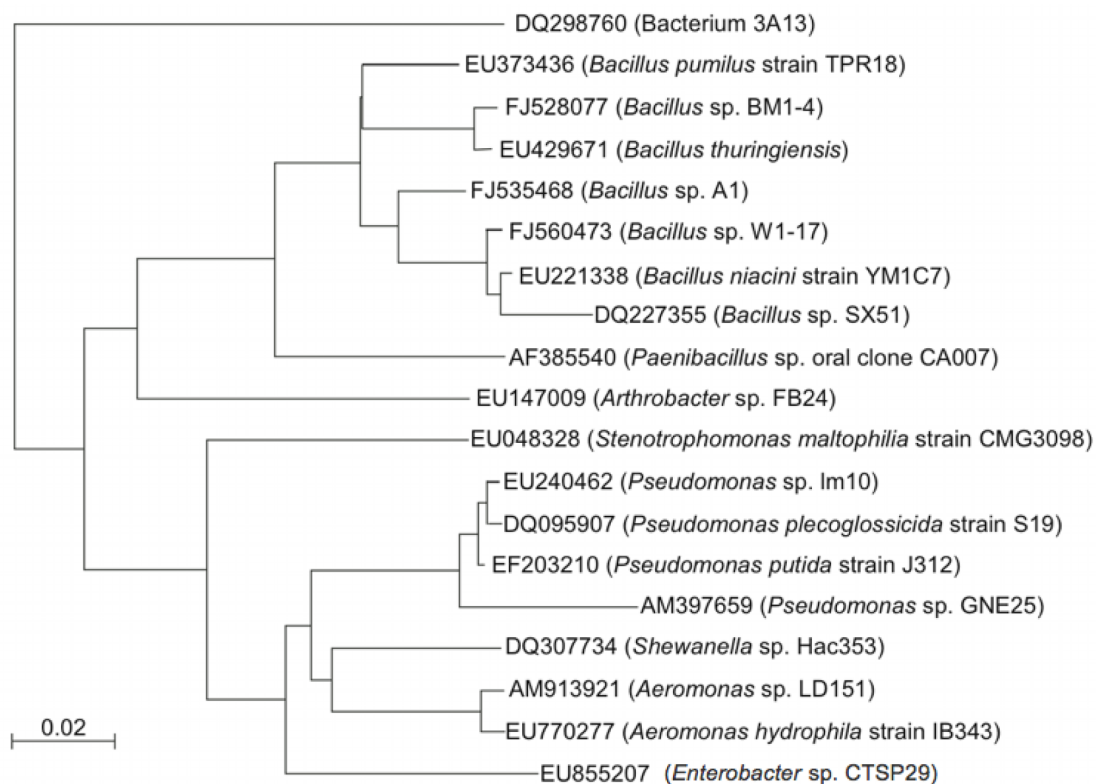
Figure 3.10 Phylogenetic tree based on 16S rDNA sequences showing relationship within of the environmental isolates obtained in the pre-screening. Most environmental isolates were members of classes *Bacilli* or γ-proteobacteria.
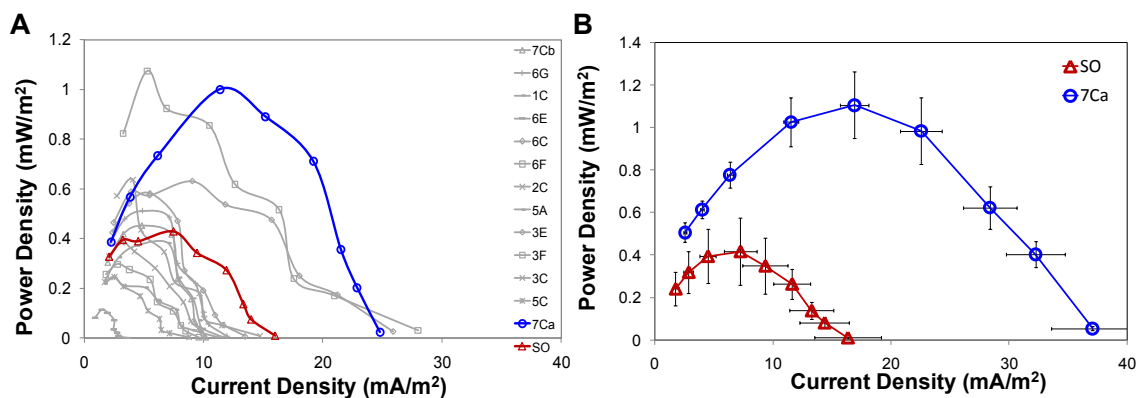
Figure 3.11 Screening results of electrochemically environmental microbes with the 24-well MFC array. A: Screening of 13 environmental isolates with *S. oneidensis* MR-1 as the positive control (SO, red) using two 24-well MFC arrays in parallel. The average power density of two replicates was shown for each isolate. **B:** The power density of 7Ca compared to the *S. oneidensis* MR-1 reference strain ($n = 8$).

sequence similarity) (**Figure 3.12**). The high power generation capability of 7Ca was

further validated in 24-hour trials in a conventional H-type MFC system (**Figure 3.13,**

Figure 3.14)[116]. In the specific conventional MFC configuration, the maximum current

density of 7Ca was 169.00 ± 10.60 mA/m^2, which was 217% higher than the current

density (78.00 ± 7.30 mA/m^2) generated by the *S. oneidensis* MR-1 control. The

maximum power density of 7Ca was also 233% higher than this reference strain.

Although gold was used as the anode material in the MFC array and carbon cloth as the

anode material in the H-type MFC system, the power density increases of 266% in the

MFC array and 233% increase in the H-type MFC system showed that findings in the

MFC array system can be translated to larger scale conventional systems. Thus, insights

garnered using gold anodes in miniaturized MFCs can be transferred to conventional

MFC formats using carbon anodes.

It is intriguing to speculate on the molecular mechanisms that contribute to the

enhanced electrochemical activity of 7Ca. For example, the presence of gain of function

mutations affecting biofilm formation, nanowire formation, cell membrane electron

transfer, metabolic and respiration capacities, regulatory components for these functions,

and/or combinations of all the above, could contribute to the observed power output. In

this regard, it is notable that previous genetic studies in *S. oneidensis* MR-1 revealed

several genes that are directly involved in electricity generation, including *mtrA, mtrB,*

omcA/mtrC, cymA, fur, and *crp*. Deletion of these genes caused severe reductions in

current production[117]. Gain of function mutations at these candidate loci may therefore

confer enhanced MFC power generating properties. Similarly, an engineered strain of

Geobacter sulfurreducens generated by Izallalen et al. displayed enhanced electrochemical activity due to increased respiration rates[104]. Despite these molecular insights, there has been a paucity of functional studies that directly measure the electrochemical activities of environmental microbes. In fact, the electrochemical activities of only a handful of microbial species have been characterized in MFC systems[16]. Although MFCs using wastewater treatment and sediment nutrient sources have defined electrochemically active microbial consortia [118], the electrochemical activities of individual species within these consortia remain largely unexplored. It is likely that the MFC array system reported here will facilitate and accelerate these kinds of studies.

3.5 Conclusions

A microfabricated MFC array system was developed and its capability to rapidly screen and characterize microbial electrochemical activity was demonstrated. The design of the system has several attractive features. First, the microbe culture chamber was easy to assemble and reusable. The PDMS and electrode could be used at least 10 times without degradation and the acryl anode chamber could be used more than 10 times with proper cleaning. Therefore, the device has the potential for widespread adoption. Second,
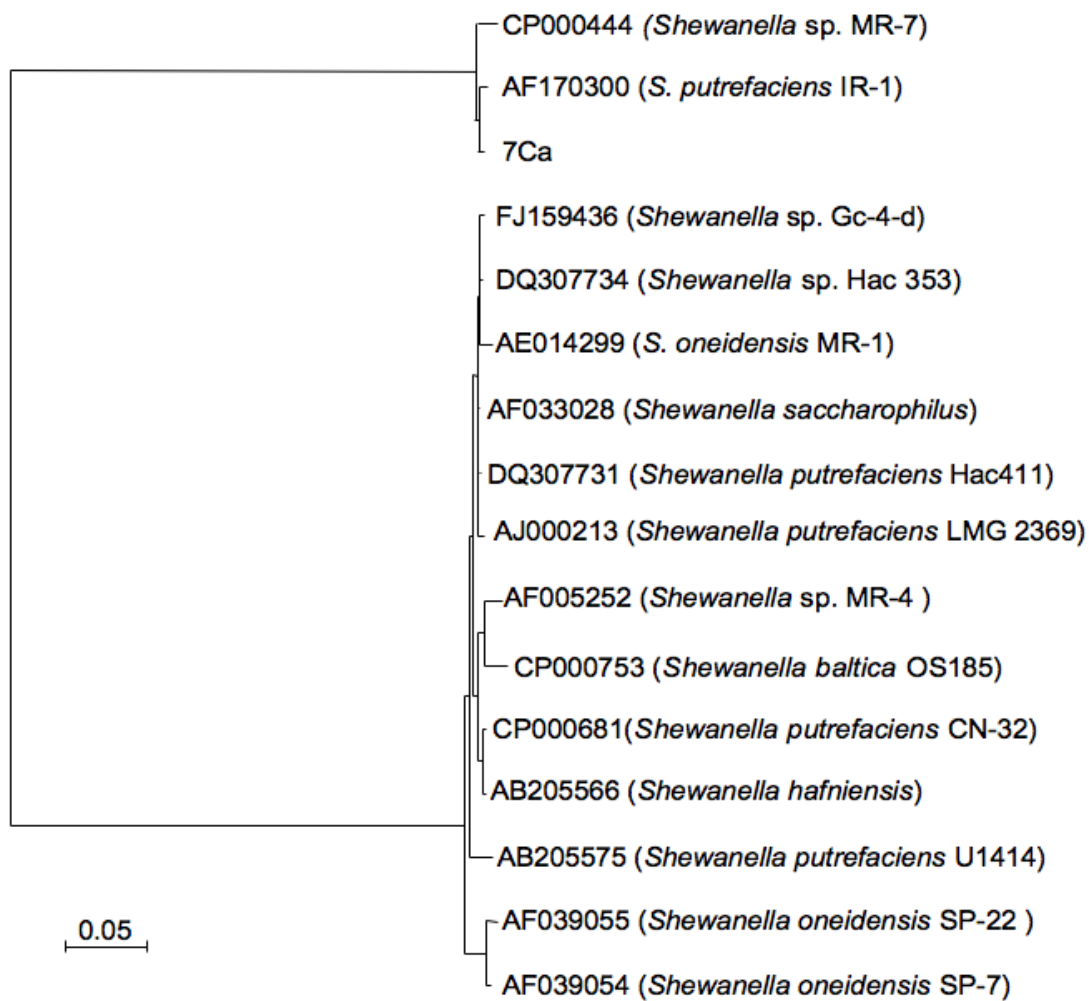
Figure 3.12 Phylogenetic tree based on 16S rDNA sequences indicating the relationship of various *Shewanella* species.
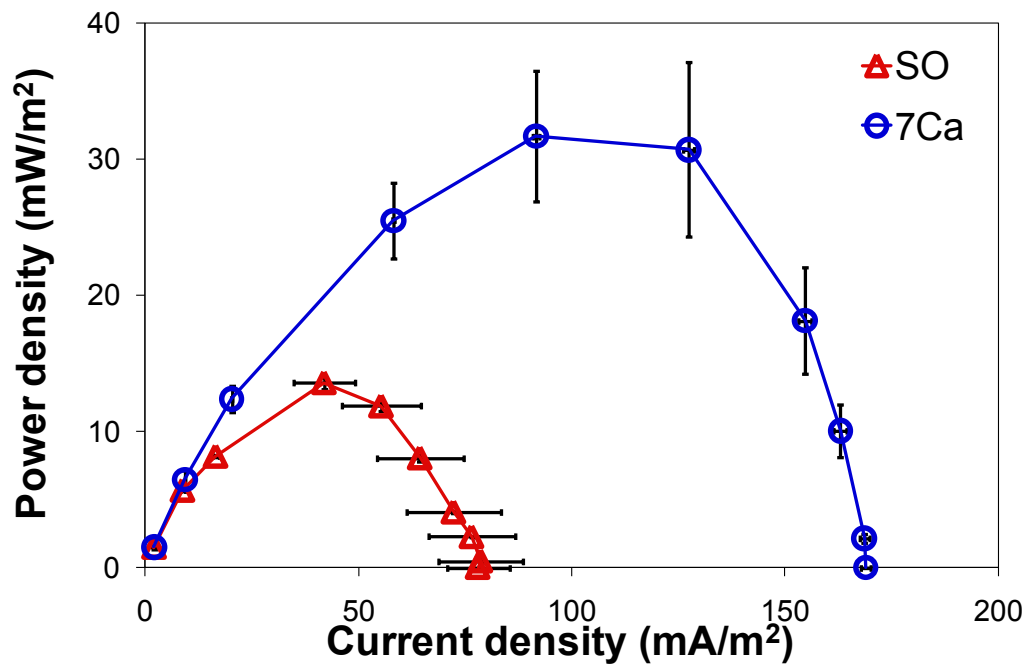
Figure 3.13 Validation of current generation by 7Ca and *S. oneidensis* MR-1 in conventional MFCs (*n* = 4).
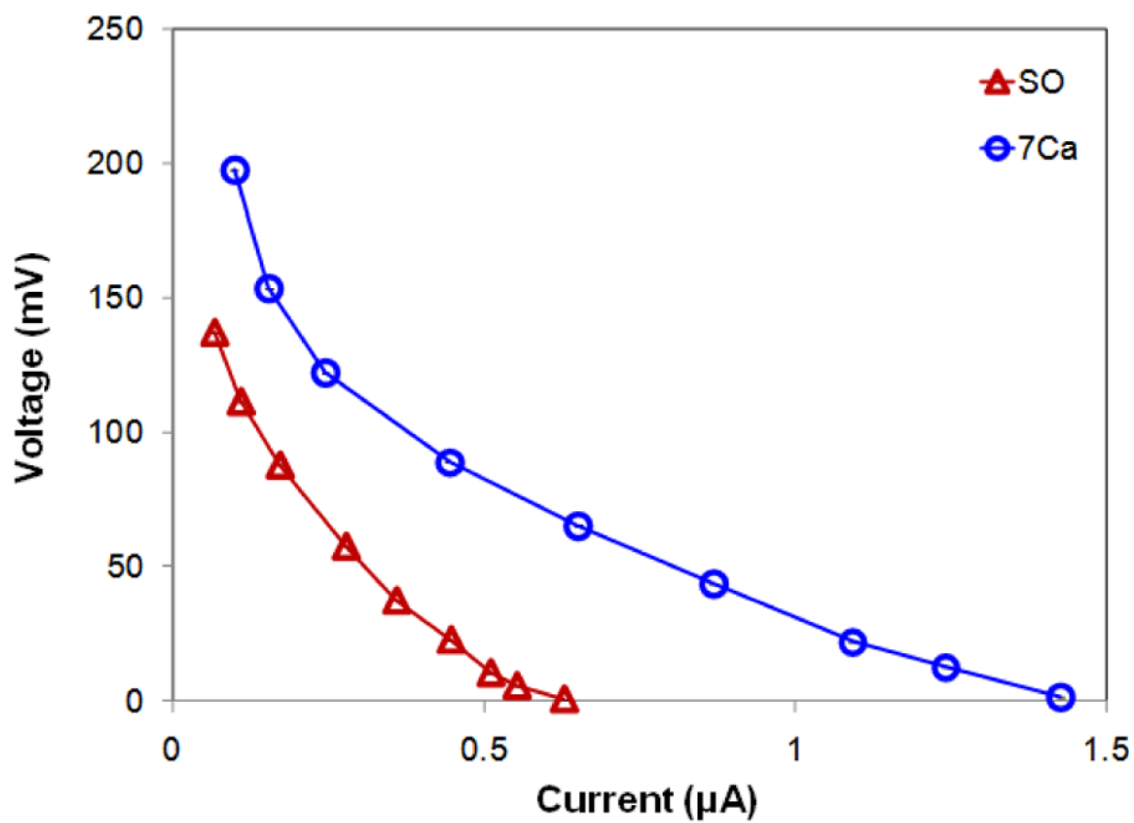
Figure 3.14 Polarization curves of 7Ca (blue) and *S. oneidensis* MR-1 (SO, red) in the MFC array.

because the individual MFC chambers in the array hold a small volume, 380-fold fewer

reagents are required than conventional MFC devices. Third, the universal design of the

array makes it possible to easily change the anode and cathode for quickly exploring

new electrode materials to further optimize the MFC architecture. Fourth, the device can

support factorial experiments in which several variables are tested and compared

simultaneously. This feature will dramatically accelerate the pace of electricigen

research. Fifth, the highly scalable approaches used to microfabricate the array set the

stage for the development of next-generation parallel devices with more than 1,000

wells. Finally, the array provides a platform for MFC performance to be assessed in

parallel (increasing MFC experimental throughput by 24-fold). This feature was

exploited to identify and characterize electricigens with high electrochemical activities.

In this regard, the fact that several microbes with enhanced electrochemical activity were

rapidly uncovered in the screen indicates that the natural environment constitutes a

plentiful reservoir for mining electricigens. For example, the screen uncovered four

Pseudomonas sp. that produce phenazine-based metabolites that can serve as electron

shuttles[119, 120]. Moreover, the screen resolved *Bacillus* sp. and *Aeromonas hydrophila*

that have been reported to be present in microbial consortia of MFCs[108]. A *Shewanella*

isolate 7Ca, which generated power density that was 2.3-fold above the reference strain,

was also uncovered.

4. AIR-CATHODE MFC ARRAY

4.1 Motivation

The MFC array system developed and demonstrated in Section 3 supported parallel, low cost, and reproducible analysis of microbial electrochemical activities[67]. Ferricyanide was used as an electron acceptor in this MFC array system. Although this system holds the advantage of low overpotential, which results in high power output, the system was not suitable for long-term continuous operation because of the depletion of ferricyanide as catholyte in the confined cathode chambers. Other than ferricyanide, oxygen dissolved in water[32] or in ambient air[31, 88, 121] is the most commonly used electron acceptor due to its low cost, sustainability, and lack of a waste product. Such devices hold the potential for practical and long-term operation. These facts led us to investigate the feasibility of developing an air-cathode based MFC array system, which holds advantages consistent with what has been observed in conventional air-cathode MFC systems[74].

Here we describe the development of an air-cathode MFC array that supports the parallel examination and direct comparison of the electrochemical activities of environmental microbes. The air-cathode MFC array is a microfabricated miniaturized MFC system comprising of 24 single-chamber air cathode MFCs with equivalent test environments. The MFC array does not need aeration of the media, instead it uses oxygen in ambient air as the electron acceptor. The air-cathode MFC array holds the advantages of air-cathode MFCs compared to ferricyanide MFCs, at the same time,

holds the ability of conducting high throughput MFC parallel studies same as the ferricyanide cathode MFC array.

4.2   Air-cathode MFC array development

4.2.1   Air-cathode MFC array design

Figure 4.1A shows the schematic illustration of the 24-well air-cathode MFC array. The system is composed of an anode layer, an anode chamber layer, an air-cathode layer, and an air-cathode interface layer. The air-cathode layer is an assembly of PEM and Pt-loaded carbon cloth heat-stacked together. The cathode interface layer has arrays of electrode pads with through-holes in the center to facilitate oxygen transport while making electrical contacts between the cathode assembly and the external load resistors. Microbes to be screened or characterized are loaded in each of the anode well chambers and then the power output from individual wells is continuously monitored.

4.2.2   Twenty-four well air-cathode MFC array microfabrication

Fabrication of the air-cathode MFC array was performed through conventional photolithography and soft lithography techniques. The anode layer with 24 addressable electrodes (electrode diameter: 8 mm) was fabricated with Ti/Au deposited on a glass substrate using as described previously [67]. The cathode interface layer fabrication is shown in **Figure 4.1B**. First, Ti (200 Å, 3 Å/sec) and Au (2000 Å, 3 Å/sec) were deposited on a solvent-cleaned PMMA substrate using E-beam evaporation. Photoresist
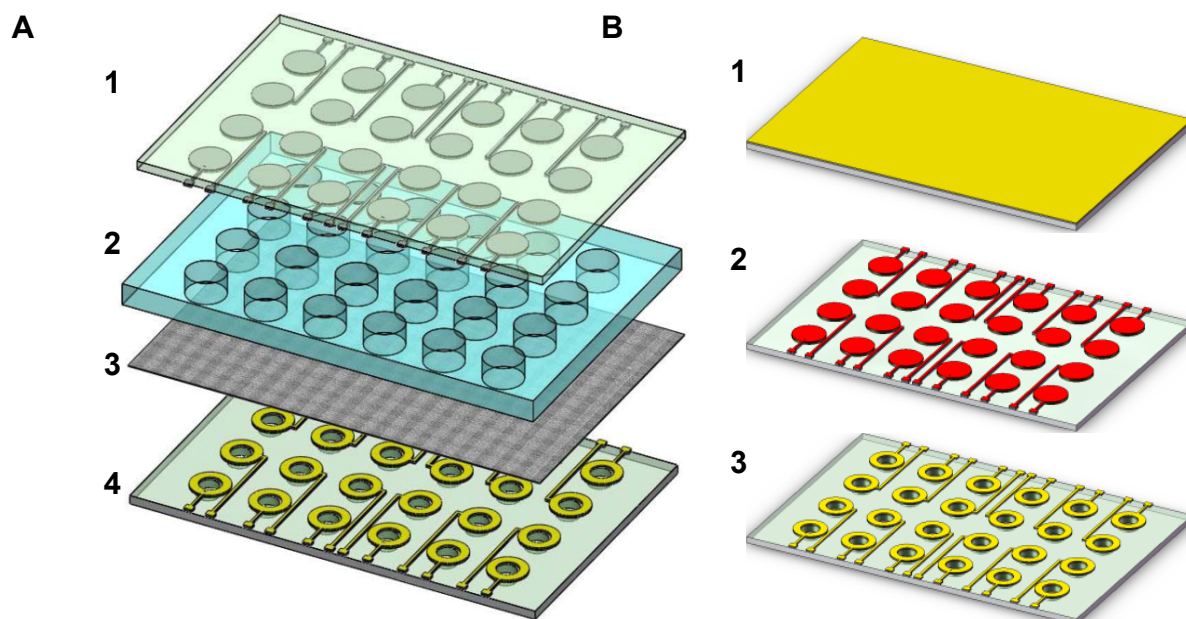
Figure 4.1 Schematic illustration of the 24-well air-cathode MFC array system and its microfabrication procedures. A: Illustration of the 24-well air-cathode MFC array. (1) Anode layer, (2) anode chamber layer, (3) air-cathode layer (PEM/carbon cloth assembly), (4) air-cathode interface. **B:** Air-cathode interface microfabrication steps. (1) Au/Ti deposited PMMA substrate, (2) photoresist patterning followed by Au/Ti etching, (3) photoresist removal followed by drilling hole in the center of the electrode pads.

(Shipley S-1818, Rohm and Haas, Inc., Philadelphia, PA) was spin-coated on the metal coated PMMA substrate at 4000 rpm, baked inside a 80°C oven for 10 min, and exposed to UV light through a photolithography mask for 18 sec using a mask aligner (MA6, SUSS Microtech, Germany) at an intensity of 8.5 mW/cm^2 (wavelength = 320 nm). The substrate was then developed in a photoresist developer (MF^{TM} 319, Rohm and Haas, Inc., Philadelphia, PA) for 20 sec. The exposed part of the Au and Ti layers were removed in Au etchant (Type TFA, Transene Company Inc., Danvers, MA) and Ti etchant (HF : H_2O = 1 : 300 v/v), and the photoresist was finally removed with acetone and cleaned with isopropanol and DI water. Finally, through-holes with 4 mm diameters were drilled in the center of the electrode pads with a laser machine (Professional series, Universal Laser Systems Inc.; Power: 100%, Speed: 5.5%, PPI: 1000). The anode chamber layer was composed of an acryl block layer sandwiched by two PDMS layers (Sylgard 184, Dow Corning, Auburn, MI) [67], and had 24 wells that were 7 mm in diameter and 16 mm in depth. The PEM/carbon cloth assembly was fabricated by placing PEM (Nafion 117^{TM}, Ion-Power, Inc., New Castle, DE) and carbon cloth (10% Pt, A1STD ECC, BASF Fuel Cell, Inc., Somerset, NJ) together and applying 600 kPa of pressure for 5 min at 150ºC. This allowed handling of the PEM/carbon cloth assembly as a single piece for easy assembly with the other layers. The assembly was stored in DI water till use.

The fabricated functional layers were then sandwiched between two acryl blocks with screws as shown in **Figure 4.2**. The acryl block directly contacting the air-cathode interface had through-holes to facilitate oxygen transportation (**Figure 4.2** inset showing the device from backside), while maintaining a tight seal between the multiple functional layers.

4.2.3 MFC array characterization, data acquisition, and preparation of environmental microbes

Environmental bacteria used for screening were isolated and prescreened as described previously , automatic data acquisition was also described similarly (section 3.2.6, 3.2.4, 3.4.2)[67].

4.2.4 Conventional air-cathode MFC setup and characterization

The conventional air-cathode MFC setup is comprised of a sterile glass container (250 ml) with a glass bridge. The PEM/carbon cloth assembly was clamped onto the end of the glass bridge and the exposed area was 0.8 cm^2. The anode chamber was sealed to keep the culture condition anaerobic. Carbon cloth (B1A, BASF Fuel Cell, Inc., NJ) was used as the anode (surface area: 7.5 cm^2). The anode and cathode were connected to a variable load resistor (Ohm-Ranger, Ohmite Mfg. Co., IL) for current-power curve characterization. A digital multimeter (34410A, Agilent Technologies, Inc., CA and 8840A, Fluke, WA) connected to a computer was used to measure current through the load resistor. Current was recorded for 1000 min for stabilized reading, and then
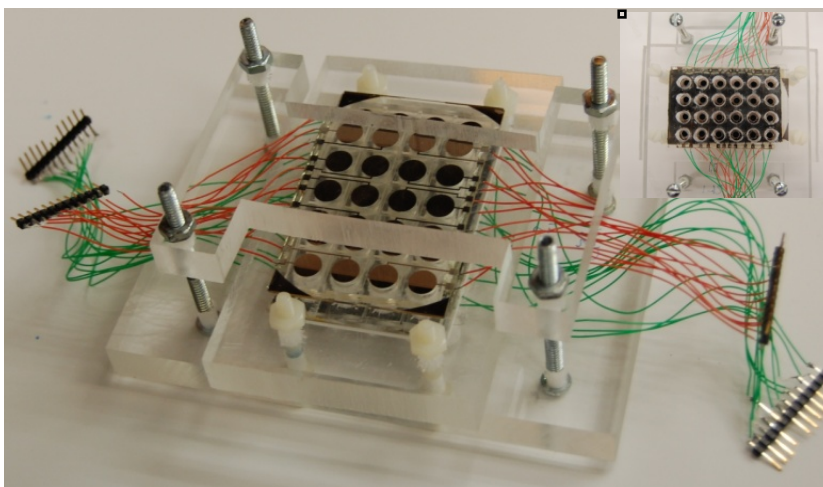
Figure 4.2 Image of a fully assembled 24-well air-cathode MFC array. (Inset: backside of the 24-well air-cathode MFC system showing open holes for oxygen transport to the air cathodes.)

recorded 20 min with each load resistor. Power was calculated using Ohm's Law (P =

I^2R).

4.3   Environmental microbe screening using the air-cathode MFC array

The performance of the 24-well air-cathode MFC array was first tested by loading

Shewanella oneidensis MR-1 (SO) (OD_{600} = 1.7) into the anode chambers and

comparing the current densities generated from each well. When 200 kΩ load resistors

were connected, SO showed a current density of 4.63 ± 1.01 mA/m^2 (ave. ± std.) (*n =12*)

compared to the negative control (TSB media) of 0.14 ± 0.11 mA/m^2 (*n =3*) 1000 min

after loading microbes into the MFC array (**Figure 4.3A**).   This current density is

equivalent or slightly higher than the density previously reported in an MFC array using

ferricyanide in the cathode well[67]. The standard deviation of 22% in the air cathode

array, however, is higher than the standard deviation of 6 - 14% in the ferricyanide

system[67], but still within an acceptable range for screening applications.

The screening functionality of the air-cathode MFC array was tested by

screening a previously characterized test set of environmental microbes with the aim of

identifying microbes that display the highest electrochemical activity in MFC systems.

The 13 isolates used in these studies were previously selected from a collection of

~12,000 microbes that were collected from the environment and pre-screened for

electrochemical activity using Reactive Black 5[67] . An analysis of current densities after

1000 min of operation in a 24-well air-cathode MFC array showed that 7Ca and 3C were

able to generate higher power than other environmental isolates (**Figure 4.3B**).   A

previous analysis of 16S rRNA sequences from these microbes indicated that they are closely related to *Shewanella putrefaciens* and *Arthrobacter sp.*[67].

To confirm this finding, these two species (7Ca and 3C) were then further characterized in a secondary screen using the air-cathode MFC array. These confirmatory experiments showed maximum power densities of 1.86 ± 0.16 mA/m^2 and 2.69 ± 0.42 mA/m^2 for 3C and 7Ca, respectively (**Figure 4.3C**), with 7Ca showing 145% higher power than 3C. Standard deviations were in the range of 8 - 16% with 5 replicates. This result was validated in experiments using a conventional air-cathode MFC ($OD_{600} = 1.7$) in which a full range I-P curve was generated. The maximum power densities of 3C and 7Ca in this conventional system were 8.11 mA/m^2 and 13.93 mA/m^2 respectively, showing that the power density of 7Ca was 171% higher than 3C. This result showed that results obtained using the 24-well air-cathode MFC array were scalable to conventional milliliter-scale systems.
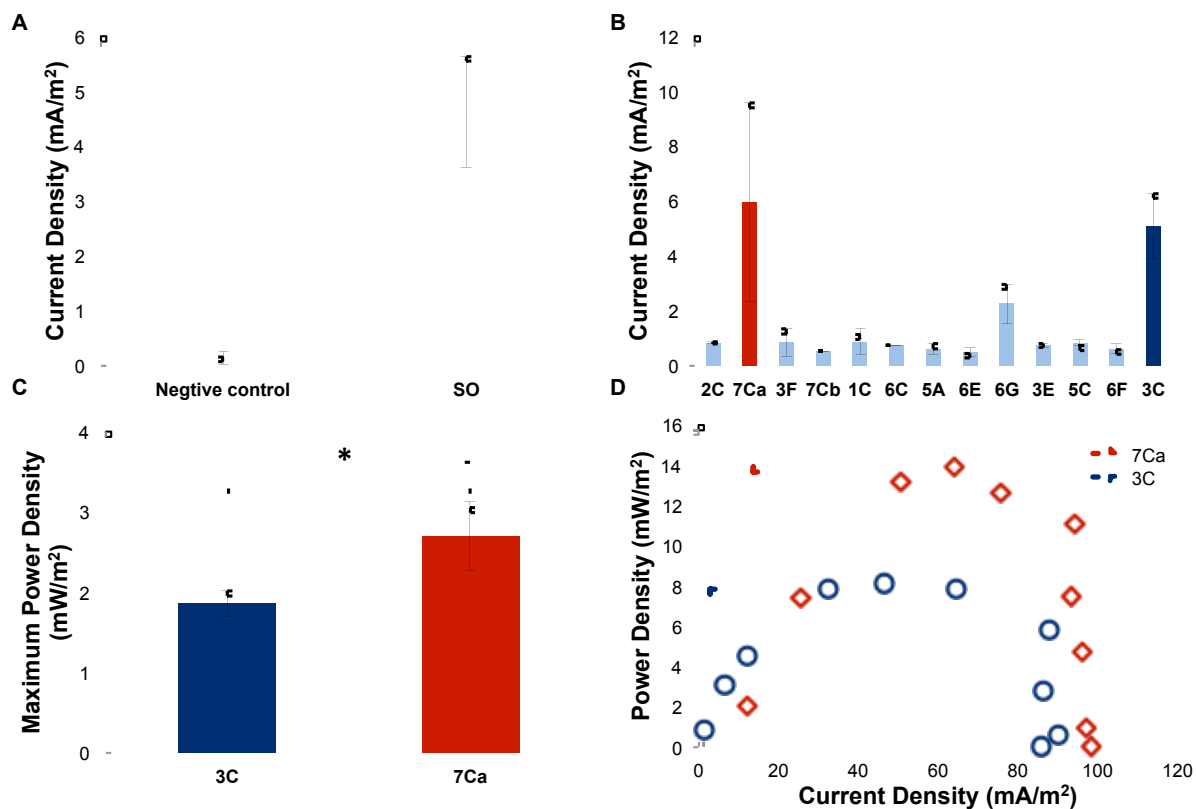
Figure 4.3 Screening of environmental microbes with the 24-well air-cathode MFC array. A: Electricity generation with *S. oneidensis* MR-1 ($n = 12$). TSB media was used as the negative control ($n = 3$). Load resistors (200 kΩ) were connected and voltages were measured 1000 min after loading microbes into the air-cathode MFC array. **B:** Primary screening with an air-cathode MFC array showing 7Ca and 3C generating higher power densities than other environmental species ($n = 1$-3). **C:** Secondary confirmation screening of 7Ca and 3C with more repeats ($n = 5$) using the air-cathode MFC array. (Two-sample t-Test: $p < 0.01$). **D:** Conventional H-type MFC validation of the two selected environmental microbes 7Ca and 3C.

7Ca gave a higher power density (2.4 times) in the air cathode array than in the ferricyanide-based system. However, standard deviations were typically higher when using the air-cathode MFC array system (22% vs. 14%). An interesting finding is that 3C (*Arthrobacter sp.*), which showed the second highest power generation capability when using the air-cathode MFC array, did not perform similarly in the ferricyanide based MFC array. This difference in performance could reflect differences in the oxygen availability at the anode surface of each system, and the concomitant ability of each isolate to maintain electrochemical activity in the presence of oxygen. In the air-cathode system, the barriers to oxygen diffusion into the anode well through the PEM are less than in the ferricyanide system. Thus, microbes that can maintain electrochemical activity in the presence of oxygen will perform better in the air cathode system. Further investigation will be required to determine if isolate 3C possesses such properties. In addition, electron transfer mechanisms such as biofilm formation, nanowire conduction, cell membrane direct electron transfer, or their combined effects need to be further investigated. Identifying and characterizing genes that contribute to the higher power generating abilities of 7Ca and 3C will open possibilities for exploiting genetic engineering approaches to generating microbes with enhanced electrochemical activity that may accelerate MFC commercialization.

The 24-well air-cathode MFC array is reusable, easy to assemble, and utilizes 400 times less reagent compared with conventional MFCs. These features will greatly reduce the cost of MFC research. The air-cathode MFC array can have several microbes or factorial parameters tested in parallel while leaving other experimental conditions

(temperature, light, humidity, etc.) undisturbed. The exacting specifications that can be achieved through the use of microfabrication techniques also helps ensure the repeatability of the results obtained using these systems. Compared with our previously developed MFC array with ferricyanide as catholyte [67], the screening results of both systems uncovered 7Ca as the species that generates the highest power among the 13 environmental microbes included in the test set, and screening results from both MFC array systems were validated by corresponding conventional bottled MFC systems. This shows that the results from both screening systems are consistent despite of the absolute power differences.

4.4   Conclusions

A 24-well air-cathode MFC array, a compact and user-friendly platform for identification and characterization of electrochemically active microbes was developed and demonstrated through environmental microbe screening. Compared with the first MFC array developed (Section 2), this air-cathode MFC array uses ambient air as the electron acceptor, which is low cost and most suitable for studies that require long-term continuous MFC operation. Environmental samples were used to validate the utility of the air cathode MFC array. Two previously identified isolates, 7Ca and 3C, were shown to display enhanced electrochemical activities, where 7Ca demonstrated 1.45 fold higher power than 3C in the air-cathode MFC array. This result was validated with a conventional air-cathode MFC, in which 7Ca showed 1.71 fold higher power than 3C. It is expected that this 24-well air-cathode can be scaled-up and become a powerful high-

throughput screening tool for environmental and genetically modified microbes with enhanced electrochemical activities.

5. MICROFLUIDIC-CATHODE MFC ARRAY

5.1 Motivation

The two MFC array prototypes in Section 3 and Section 4 were successfully demonstrated as high-throughput screening and parallel study tools, and were used to identify electricigens with enhanced power generation abilities from the environment[67, 122]. Several electricigens showing higher electricity generation capabilities (up to 270%) compared to the reference strain *Shewanella oneidensis* MR-1 were successfully uncovered. However, these MFC arrays are not suitable for long-term parallel studies. The air-cathode MFC array, although designed for long-term operation, showed larger device-to-device and unit-to-unit variation compared to ferricyanide based MFC array, making it less attractive for parallel comparison studies. The batch-mode MFC array, on the other side, demonstrated good device-to-device and unit-to-unit repeatability, however, did not support studies beyond a few days of operation due to the depletion of electron acceptors in the limited volume (less than 1 ml) cathode chambers. Electricity production in MFCs changes over time, hence long-term characterization over periods of weeks is critically needed to gain a better understanding of the dynamics of MFC performance. In addition, even though all cathode chambers are initially filled with the same concentration of ferricyanide, the amount of electron acceptors will vary among different chambers during operation because of the differences in electrochemical reaction speeds in each of the miniature MFC units which possess distinct anodic parameters (e.g. different microbial species and substrate types). Therefore, providing

sufficient amount of electron acceptors to all cathode chambers becomes essential for parallel comparisons of anodic parameters of interest.

Recently, few reports start to emerge on flow-through type miniature MFCs [80, 99, 123-125]. Both anolyte and catholyte replenishment have been reported with such systems. Power densities from these miniature MFCs (µl scale) were comparatively low to those from larger volume MFCs (ml scale) due to higher internal resistance as well as evaporation issues related with such a small volume to name a few. However, they provide potentials for rapid studies on electrode materials, microbial metabolisms, and as on-chip power sources. So far, all published works were single unit based MFCs and no microfluidic flow-through type MFC array has been reported, thus were not suitable for long-term high throughput parallel studies.

To address the long-term operability challenge while still providing high-throughput parallel screening capability, a catholyte flow-controllable (continuous or periodic) microfluidic-cathode MFC array that supports long-term multiplexed studies is proposed. The 24-array microfluidic MFC system utilizes integrated microfluidic channels and a microvalve array to periodically or continuously replenish catholytes from all 24 cathode chambers, while maintaining individual unit to unit isolation during operation and power output characterization. Hence, the system functions as 24 independent miniature flow-through MFCs on a single chip.

5.2 Design, fabrication, and characterization methods of the 24-well microfluidic-cathode MFC array

5.2.1 24-well microfluidic-cathode MFC array design and fabrication

Schematic illustration of the 24-well microfluidic-cathode MFC array is shown in **Figure 5.1A**. The device consists of 5 functional layers: an anode electrode layer, an anode chamber layer, a PEM layer, a microfluidic-controlled cathode chamber layer, and a cathode electrode layer. The anode electrode layer consists of 24 addressable electrode pads, each corresponding to one of the 24 anode chambers (diameter: 7 mm) on the anode chamber layer. The cathode chamber layer consists of three functional layers: a microfluidic channel layer, a hydraulic-pressure control layer, and a membrane that separates those two. A single microfluidic channel connects all 24 cathode-chambers so that catholyte can be continuously or periodically replenished during operation through a syringe pump. The hydraulic-pressure control channel layer has grid channels that can isolate all 24 cathode chambers when pressure is applied to block the microfluidic channel. This allows complete isolation among the cathode chambers during power measurement to prevent any cross talk. **Figure 5.1C** shows the fabricated and fully assembled microfluidic-cathode MFC array. The use of hydraulic-pressure for integrated microvalve control instead of pneumatic-pressure prevented gas bubbles from forming in the gas permeability PDMS chambers[126]. These bubbles, if not controlled, can travel into the catholyte flow channel and eventually block the catholyte flow. The use of hydraulic pressure successfully allowed reliable operation of the microfluidic-

A: Anode Electrode Layer
Anode Chamber Layer
Proton Exchange Membrane
Control Channel Layer
Flow Channel Layer
Cathode Electrode Layer

B: Chamber A — Chamber B
During Catholyte replenishment

Chamber A — Chamber B
During Power measurement

Control channel | Flow channel | PDMS membrane

C: Catholyte in/out | Control pressure +/-
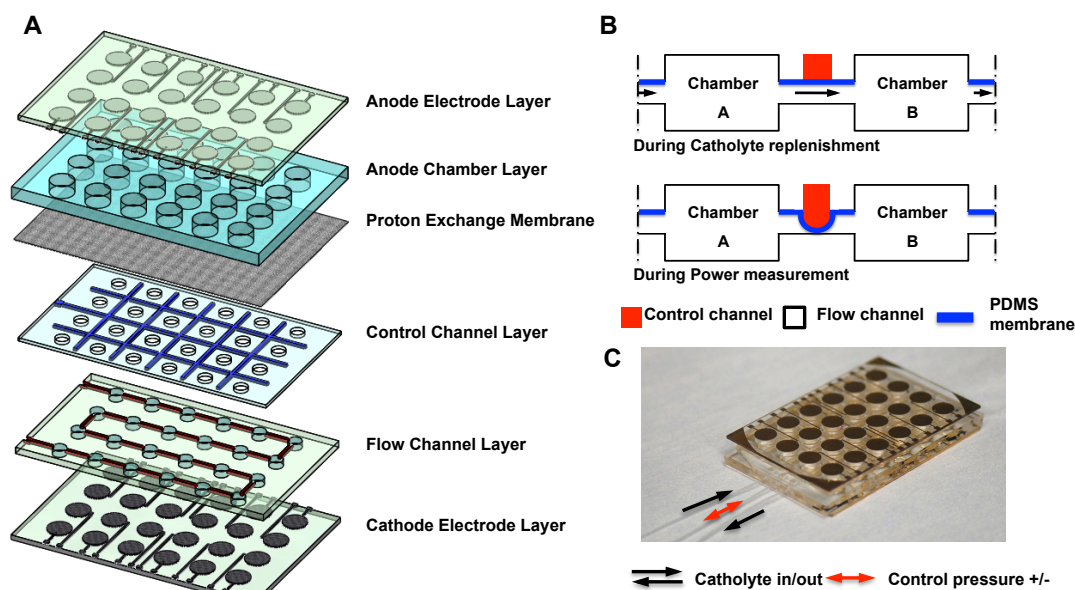
Figure 5.1 A microfabricated 24-well microfluidic-cathode MFC array as a high-throughput MFC screening platform. **A:** Schematic illustration of the MFC array. The MFC array is comprised of 5 functional layers. The control channel layer, PDMS membrane layer, and flow channel layer are permanently bonded together as a microfluidic-controlled cathode chamber layer. **B:** Operation of the microfluidic-cathode MFC array for catholyte replenishment and chamber to chamber isolation scheme. During catholyte replenishment, the normally open microvalve remains open so that all 24 cathode chambers connected through a single catholyte replenishment channel can be replenished using a single inlet. During power measurement, positive pressure is applied through the control channel to close the microvalves between chambers to isolate the chambers from each other. **C:** Image of a fully assembled microfluidic-cathode MFC array device.

cathode MFC array for more than 2 weeks. Successful isolation between the neighboring cathode chambers during microvalve closure was confirmed through color dye testing and resistance measurement analysis between chambers (data not shown).

The device was fabricated through conventional photolithography and soft lithography similarly as previously described[67, 122], except for the microfluidic cathode layer. In brief, the 24 individually addressable anodes were fabricated in Ti/Au (thickness: 3000 Å), each corresponding to an anode chamber (thickness: 5 mm, diameter: 7 mm) made on a PDMS substrate. The cathode electrode layer was fabricated by assembling Pt loaded carbon paper disks (EC-10-05-7, Electrochem Inc., Woburn, MA) on Au pads identical to the anode electrodes. To fabricate the microfluidic channel (height: 200 μm, width: 1 mm) on the microfluidic cathode chamber layer, SU-8 2075[TM] (MicroChem Corp., Newton, MA) was patterned to form a soft-lithography master mold. The PDMS microfluidic channel layer was then replicated from this master through a soft-lithography process. A PDMS membrane (thickness: 10 μm) separating the microfluidic channel layer and the control channel layer was fabricated by spin coating a PDMS/hexane mixture (weight ratio: 1:1) at 3000 rpm for 20 sec, followed by baking at 85°C for 20 min. The PDMS hydraulic grid control channel (height: 1 mm, width: 1mm) was replicated from an acrylic master mold fabricated with a rapid prototyping machine (MDX-40, Roland Inc., Los Angeles, CA). The three PDMS layers were then permanently bonded together with oxygen plasma treatment. Through-holes were then punched to form the 24 cathode chambers on the bonded layer. The assembled microfluidic cathode chamber layer was then bonded on the cathode electrode layer.

Proton exchange membrane (Nafion 117[TM], Ion-Power, Inc., New Castle, DE) was treated before use (section 3.2.2)[67].

5.2.2 Experiment protocol and data acquisition

Before chip assembly, tubings for catholyte inlet/outlet and control channel inlet/outlet were connected. De-ionized (DI) water was injected into the control channel gradually until no gas bubbles exist in the channel. Ferricyanide (100 mM) was first manually filled into the cathode chamber and then the PEM and anode chamber layer were aligned and assembled together with the cathode chamber layer. Microbes were loaded to each anode chamber and then the anode chamber layer was enclosed with the anode electrode layer. The assembled device was then connected to a circuit board having series of load resistors. Voltages across external load resistors connected to each of the 24 miniature MFC units on the device were continuously recorded with a digital multimeter connected through a multiplexer controlled by a LabView[TM] (National Instruments, Austin, TX) interface.

During operation, catholyte was periodically replenished with a certain duty cycle using a syringe pump (Harvard Apparatus, Holliston, MA). During power measurement, positive pressure was applied through the hydraulic-controlled channel so that all 24 cathode chambers are isolated, preventing cross-talk. Hence, the microfluidic-cathode MFC array worked as 24 individual miniaturized microfluidic MFCs. Polarization curves (voltage density vs. current density) were acquired by connecting each of the 24 miniature MFC units to varying load resistors and measuring

the voltages across the resistors. This can be repeated over time, thus results in full polarization curves for each of the 24 microfluidic MFCs over time. Maximum power from each MFC unit was then identified from these polarization curves for further analyses. The microvalves were only opened when replenishing all 24 cathode chambers with fresh catholyte (flow rate: 200 µl/min, flow time: 15 min). Power measurements were taken both before and after each catholyte replenishment cycle to characterize how catholyte replenishment influenced the instant power output.

5.2.3   Microbe cultivation and biomass analysis

S. oneidensis MR-1 was used as a reference strain for the microfluidic-cathode MFC array characterization. A previously uncovered environmental species, *Shewanella* sp. Hac353 (DQ307734.1) (7Ca)[29], was used for parallel comparison studies. Detailed microbial cultivation and preparation practices were described in our previous work[67]. For biomass analyses, cells were collected from anode chambers and lysed in 0.2 M NaOH and 1% SDS, followed by cell debris removal by centrifugation at 14,000 rpm for 10 min.

5.2.4   Biofilm characterization

Shewanella oneidensis MR-1 was collected from both microfluidic-cathode MFC array and batch-mode MFC array chambers after 234 hours of operation. Biofilms were fixed with 4% paraformaldehyde, stained with 2µg/ml DAPI (4', 6-diamidino-2-phenylindole),

and then images take using the Olympus BX51 fluorescent microscope (Olympus America, NY).

5.3 Characterization of the microfluidic-cathode MFC

5.3.1 Short-term study on power output improvement through catholyte replenishment

The microfluidic-cathode MFC array was first used to characterize power improvement induced by catholyte replenishment for *S. oneidensis* MR-1. All anode wells were inoculated with *S. oneidensis* MR-1. Twelve of the cathode chambers were periodically replenished with ferricyanide, and whereas the remainder were unreplenished. As shown in **Figures 5.2A** and **5.2B**, similar maximum power densities were observed during early time points after inoculation (200 min post-inoculation) in units with or without catholyte replenishment (13.8 mW/m^2, **Figure 5.2B**, or 14.9 mW/m^2, **Figure 5.2A**, respectively). After 1100 min (18.3 h), however, the maximum power density of the MFC units without catholyte replenishment dropped by 234% to 5.9 mW/m^2, whereas units with catholyte replenishment did not show significant changes in maximum power output (15.9 mW/m^2 at 1100 min vs. 14.9 mW/m^2 at 200 min) (**Figure 5.2B**). Therefore, catholyte replenished units provided a 270% higher power output than units without replenishment (15.9 mW/m^2 vs. 5.9 mW/m^2).

This initial short-term study (< 24 h) comparing batch-mode and microfluidic controlled MFCs readily revealed that batch-mode MFC arrays were not suitable for

long-term MFC studies due to power drop caused by electron acceptor depletion in the catholyte. At 200 min (< 4 h), catholyte replenishment had no obvious advantage because there was still sufficient amount of electron acceptors (ferricyanide in this case) in the catholyte to support power generation. However, as MFC array operation was carried on where electron acceptors in catholyte were continuously consumed during the electrochemical reaction, power output started to drop. This can be clearly seen from the result at 1100 min (~ 18 h) comparing the microfluidic-cathode MFC array units with and without catholyte replenishment (270% difference), confirming that batch-mode MFC arrays are not able to show the true electricity generation capacity of microbes over time due to catholyte depletion. However, with catholyte replenishment, power drop caused by catholyte depletion could be effectively eliminated (i.e. similar power output level between 200 and 1100 min with catholyte replenishment), providing a feasible strategy for long-term MFC studies in an array format.
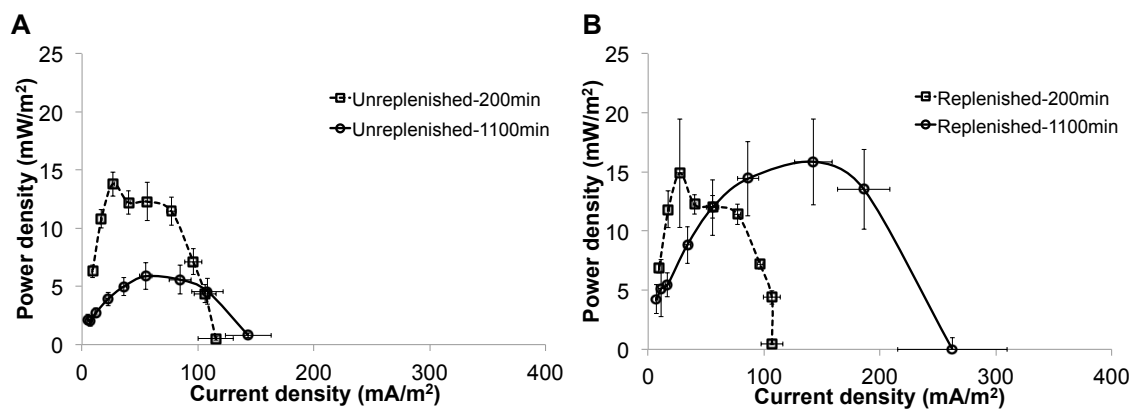
Figure 5.2 Power generations of *S. oneidensis* MR-1 A: without and B: with catholyte replenishment. Power densities of MFC units with and without catholyte replenishment were measured and compared at 200 min and 1100 min after cell loading (average and standard deviations are shown, *n* = 7-8 for each case).

5.3.2   Long-term power generation capability with catholyte replenishment

To further investigate the long-term power generation capability of the microfluidic-cathode MFC array developed here, two-week long studies were conducted in which the power outputs of *S. oneidensis* MR-1 and *Shewanella* sp. Hac353 (DQ307734.1) (7Ca) with catholyte replenishment were compared. In these experiments power densities from 24 microfluidic MFC units (12 containing MR-1 and the remainder containing 7Ca) were measured initially every 2 hrs and then twice a day both before and immediately after catholyte replenishment for a two-week period (307 hrs). **Figure 5.3** shows several selected polarization curves obtained for MR-1 with and without catholyte replenishment during 0 to 170 hours of MFC array operation.

For ease of comparison and analysis, maximum power densities after catholyte replenishment at each time point were calculated from the polarization curves and plotted (**Figure 5.4**). After initially showing the same maximum power output when using MR-1 (**Figure 5.4B,** 3 - 5 hrs), the microfluidic MFC units with catholyte replenishment showed increased power and then stabilized at a median value of 18.7 mW/m^2 (average: 16.9 mW/m^2). During the same time period, microfluidic MFC units without catholyte replenishment stabilized at a much lower maximum power density with a median value of 5.1 mW/m^2 (average: 5.0 mW/m^2). The overall maximum power output of MR-1 during the 2-week operation was 23.5 mW/m^2 with catholyte replenishment compared to 6.5 mW/m^2 without catholyte replenishment, a 362% difference in maximum power output (Fig. 4A). Similar analyses were conducted using 7Ca. **Figure 5.4C** and **Figure 5.4D** show that 7Ca and MR-1 displayed similar trends in
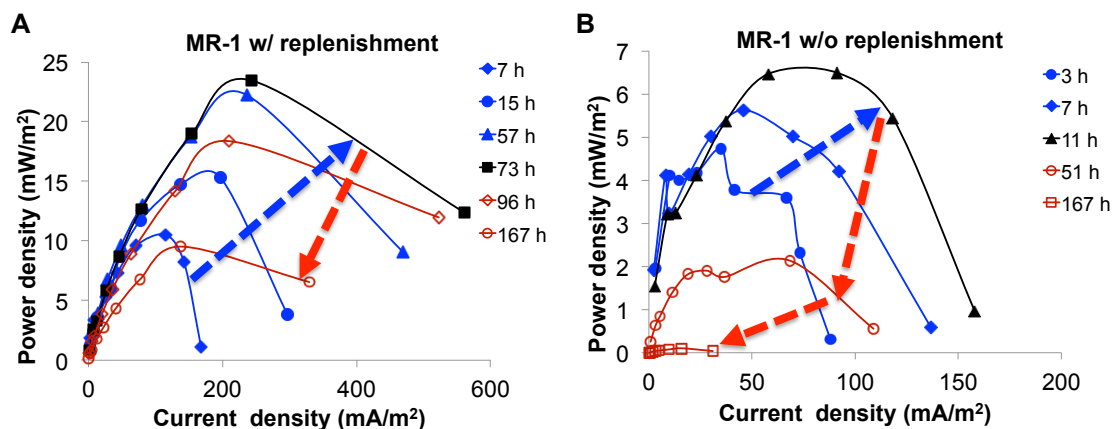
Figure 5.3 Polarization curves of *S. oneidensis* MR-1 (SO) A: with and B: without catholyte replenishment at different time points after cell loading. Polarization curves before reaching the maximum power density (black lines) were plotted in blue lines (filled marker) and curves after reaching the maximum power density were plotted in red lines (unfilled marker). The trends are pointed out with arrows. Note the different Y-axis ranges in A (0 to 25) and B (0 to 7). (n = 9-11 of each type)
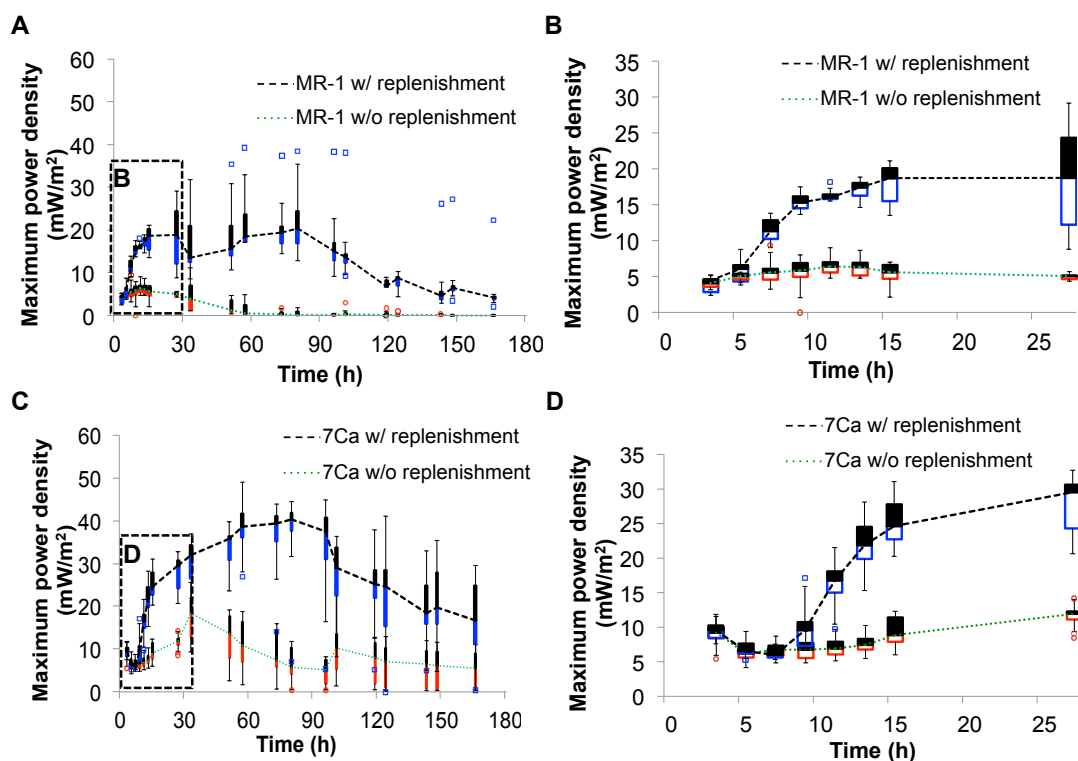
Figure 5.4 Box-and-whisker plots showing power generations of (A & B) *S. oneidensis* **MR-1 (MR-1)**
and (C & D) 7Ca with and without catholyte replenishment. Power outputs of (A) MR-1 and (C)
7Ca between 0 - 30 h were plotted in (B) and (D) respectively to better show the initial stage of
power change. Data points analyzed represents maximum power densities calculated from the
polarization curves. The medians of the data are connected through black dashed line (with
replenishment) and green dotted lines (without replenishment). Boxes above (black color) and below (red
color: MR-1 or 7Ca without catholyte replenishment; blue color: MR-1 or 7Ca with catholyte
replenishment) the median represent 25% and 75% percentiles. Bars above and below the percentiles
represent 1.5*IQR (interquartile range) above and below the 25% and 75% percentile or the
maximum/minimum, whichever is lower/higher. Scattered dots fall out of the bars and are outliers (Blue
□: MR-1 or 7Ca with catholyte replenishment; Red O: MR-1 or 7Ca without catholyte replenishment). (*n*
= 9-11 for each case)

these experiments. After initially producing the same maximum power output regardless of catholyte replenishment (**Figure 5.4D,** 3 - 7 h), the microfluidic MFC units with catholyte replenishment producing increased power outputs of up to a median value of 29.6 mW/m^2 (average: 27.9 mW/m^2) within 27 hours of operation. During the same time period, however, 7Ca loaded units without catholyte replenishment produced a much lower maximum power density at a medium value of 11.9 mW/m^2 (average: 8.0 mW/m^2). The overall maximum power output of 7Ca during 2-weeks of operation was 38.2 mW/m^2 with catholyte replenishment compared to 17.5 mW/m^2 without catholyte replenishment, a 217% difference in maximum power output (**Figure 5.4C**).

The power generation improvement induced by catholyte replenishment during the 7 days of microfluidic-cathode MFC array operation was confirmed with the two-tail Student's t-test analyses for the 33 measurements (0-167 h) (**Table 5.1**). Power outputs between catholyte replenished MFC array units and batch-mode operated MFC array units continued to show significant differences. This was the case for both MR-1 and 7CA, where initially no statistical differences were observed between catholyte

replenished units and those without replenishment ($p > 0.1$). However, after the initial start-up time period (~ 7 h), units with replenishment showed statistically higher power output than the batch-mold operated microfluidic-cathode MFC array units for up to 7 days ($p < 0.05$).

To examine whether power output from the microfluidic MFC units without any replenishment for a long period of time could be revived with catholyte replenishment, at 166 h post inoculation fresh catholyte was added to previously batch-mode operated microfluidic MFC. At this time point, MFC units without catholyte replenishment showed significant drops in power (from max. power of 6.5 mW/m^2 to 0.12 mW/m^2 for MR-1 and from max. power of 17.5 mW/m^2 to 3.68 mW/m^2 for 7Ca). Interestingly, the power outputs of both MR-1 and 7Ca increased immediately after catholyte replenishment by more than 363% (from 0.12 mW/m^2 to 0.42 mW/m^2) and 233% (from 3.68 mW/m^2 to 8.56 mW/m^2), respectively, a strong indication that the lower power output without replenishment was indeed due to catholyte depletion.

Table 5.1 Two tail t-test results comparing differences between catholyte replenishment and no replenishment when using *S. oneidensis* MR-1 and 7Ca (up to 167 hours of operation). 'x' represents $p > 0.05$ where the two series of data were statistically not different, and 'o' represents $p < 0.05$ where the two series of data were statistically different. Shaded measurements indicate measurements after catholyte replenishment and others indicate measurements before catholyte replenishment. MR-1-unrep and 7Ca-unrep were measured simultaneously with MR-1-rep and 7Ca-rep. (n = 9-11 for each case)

Measurements	1	2	3	4	5	6	7	8	9	10	11	12	13	14	15	16	17	18	19	20	21	22	23	24	25	26	27	28	29	30	31	32	33
SO-rep&unrep	x	x	o	o	o	o	o	o	o	o	o	o	o	o	o	o	o	o	o	o	o	o	o	o	o	o	o	o	o	o	o	x	o
7Ca-rep&unrep	x	x	x	o	o	o	o	o	o	o	o	o	o	o	o	o	o	o	o	o	o	o	o	o	o	o	o	o	o	o	o	o	o

5.3.3 Lifetime improvement of the microfluidic-cathode MFC array

Operation longevity was also improved with catholyte replenishment. For MR-1 with catholyte replenishment, power outputs kept increasing until 73 h after MFC array inoculation, at which point it reached the maximum compared to 11 h without catholyte replenishment (**Figure 5.4A**). This is about 700% longer in MFC array operating time compared to the batch-mode MFC array. For 7Ca, MFC units with catholyte replenishment kept increasing until 57 h after MFC array inoculation, compared to the MFC units without catholyte replenishment that showed power a drop at around 33 h. This translates to a 170% increase in MFC array operation time before the power output reaches the maximum.

The improved operation longevity by integrating the catholyte replenishment microfluidic system clearly demonstrated that drops in power generation in the batch-mode MFC array due to the depletion of electron acceptor could be effectively mitigated. For batch-mode operated MFC arrays, power dropped at a much earlier time point (11 h for MR-1 and 33 h for 7Ca) than the microfluidic MFCs (73 h for MR-1 and 57 h for 7Ca). This was mainly due to electron acceptor depletion in the cathode side but not substrate depletion in the anode chambers because the side by side operated microfluidic MFCs supplied with sufficient catholyte still showed higher power output, suggesting sufficient substrate remaining in the anode chambers. However, the eventual drop in power even in the microfluidic MFC units operating in catholyte replenishment mode is thought to be due to anode substrate depletion. A microfluidic MFC array that supports anode chamber replenishment capability as well to study how different substrates or

mixtures of substrates influences MFC power output over time is shown in the following section (Section 6)

5.3.4   Instant power output improvement through catholyte replenishment

The immediate increase in power output caused by catholyte replenishment in the microfluidic-cathode MFC array was also characterized by comparing maximum power densities right before and after catholyte replenishment. For MR-1, as shown in **Figure 5.5A** and **5.5B**, a striking power increase right after each replenishment cycle was observed, with a maximum improvement of 246% and average improvement of 160%. The same trend was observed when using 7Ca. This strain showed a maximum improvement of 200% and an average improvement of 141% (**Figure 5.5C&D**). However, the amount of power increase right after catholyte replenishment greatly depended on the duty cycle that it is depended upon on how much time elapsed from the last replenishment. Initially, the power densities increased about 150% after
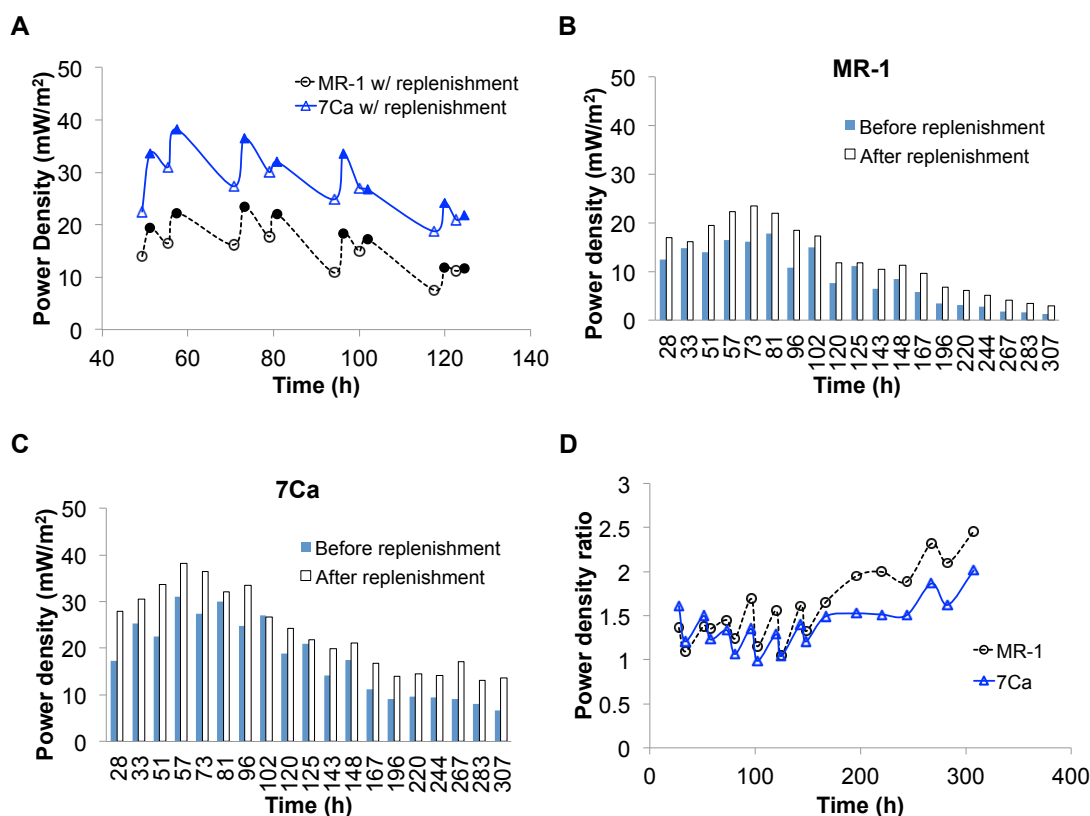
Figure 5.5 Power density improvement induced by catholyte replenishment for both *S. oneidensis* MR-1 and 7Ca. Maximum power densities calculated from polarization curves obtained at each time point were plotted. **A:** Measurements were taken right before (empty markers) and after catholyte replenishment (filled markers) in a sequence of: 1) power measurement, 2) catholyte replenishment, and 3) power measurement. **B&C:** Power density before and after each catholyte replenishment cycle. **D:** Ratio of improvement induced by catholyte replenishment (ratio = power density after replenishment / power density before replenishment). *(n = 9-11 for each case).*

replenishment when catholyte was replenished every 12 h. However when catholyte was replenished every 24 h, the effect of catholyte replenishment was much more significant, typically showing more than a 200% increase in power.

The findings above showed that the power increase ratio is dependent on catholyte replenishment duty cycle. Since concentrations of electron acceptors will gradually drop during operation and results in decreasing power output, a longer duty cycle between replenishment means less available electron acceptors compared to a shorter duty cycle. This means more significant power drop when a longer duty cycle is used, resulting in larger power increase percentage back to the maximum power level once catholytes are replenished. Immediate power improvement of microfluidic MFCs right after catholyte replenishment further confirmed that catholyte depletion is a major factor hampering miniature MFC array based parallel studies, unless there is a mechanism to periodically or continuously replenish depleted electron acceptors as presented in this study through the use of a microfluidic-cathode MFC array.

5.3.5   Biomass and biofilm characterization

To determine whether power output increases due to catholyte replenishment were due to differences in microbial growth in the anode chambers of the MFC units, biomass analyses of anode chambers with or without catholyte replenishment were conducted at the end of the experiments. **Figure 5.6** shows no statistical differences in biomass between replenished and un-replenished units for both MR-1 (0.22 µg/µL vs. 0.28 µg/µL) and 7Ca (0.34 µg/µL vs. 0.31 µg/µL) ($p > 0.1$). These data indicate that there are no

obvious differences in microbial growth as a consequence of catholyte replenishment, thereby supporting the hypothesis that the observed power improvement is indeed induced by the replenishment of depleted electron acceptors in the cathode chambers of the MFC array units.

Biofilm formed on electrodes of both batch-mode MFC array and microfluidic-cathode MFC array were examined and compared. Two types of MFC array were run side by side, and biofilms on anode electrodes were examined after 234 hours of operation. Both MFC array formed thick biofilm on anode electrodes (**Figure 5.7**). However, biofilm formed on electrode with catholyte replenishment appears brighter and thicker under microscope observation. This demonstrates that the catholyte replenishment may promote biofilm formation on anode electrode, which might be one reason why catholyte-replenished MFCs show higher power outputs than batch-mode MFCs.
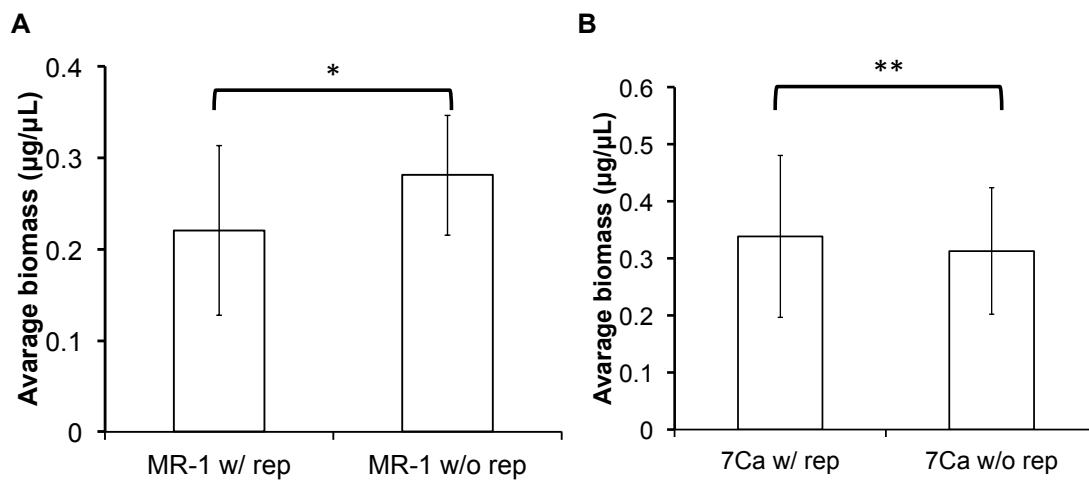
Figure 5.6 Biomass characterizations of (A) *S. oneidensis* **MR-1 and (B) 7Ca after 300 hours of operation with and without catholyte replenishment.** Two tail t-tests showed $p > 0.1$. (Average and standard deviations were calculated from $n = 7\text{-}11$ for each case).
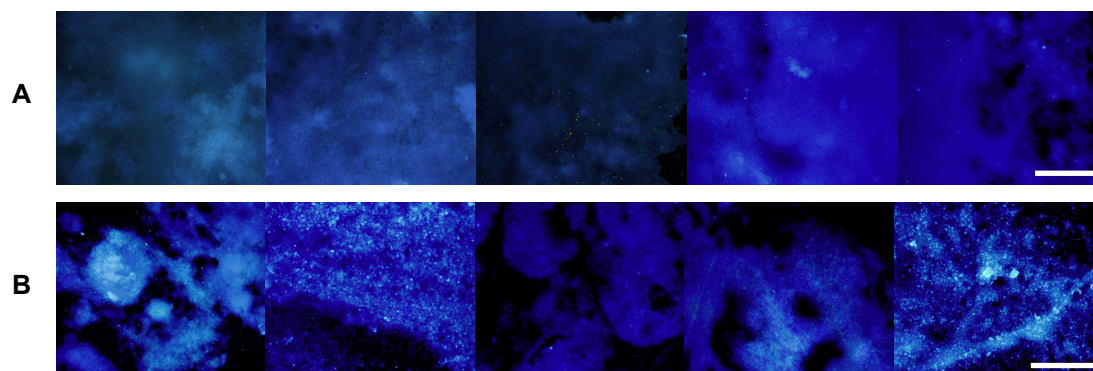
Figure 5.7 Biofilm formed on anode electrodes of A: a batch mode MFC array and B: a microfluidic-cathode MFC array. Five electrodes of each type were examined. Scale bar: 250 μm.

5.3.6   **Paralel study using the microfluidic-cathode MFC array**

To further demonstrate the ability of the microfluidic-cathode MFC array to support parallel MFC studies, MR-1 and 7Ca were tested side by side both with and without catholyte replenishment using a single microfluidic-cathode MFC array (12 anode chambers with MR-1 and 12 with 7Ca, 6 of each with or without catholyte replenishment). For chambers with catholyte replenishment, no statistical differences between MR-1 and 7Ca ($0.05 < p < 0.6$) were found during the startup period ($0 \sim 26$ h, **Table 5.2**). After the startup period however, MR1 and 7Ca showed differences in power output, with 7Ca producing higher power compared to MR-1 as expected ($p < 0.05$). However, no statistical differences between 7Ca and MR-1 were found after about 80 hours of operation ($0.05 < p < 0.19$) even though the average power of 7Ca was much higher than MR-1 (32.00 mW/m^2 vs. 22.04, 145% difference). In the case of batch-mode MFC units without catholyte replenishment, statistical differences were found between MR-1 and 7Ca after the startup period (0-13 h, **Table 5.2**), and 7Ca continued to show higher power until the end of the experiment ($p < 0.05$).

The parallel study results showed that the microfluidic-cathode MFC array could fully characterize two different microbial species (MR-1 and 7Ca) with different electricity generation abilities over a two-week MFC operation period. The result that microfluidic-controlled MFC array showed a narrower distinguishable time window between the two microbial species (26 h – 80 h for microfluidic MFCs vs. 13 h -167 h for batch-mode MFCs) is probably due to the fact that substrates in the anode chambers are depleted faster in MFCs with catholyte replenishment due to higher electrochemical

Table 5.2 Two tail t-test results comparing differences between *Shewanella oneidensis* MR-1 and 7Ca with catholyte replenishment and without catholyte replenishment (up to 167 hours of operation). 'x' represents $p > 0.05$ where the two series of data were statistically no different and 'o' represents $p < 0.05$, where the two series of data were statistically different. Shaded measurements indicate measurements after catholyte replenishment and others indicate measurements before catholyte replenishment. MR-1-unrep and 7Ca-unrep were measured simultaneously with MR-1-rep and 7Ca-rep. (n = 9-11 for each case)

Measurements	1	2	3	4	5	6	7	8	9	10	11	12	13	14	15	16	17	18	19	20	21	22	23	24	25	26	27	28	29	30	31	32	33
SO-rep&7Ca-rep	o	x	o	o	x	o	o	x	o	o	o	o	o	o	o	o	o	o	x	o	x	o	x	o	x	o	x	x	x	o	x	x	x
SO-unrep&7Ca-unrep	o	o	x	x	x	x	o	o	o	o	o	o	o	o	o	o	o	o	o	o	o	o	o	o	o	o	o	o	o	o	o	o	o

reaction speed. Lower substrate consumption speed is probably resulting in faster substrate-limited state. When substrate concentration decreases to a level that limits the electrochemical reaction speed (i.e. power output), the true power generation capabilities of different microbial species cannot be fully analyzed any more.

5.4   Environmental soil sample screening

5.4.1   Environmental soil sample preparation

Five gram of soil (wet weight) was homogenized in 90 ml of PBS in a Waring blender (blenders were autoclaved prior to use) for 3 x 60 sec, with cooling in an ice bath in between each run. The homogenate was place in 250 ml centrifuge bottle and PBS was added to bring final volume to around 250ml. The solution was then centrifuged for 20 min at about 2,000 g in a refrigerated centrifuge (centrifuge speed was increased for better settlement of the soils). The supernatant was collected and the soil was resuspended in PBS (bring volume to about 250 ml) and mix/shaken/homogenized and centrifuged again. This was repeated twice and the combined supernatants from the low speed centrifugation were centrifuged at 10,000g for 30 minutes. The supernatant from this centrifugation was discarded and the final pellet should contain live bacterial cells. The pellet can be resuspended in PBS and measured for O.D. and stored at 4 °C. Cells were then enriched by growing overnight at RT. O.D. of all samples was adjusted to 0.8 before screening.

5.4.2   Environmental soil sample screening result

Based on the results that the microfluidic-cathode MFC array can be used for parallel studies of anode parameter by eliminating cathodic factors with high power generation abilities, the device was used for environmental microbe screening from soil samples collected at different locations throughout the USA (**Table 5.3**). Twelve environmental samples were loaded on to two microfluidic-cathode MFC array chips, each with *Shewanella oneidensis* MR-1 and TSB media as positive and negative control respectively (**Figure 5.8A, B**). Power outputs of all samples were measured for 330 h and maximum power output through out the experiment of each sample was calculated and plotted. Because two different chips were used, and the positive control on two chips (*Shewanella oneidensis* MR-1) showed different maximum power outputs, the power outputs of environmental samples were normalized to the positive control on the same chip and were then compared side by side (**Figure 5.8C**). Four environmental samples (BWR1, WSH10, WHS10(-80), BIG19) showed higher power outputs than the positive control strain MR-1, with WHS10(-80) showing the highest power (1.78-fold higher than the reference strain). The result shows that electricigens are rich in soil at diverse locations. Besides, since soil samples tested contained diverse cell mixtures, the final power generation of the tested sample might be from one dominating group in the culture or from the cooperation of several different microbial species completing the electron transfer chain. The identifies of the four samples that showed higher power outputs than MR-1 will be analyzed and the dominating species in each environmental

Table 5.3 Environmental soil sample site information.

Site Name	State	Sample	Site ID	Temperature (°C)	Side description
Big Bend NP	TX	Soil	Big19	31.00	Possible second source for the Gravel pit spring in the middle of the pool
Wilson Hot Springs	UT	Thermal soil	WHS10	54.90	Edge of the pool, crystal red, orange on the surface
Laguna Bouqueron NWR	PR	Soil	BWR1		
New Mexico Sulfur Springs	NM	Thermal soil	NSS1	58.70	White silt 1" deep manmade pool
Hot Creek at Mammoth	CA	Thermal soil	HCMA	73.30	Blue pools across the river
Hawaii	HI	Brakish soil	KKHW2	27.5	Alcidine pond, med dryness of three pond nearby, lots of organic matter, very light and stinky, boggy covered
Braziria NWR	TX	Brakish soil	Bra5-9		Near shore of salt lake under 1 inch of water, next to grass and rocks
Hawaii, Alchiline ponds	HI	Brakish soil	APHW2	26.20	Alcidine pool 2, natural, more rocks, smelly soil
Great Salt Plains	OK	Bio rich	GSP 8	19.10	Quick sand, black
Rosswel-Carlsbad	NM	Bio rich	LL2	13.89	Lazy Lagoon, edge of the water
New Mexico Sulfur Springs	NM	Thermal soil	NSS1 (-80)	58.70	White silt 1" deep manmade pool
Wilson Hot Springs	UT	Thermal soil	WHS10 (-80)	54.90	Edge of the pool, crystal red, orange on the surface
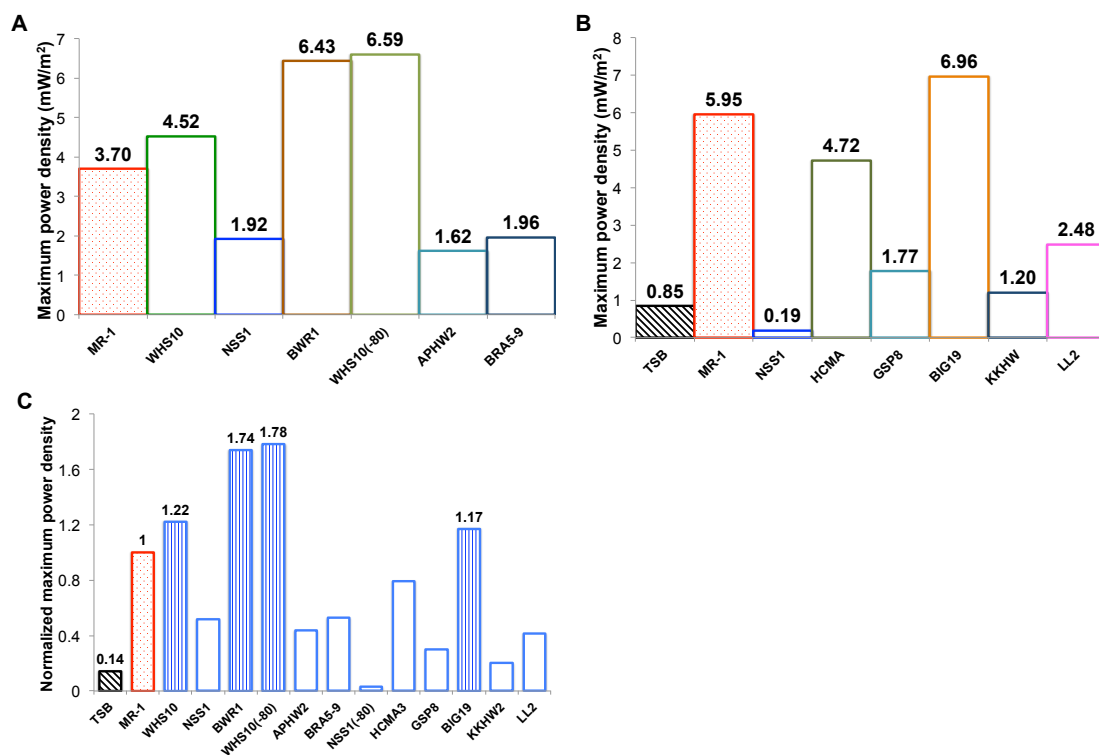
Figure 5.8 Maximum power output of environmental soil samples screened with the microfluidic-cathode MFC array. Twelve environmental samples and *S. oneidensis* MR-1 (MR-1) reference strain were loaded into two chips (**A:** Chip 1 and **B:** Chip 2)) each with 2-3 replicates. Maximum power output from each sample during the 330 h screening was calculated and plotted. **C:** Maximum power outputs from environmental samples in Chip 1 and Chip 2 normalized to power output of the reference MR-1 from each chip.

sample will be further characterized in the future to better understand their high electrochemical activities.

5.5   Conclusions

A 24-chamber microfluidic-cathode MFC array capable of long-term MFC parallel studies through continuous/periodic catholyte replenishment was developed. The microfluidic-cathode MFC array provides critical strategies for precise MFC parallel studies. With the catholyte replenishment feature, the operation longevity of MFC arrays was increased by 700% and the power output was increased by up to 360%. More importantly, the developed device eliminated the power fluctuation issue associated with catholyte depletion in miniaturized MFC devices, allowing reliable and repeatable long-term parallel MFC studies to screen and fully characterize electricity generating microbes and their performances in MFC systems.

The developed microfluidic-cathode MFC array is versatile that it can be easily reconfigured depending on its application. For example on top of screening and analyzing various electricity producing microbes on the anode side, different cathode conditions such as different types of electron acceptors can be applied to a set of cathode chambers by using two or more separately controllable microfluidic catholyte channels. One example of such reconfiguration was demonstrated here where both MR-1 and 7Ca with and without catholyte replenishment (2 different anode and 2 different cathode conditions with 6 replicates each = 2 x 2 x 6 = 24) were tested using a single microfluidic-cathode MFC array chip. Other parallel studies such as testing different

substrates and co-culturing different microbial species are some of the future studies planned using the anode and cathode replenishable microfluidic MFC array (shown in the subsequent section). The versatile design and precise fabrication process make this device a multifunctional high-throughput screening platform for MFC parallel studies.

The high-throughput and long-term screening and analyses capability of the developed microfluidic-cathode MFC array is expected to significantly enhance strategies for precise MFC parallel studies. MFC research such as environmental electricigen screening and anodic/cathodic operating condition optimization could be greatly speed up, and the MFC arrays could ultimately contribute to make MFC a practical renewable energy resource. Besides, the scalability of the microfabricated 24-chamber microfluidic-cathode MFC array is expected to further improve the throughput in the near future.

6. MICROFLUIDIC MFC ARRAY

6.1   Background

As described previously, MFCs as potential solutions for both bioelectricity generation and wastewater treatment have not yet been implemented in practice due to low power generation and difficulties of scaling up. Breakthroughs are possible through thorough understanding of electrochemical mechanisms of microbial bioenergy conversion from carbon sources in MFCs[83, 127-129]. Platforms enabling direct comparison of various factors such as different carbon substrates used by different microbes in MFC bioelectricity generation with high precision and throughput are highly desirable.   The previously developed MFC arrays (ferricyanide-cathode MFC array, air-cathode MFC array, microfluidic-cathode MFC array) have been used for environmental microbe screening to uncover electricigens with high bioelectricity generation capabilities. However, long-term parallel studies of different microbes under different carbon substrates are not possible due to the limited anode chamber volume. Here we present an anolyte and catholyte replenishable microfluidic MFC array for multiplexed analysis of microbial activities. The proposed device allows screening of 24 conditions (6 different microbial species with 4 different substrates) to be performed in parallel on a single device through periodic anolyte replenishment.

6.2   Materials and Methods

6.2.1   Device configuration and fabrication

The device consists of 6 functional layers (**Figure 6.1**): an anode electrode layer, an anode inflow channel/control channel layer, an anode outflow/control channel layer, a PEM layer, a microfluidic cathode chamber layer, and a cathode electrode layer. The 24 cathode chambers (110 μl) are connected by a fluid channel through which catholyte can be continuously/periodically replenished via one single catholyte inlet (see section 5.2.1). All chambers could be subsequently isolated by closing microvalves separating the cathode chambers during power output measurement. The anode chamber layer consists of an inflow channel/control layer and an outflow channel/control layer. Four inflow channels are connected to 4 rows of chambers with 6 anode chambers in each row, such that 4 different substrates can be tested against 6 different microbes. Substrate in each anode chambers is flushed out through the outflow channel. Microvalves are integrated on each layer to control both inflow and outflow channels to realize sequential replenishment while preventing chamber-to-chamber cross-contamination (**Figure 6.2**).

The anode/cathode electrode layer was fabricated as previously described[67, 122]. The inflow and outflow channel/control layers were fabricated through soft lithography by making PDMS replicas from acryl master molds, resulting in channels with 1 mm width and 1 mm height and chambers (diameter: 6 mm) of 3 mm thick. PDMS membrane separating flow channel layer and control channel layer were fabricated by spin coating PDMS mixture (base: curing agent = 1: 1 (weight ratio)) at 3000 rpm for 20

sec with acceleration speed of 300 rpm/sec, which resulting in a membrane about 30 μm thick. To fabricate the inflow or outflow channel/control layer assembly, the control channel layer was firstly bonded with the PDMS membrane through oxygen plasma treatment and then tubings for valve controls were inserted. The control channel/membrane layer was then permanently bonded with the flow channel layer. Negative pressure was applied to all control channels to buckle down the membrane during the bonding process to prevent the valve sites from bonding to the flow channel layer.

6.2.2 Replenishment efficiency characterization

Light transmittances (365 nm) of color dye at different concentrations were measured with a colorimeter (COL-BTA, Vernier Software & Technology, OR) and used for calibration. Color dye diluted with DI water (20%) was filed into anode chambers, and was then replenished with DI water (200 μl/min for 5 min). Light transmittances after replenishment were measured and the concentrations were calibrated through the transmittance calibration curve. Replenishment efficiency, defined as percentage of the first solution replenished with the second solution, was characterized by equation 6.1.

$$Efficiency = 1 - \frac{C_1}{C_2} \qquad\qquad 6.1$$

Here C_1 is the concentration of color dye after replenishment and C_2 is the concentration of color dye before replenishment.
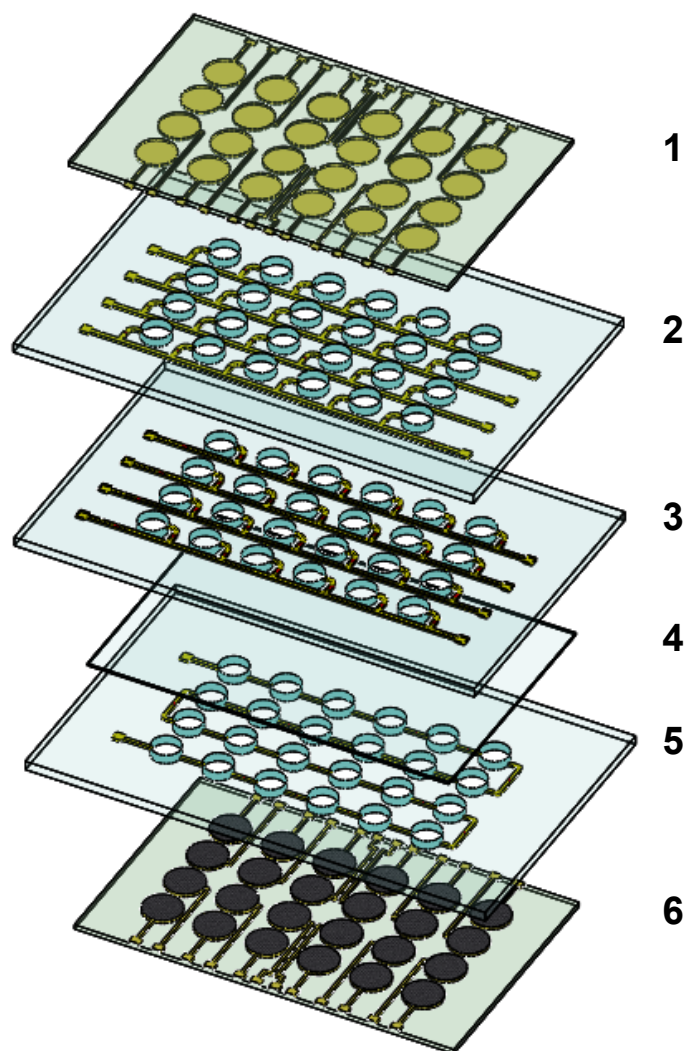
Figure 6.1 Illustration of the anolyte and catholyte replenishable MFC array. The
MFC array consists of 6 functional layers: the anode electrode layer (1), the inflow
channel/control layer (2), the outflow channel/control layer (3), the proton exchange
membrane layer (4), the microfluidic cathode layer (5), and the cathode electrode layer
(6).
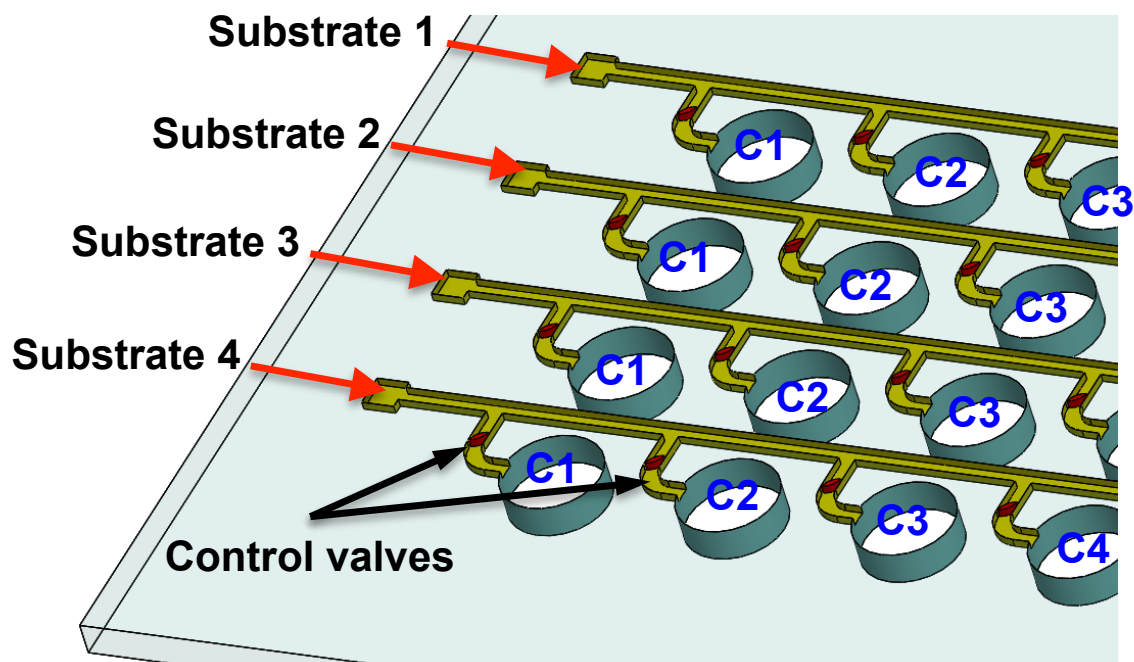
Figure 6.2 Schematic illustration of the inflow/control channel layer. The layer consists of 4x6 arrays of chambers. Four types of substrate could be replenished to 4 rows of chambers, each connecting 6 anode chambers loaded with 6 different types of microbes (C1-C6, C5 & C6 not shown). Control valves were integrated at each chamber entrance for sequential replenishment control.

6.2.3 Microbe growth and preparation

Xylose (X1500, Sigma-Aldrich, Inc., MO), acetate (#71183, Sigma-Aldrich, Inc., MO), lactate (L7022, Sigma-Aldrich, Inc., MO), Tryptic soy broth (TSB) (#211768, BD,NJ) were prepared at 50 mM concentration and used for the substrate screening characterization. *Shewanella oneidensis* MR-1 and 7Ca[67] were grown in TSB for 2 days and resuspended in xylose, acetate, lactate and TSB, with O.D. adjusted to 1 before use.

6.2.4 Device assembly and substrate screening

The whole device was sterilized in 70% ethanol before use. To assemble the device, cathode chambers were firstly filled with ferricyanide and then PEM and anode chamber layers were aligned and stacked on top of the cathode chamber layer. *Shewanella oneidensis* MR-1 and 7Ca with different substrates were loaded into the anode chambers with all control valves closed. Anode electrode layer and acryl cap were then assembled with the valves controlling the chamber outflow opened, such that solution in chambers could flow into waste ports due to pressure applied during the capping procedure. An assembled device image is shown in **Figure 6.3.** Hydraulic pressure was used for valve control by filling sterilized DI water into the control channels. Solenoid valve array were used for automatic pressure control through a LabView™ (National Instruments, Austin, TX) program, and voltages of all 24 wells were measured through a digital multimeter controlled with a multiplexer. The illustration of the whole setup and data acquisition is shown in **Figure 6.4**. For each screening, catholyte (ferricyanide, 100 mM) was either continuously or periodically replenished. Before each anolyte
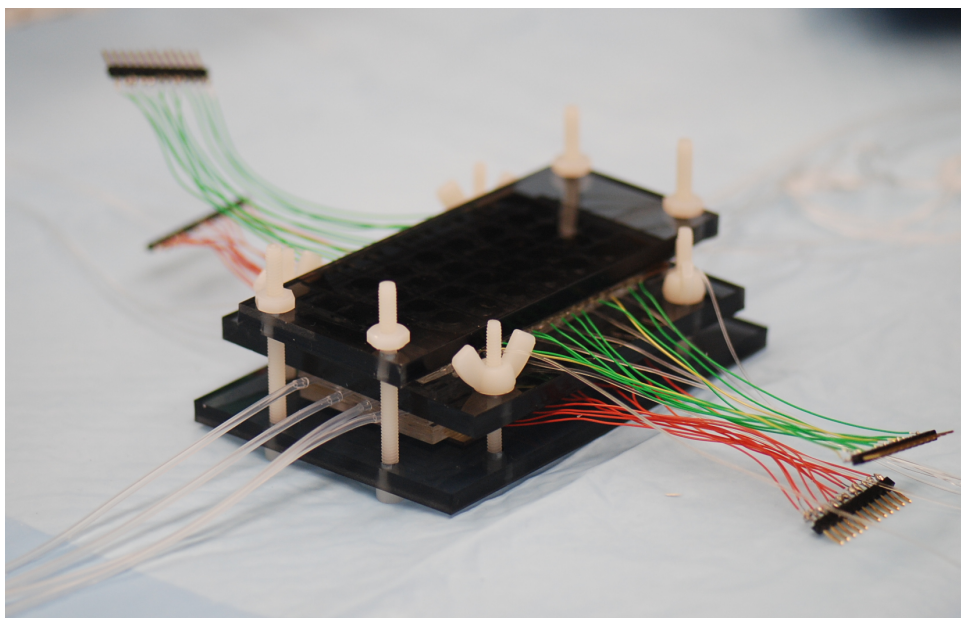
Figure 6.3 A fully assembled microfluidic MFC array.
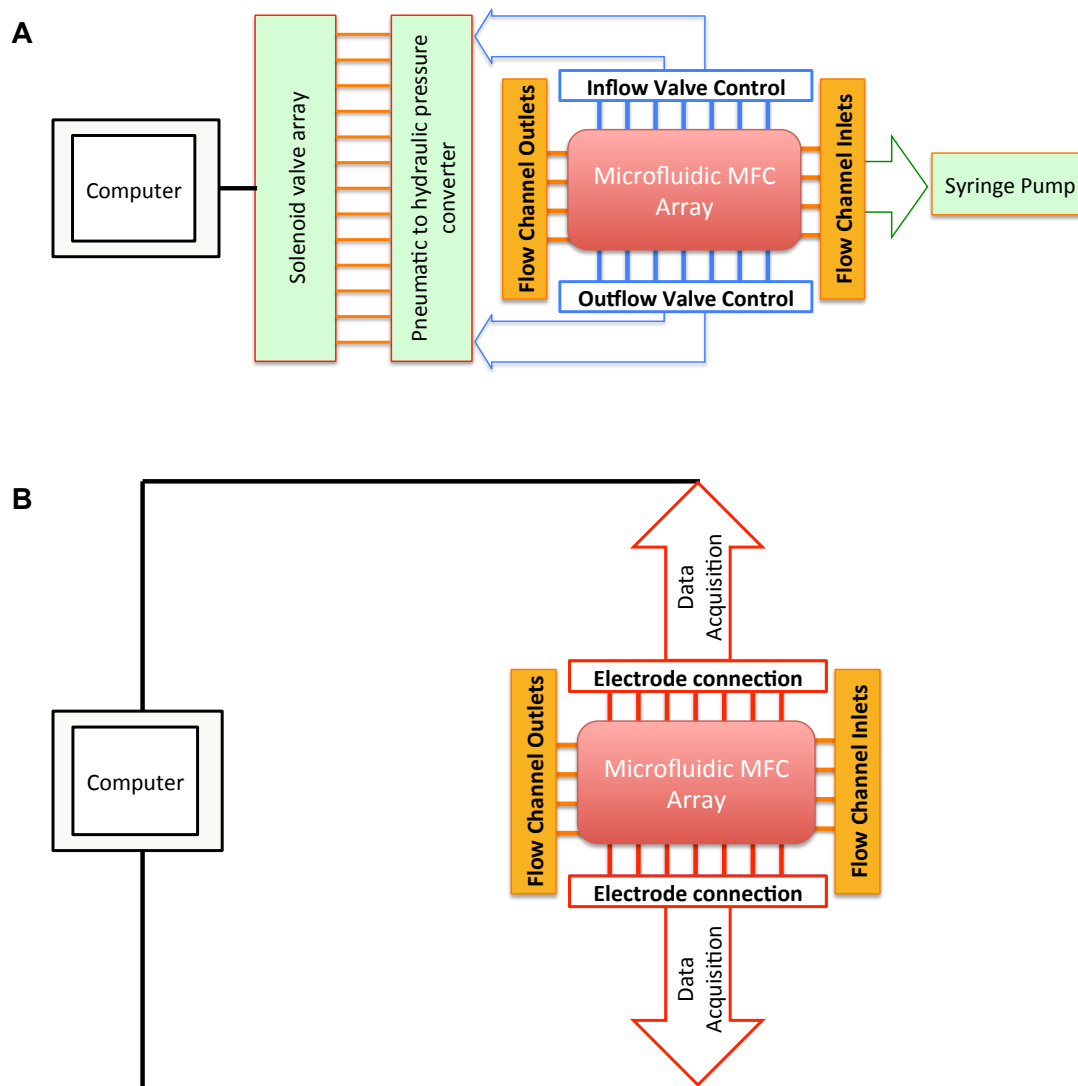
Figure 6.4 Flow charts of **A:** microfluidic control and **B:** data acquisition of the microfluidic MFC array.

replenishment, sterialized DI water was used to flush the inflow and outflow main flow channel (1 ml/min, 1 min). The anode chambers were then replenished sequentially with fresh substrates. Finally, the inflow and outflow main flow channel were flushed again with sterilized DI water. Both anolyte and catholyte replenishments were controlled with syringe pumps to realized precise flow speed control.

6.3   Results and discussion

We firstly characterized the anolyte replenishment efficiency by measuring anolyte light transmittance differences before and after anolyte replenishments. The result showed that 92% solution in anode chambers (400 μl) could be replaced in one cycle (**Figure 6.5**), demonstrating high replenishment efficiency.

The multiplexed microbial analysis capability of the microfluidic MFC array was characterized through continuous monitoring of the voltages from *Shewanella oneidensis* MR-1 and 7Ca (*Shewanella* sp. Hac353) using TSB, lactate, acetate and xylose (50 mM) as anolyte with periodic anolyte replenishment. Immediate increase in voltage could be observed after anolyte replenishment (at 40 h and 85 h) showing that power drop caused by anolyte depletion could be effectively revived (**Figure 6.6**). For anode chambers loaded with 7Ca, lactate, acetate and xylose were replenished periodically. Lactate and acetate showed identical performances, while voltage outputs from chambers replenished with xylose were 15-18 fold lower (average between 42 h and 52 h), showing the capability of the MFC array for characterizing performances of microbes under different substrate conditions in parallel. Significant voltage drop was observed
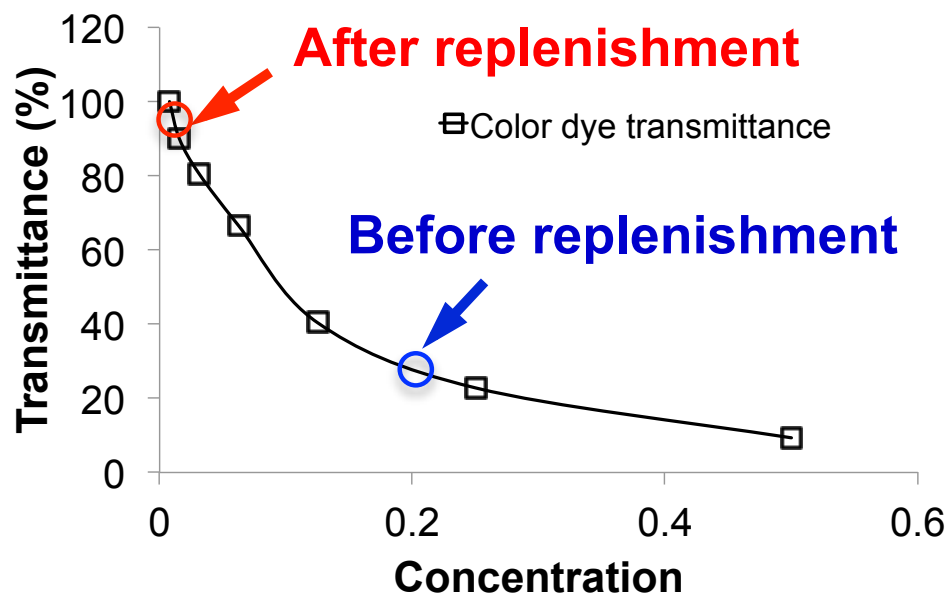
Figure 6.5 Anolyte replenishment characterization. Light transmittances (365 nm) of color dye at different dilution ratio with DI water were measured and were used for calibration. Anode chambers were filled with color dye (20%) and were replenished with DI water (200 μl/min for 5 min). Light transmittances after replenishment were measured and the concentrations (1.7%) were calibrated through the transmittance calibration curve.
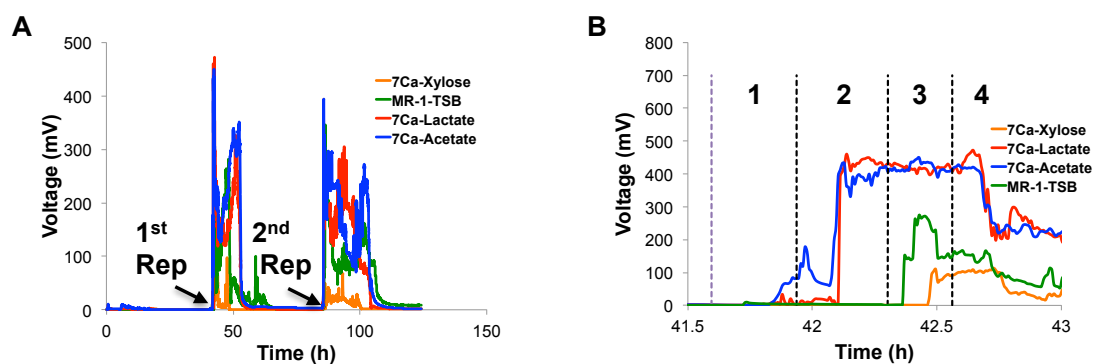
Figure 6.6 Substrate screening with *Shewanella oneidensis* MR-1 and *Shewanella sp.* Hac353 (7Ca). **A:** Two anolyte replenishment cycles to all chambers were conducted at 40 h and 85 h after cell loading, respectively (pointed with arrows). Immediate voltage revivals were observed after anolyte replenishment. **B:** Voltage output during the 1st substrate replenishment cycle (40 h). 1: Inflow/outflow main flow channels flushed with sterilized DI water; 2: Substrate replenishment of units containing 7Ca; 3: Replenishment of units filled with MR-1; 4: Inflow/outflow main channel flush.

approximately 8-10 h (1st rep) after anolyte replenishment, however voltage outputs were successfully revived through the 2nd anolyte replenishment. For the 2nd replenishment, the voltage stayed at a high level for about 15 h (2nd rep) before a sharp drop, which was longer than the 1st replenishment (8-10 h). This result clearly proves that the presented high-throughput device is capable of continuous monitoring/quantitating of MFCs under different substrate conditions over time in parallel.

6.4   Conclusions

We have developed a microfluidic MFC array that enables both catholyte and anolyte replenishments for high throughput MFC parallel studies. The fabricated device provides a feasible method for long-term operation of miniature MFCs at a high throughput fashion. The microfluidic MFC array has 4 substrate channels, where 4 types of substrates could be replenished to 6 different anode chambers, resulting in 24 different testing conditions. The influence of substrate types and concentrations on microbial fuel cell performances, such as power outputs and Coulombic efficiencies could be studied. Also, efficiencies of different carbon source conversions through different microbial species could be compared, which will assist understanding of exoelectron transfer mechanisms of different microbial species. Together with the catholyte replenishment capability of the device that eliminates influences from cathodic factor, precise parallel comparison of anodic factors could be realized with the device by testing different substrate types on the same device at identical experiment conditions.

7. NINETY-SIX WELL MFC ARRAY

7.1   Background

We have described several platforms of MFC array in 24-well formats in previous sections. All previously described MFC arrays have 24 anode and cathode chambers, which allow 24 studies conducted in parallel. To further improve the throughput, we fabricated two versions of 96-well MFC array: the batch-mode MFC array and the microfluidic-cathode MFC array. The MFC arrays provide important "proof of concept" of high throughput screening devices, demonstrating potentials to innovate schemes for MFC parallel studies, especially screening environmental electricigens and identifying novel genes that regulate the electrochemical activities of several model electricigenic microbes.

7.2   Design principle

Based on the experience of the previously developed MFC arrays, we developed a 96-well MFC array equipped with both catholyte and anolyte replenishment systems. **Figure 7.1** shows the illustration of the design concept. The anode electrode layer is similar as previously described. The anode chamber layer has 8 independent substrate channels each connecting 12 anode chambers, such that a total of 96 conditions (e.g. 12 different microbes with 12 substrate types) could be tested simultaneously on the same chip. Microvalves are integrated to isolate chambers after anolyte replenishment and at
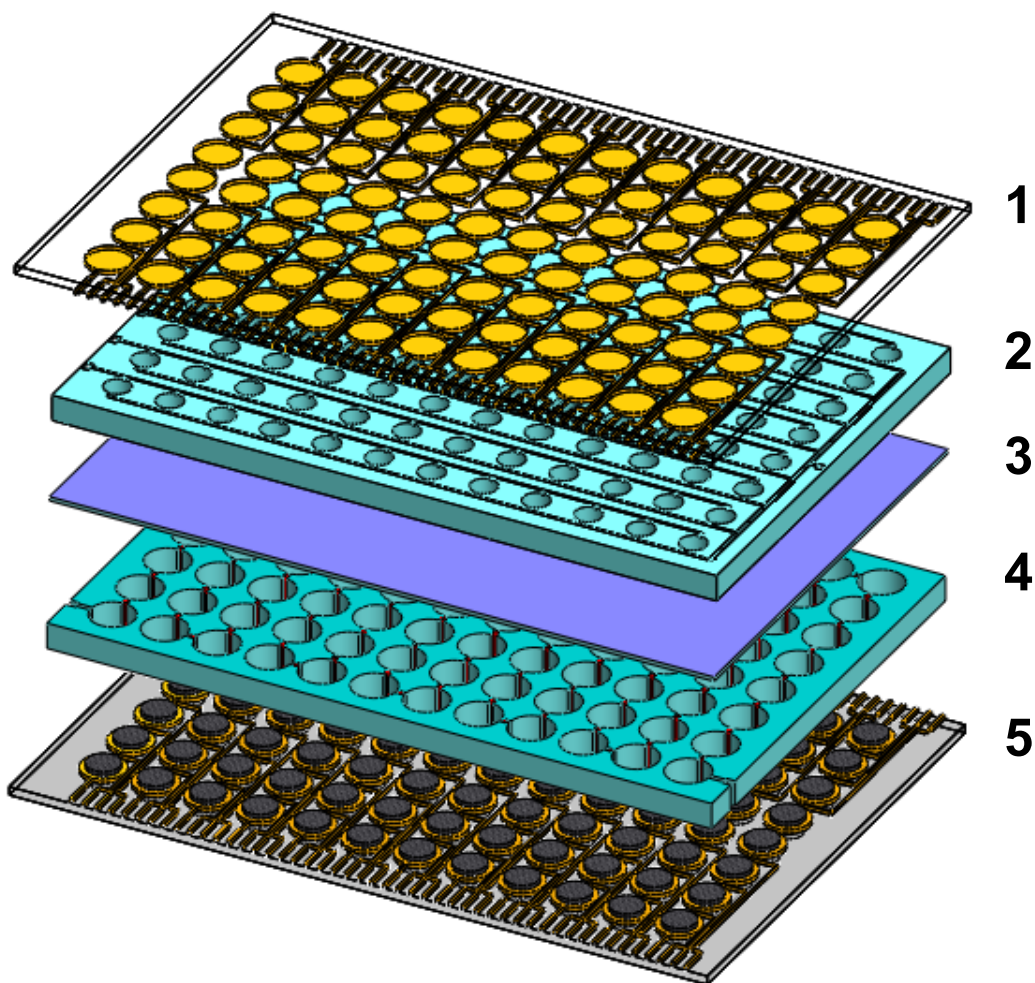
Figure 7.1 Illustration of the 96-well MFC array. The MFC array system is composed of 1: an anode electrode layer; 2: a microfluidic anode chamber layer; 3: a PEM layer; 4: a microfluidic cathode chamber layer; and 5: a cathode electrode layer.

the same time prevent cross-contamination among anode chambers. The cathode chambers are connected through a single microfluidic channel, such that catholyte could be either periodically or continuously replenished. Microvalves are integrated between each cathode chambers to isolate them while taking power measurement. For the design of the cathode electrode layer, electroplated Pt is used instead of Pt loaded carbon cloth, which was used in the 24-well MFC arrays, due to the fact that carbon cloth is not suitable for microfabrication.

7.3   Parameters tested for the development of the 96-well MFC array

7.3.1   Different concentrations of ferricyanide as catholyte

Ferricyanide concentration on the cathode side can influence power generation of the MFC array. For anodic parameter comparison, it is essential to supply enough electron acceptors such that the cathode side is not limiting the power generation. A 24-well batch-mode MFC array was used to find out the critical concentration. 1M, 100 mM, 50 mM and 10 mM ferricyanide solutions were loaded into the cathode chambers with *Shewanella oneidensis* MR-1 loaded in anode chambers. Current densities at 1000 min after microbe loading showed higher current densities with increasing ferricyanide concentrations from 10 mM to 100 mM (**Figure 7.2**). However, 100 mM and 1M ferricyanide as catholyte did not show dramatic difference in terms of current densities during the 1000 min operation, which show that 10 or 50 mM of ferricyanide are indeed
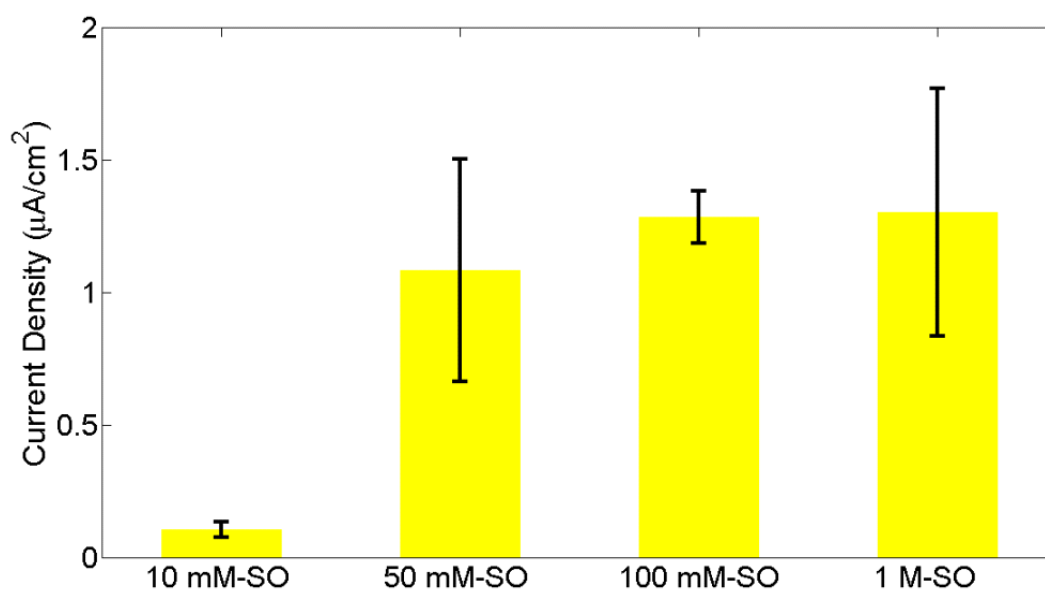
Figure 7.2 Current densities of *Shewanella oneidensis* MR-1 with different concentrations of ferricyanide as catholyte at 1000 min of operation. (load resistance = 200 kΩ, *n* = 4-6)

limiting the power generation after 1000 min of operation. Based on this characterization, it was decided that 100 mM of ferricyanide would be used as catholyte with the replenishment cycle being no longer than 1000 min.

7.3.2 Cathode materials

7.3.2.1 Carbon paste loaded with Pt

When integrating 96-well MFC array on a 50 x 70 mm substrate, the geometry of anode and cathode will have to be decreased compared with 24-well MFC array (3 mm compared to 7 mm in diameter). Applying carbon cloth/Pt disks onto the cathode electrode pads, which was the case of the 24-well MFC array fabrication, will become close to impossible. More importantly, the variations of size difference will greatly influence the repeatability of the MFC array. We have tested carbon paste/Pt mixer and

The feasibility of using carbon paste mixed with Pt catalyst to replace carbon cloth as electrode was tested on both anode and cathode side with two different microbe species: *Shewanella oneidensis* MR-1 (SO) and 7Ca (**Figure 7.3**). Result showed that when using Au anode, both SO and 7Ca with carbon paste (CP) cathode generated higher current than carbon cloth (CC) cathode. However, when CC was used as cathode, CP anode did not show obvious improvement over Au anode. Thus, Au anode is used in the 96-well MFC device fabrication. Although carbon paste cathode showed higher
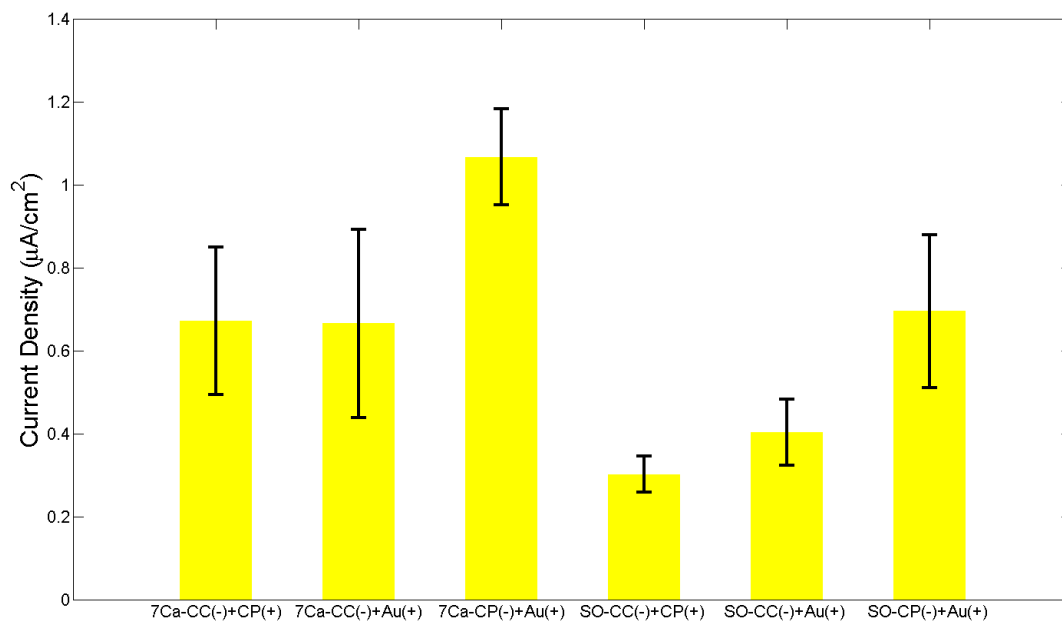
Figure 7.3 Feasibility of carbon paste/Pt mixture (CP) as cathode material and anode material. Carbon cloth (CC) and Au was tested at the same time for comparison ($n = 4$-6). (The x-axis was named as: cell type-cathode type(-)-anode type(+))

current generation ability compared to carbon cloth cathode, it was hard to uniformly apply the same amount of paste on the electrodes.

7.3.2.2 Electroplated platinum as cathode material

As described above, although Pt loaded carbon paste cathode showed better performance than carbon cloth cathode, it's not suitable for the 96-well MFC array fabrication due to the small electrode size (less than 3 mm in diameter), which make it hard to control the amount of paste applied. Electroplating has been widely used in microfabricated devices for electrode fabrication. Here we electroplated Pt on Au electrode directly and the performance was characterized with the 24-well microfluidic-cathode MFC array by comparing power outputs of electroplated Pt cathode to carbon paper cathode. The 24-well MFC array was divided to two parts, with 12 MFC units having electroplated cathode and the other 12 having Pt loaded carbon paper cathode. Each part was controlled with separate catholyte replenishment channel. Catholyte was replenished to all cathode chambers before each power measurement (100 mM ferricyanide, 200 µl/min, 3 ml in total for half chip, which has 12 chambers). Power outputs were measured and the maximum power densities after each replenishment were calculated and plotted (**Figure 7.4**). Pt loaded carbon paper and electroplated Pt showed identical performance in terms of power output and coefficient of variation through out the 45 hours' operation (average variance coefficient of all four power measurements: 20.6% vs. 20.3% for electroplated Pt and Pt loaded carbon paper). Since electroplating has better control on geometry and thickness distributions once the electrode pattern
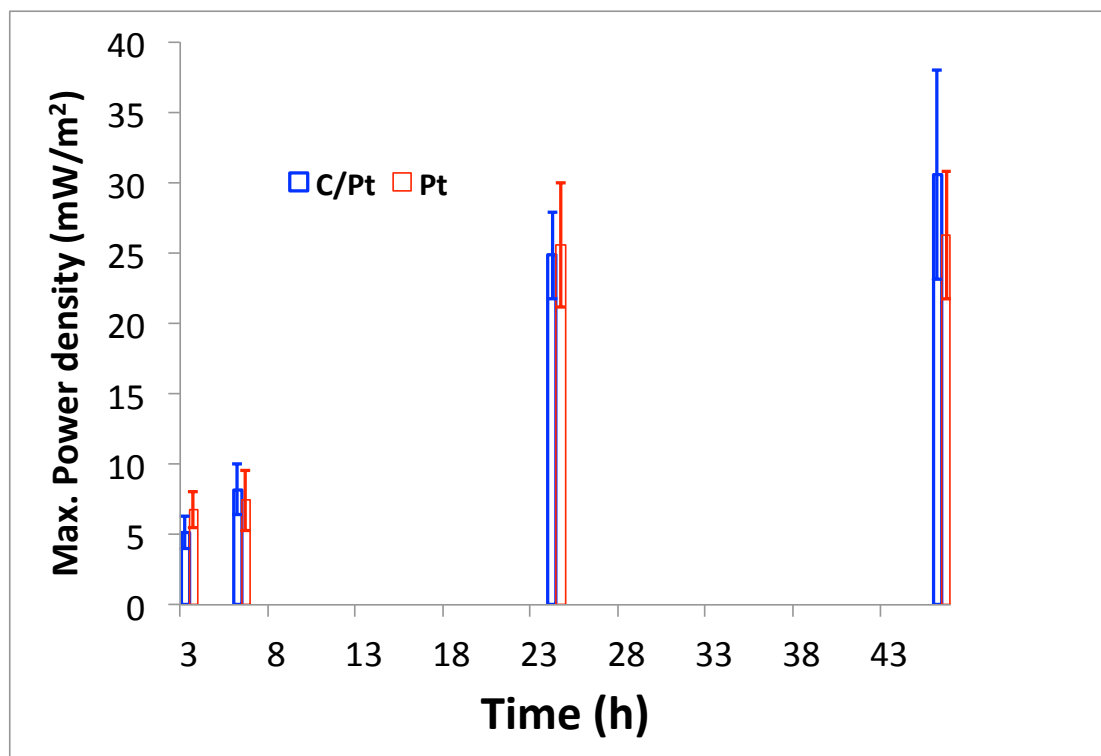
Figure 7.4 MFC performances with Pt loaded carbon paper and electroplated Pt as cathode electrode. 24-well microfluidic-cathode MFC array was used for characterization. Power output over a series of resistors was measured after each catholyte replenishment and the maximum power outputs were selected and plotted. (Electroplated Pt: 55.2 nm, Pt loaded carbon paper: 0.5 mg/cm^2)

becomes smaller (7 mm in diameter for 24-well MFC array vs. 3 mm in diameter for 96-well MFC array), electroplated Pt is expected to have better performance (e.g. better well to well repeatability) when 96-well MFC array is tested. Besides, with electroplated Pt electrode, no glue is needed as pasting carbon paper electrode on the Au pads, in which case electrode could detach during the experiment, the device will be more stable for long-term operation.

7.3.3 Platform geometry

To integrate 96 MFC units into a 50 x 75 mm format, the chamber size will have to be dramatically reduced compared to the 24-well MFC array. To have an estimated performance evaluation of the 96-well MFC array, the effects of reducing chamber size and varying the anode chamber thickness to overall power outputs and system internal resistance were characterized. A multi-size MFC array made of chambers with different sizes and thicknesses was used for characterization (**Figure 7.5 and Table 7.1**). Our preliminary results show that, with a larger chamber size (10 mm in diameter), the internal resistance was reduced from 500 kΩ to 50 kΩ when decreasing the chamber thickness from 18.7 mm to 13.5 mm. There was no significant internal resistance change of chambers with 5 mm diameter but with different thicknesses, both thickness generated internal resistances closed to 1 MΩ. When it comes to the 96-well design, which will have anode chambers with diameter even smaller than 5 mm, a much higher internal resistance is expected (higher than 1 MΩ) if the same chamber thickness was
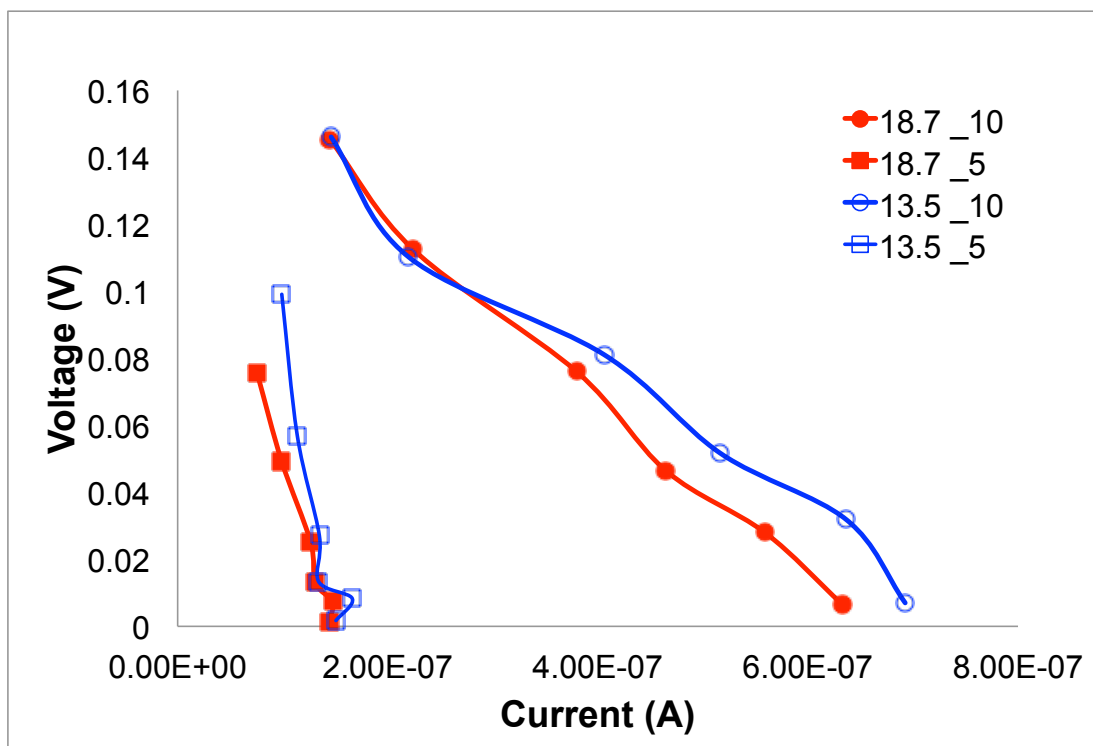
Figure 7.5 Polarization curve of multi-size MFC array with different thickness (18.7 mm and 13.5 mm) and different chamber diameter (10 mm and 5 mm). All cathode chambers were 2 mm thick with diameter same as anode chambers. *Shewanella oneidensis* MR-1 (O.D. =1) was used in the anode chamber and 100 mM ferricyanide was used as catholyte.

Table 7.1 Internal resistance calculated by polarization curve shown in Figure 7.5.

Thickness (mm)	Diameter (mm)	Linear equation	R (V=Eb-Rint*I) (kΩ)
18.7	10	y = -258702x + 0.171	259
18.7	5	y = -906328x + 0.1379	906
13.5	10	y = -192676x + 0.1544	193
13.5	5	y = -856366x + 0.144	856

used. Since the diameter of chambers is limited by the chip geometry (50 mm x 70 mm),
both anode and cathode chamber thickness need to further reduced (much thinner than
13.5 mm) to get dramatic internal resistance reduce in order to improve power
generation of the system.

7.4   96-well batch-mode MFC array

A 96-well batch-mode MFC array with ferricyanide cathode was firstly designed and
fabricated (**Figure 7.6**). Design of the chip is similar to the 24-well batch-mode MFC
array, which has an anode electrode layer, anode chamber layer with isolated anode
chambers, PEM layer, cathode chamber layer with isolated cathode chambers, and a
cathode electrode layer. The diameter of each anode and cathode chamber is 3 mm,
which is limited by the size of glass substrate used to fabricate the chip (50 x 70 mm).
The total thickness of anode chambers is 7 mm (two PDMS anode chamber layers with
thickness of 2 mm and an acryl chamber layer with thickness of 3 mm) and the thickness
of the cathode chamber layer is 2 mm.

 Shewanella oneidensis MR-1 was loaded into the anode chambers to examine the
performance of the 96-well batch-mode MFC array (**Figure 7.7**). A maximum power
density of 0.047 mW/m^2 was obtained at a resistance of 2 MΩ, which is about 10 times
lower than the 24-well MFC array (0.0467 mW/m^2 vs. 0.416 mW/m^2). The low power
density from the 96-well MFC array with enclosed anode and cathode chambers was
expected because of high internal resistance (about 10-folds higher) with reduced
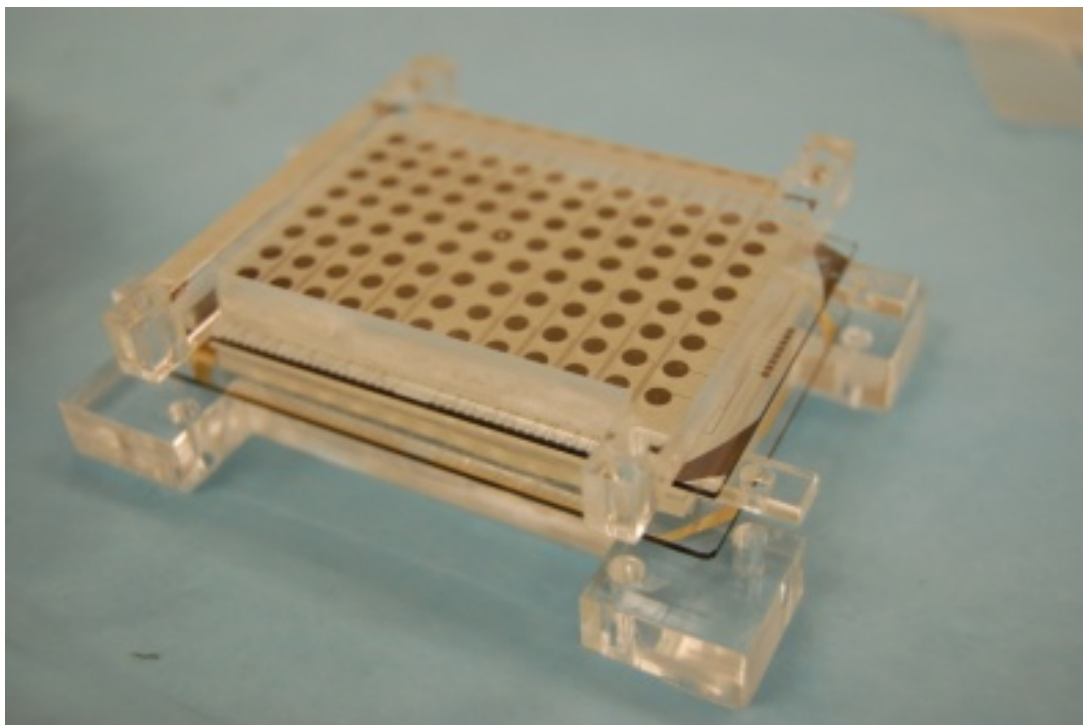chamber sizes.   The average variance coefficient of power outputs was 30.7%,

Figure 7.6 A microfabricated 96-well batch-mode MFC array.
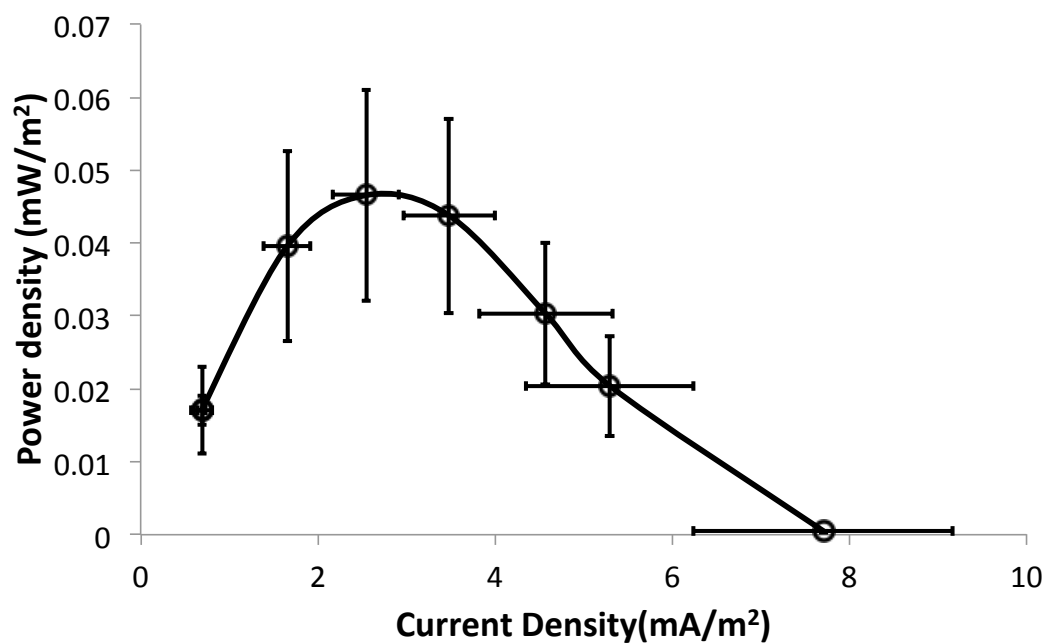
Figure 7.7 Power generation from *Shewanella oneidensis* MR-1 (O.D. = 1) tested with a 96-well batch-mode MFC array. Resistors with resistances of 1K, 100k, 200k, 500k, 1M, 2M, 5M, 10MΩ were connected for power measurement. Maximum power was obtained with 2MΩ resistor. ($n = 12$)

which was much higher than the 24-well batch-mode MFC array (C.V. = 12.5%). This shows that further optimization is needed to have the 96-well batch-mode MFC array to perform as good as the 24-well MFC array.

7.5   Microfluidic control of the 96-well MFC array

As described above, high internal resistance induced low power generation and high coefficient of variation from the 96-well batch-mode MFC array. To improve the performance, several factors have to be improved: First, the chamber thickness has to be further decreased to reduce internal resistance and thus increase power outputs. Second, to perform long-term MFC studies, both anolyte and catholyte have to be replenishable. The successful experience with the 24-well microfluidic MFC array would benefit the design of the 96-well microfluidic MFC array. Third, in the 24-well microfluidic MFC array, both catholyte and anolyte were manually loaded into the cathode and anode chambers. However, it will be very time consuming to do manual catholyte and anolyte loading with the 96-well MFC array. To realize automatic cell loading and catholyte loading, one important design regime is to eliminate bubble forming inside chambers. The 96-well microfluidic MFC array is designed to improve the high-throughput screening performance of MFC parallel studies in terms of increasing power outputs through reducing chamber thickness, enabling long-term multiplexed studies through integrated anolyte and catholyte replenishment system, and realizing automatic chip control through automatic cell loading and data acquisition.

Figure 7.8 shows the illustration of the microfluidic cathode chamber layer. The cathode chamber layer comprises of three functional layers: the control channel layer, the flow channel layer, and the membrane layer separating the two channel layers. The total thickness of the three bonded layers is controlled below 400 μm (flow and control channel layer: 160 - 190 μm, membrane: 10 μm) to reduce the system internal resistance, and also, this thin layer is the key feature that prevents air bubble capture inside the cathode chambers. Besides, sharp corners of the fluidic channel are rounded to reduce dead volume (**Appendix Figure B.12**) that helps removing bubbles formed inside chambers. With this design, ferricyanide catholyte could be automatically filled into all 96 chambers through a microfluidic channel without bubble captured inside the cathode chambers (**Figure 7.9**).

Both normally closed valve and normally opened valve were used for the cathode chamber layer characterization. When using normally opened valves for chamber isolation, fluid cross-talking/diffusion can be neglected (**Figure 7.9**). On the other hand, because the rectangular geometry of the flow channel, high pressure is needed to realize better vavle closure and electrical isolation, however, even with the highest pressure without breaking the membrane, it's hard to get 100% electrical isolation between chambers. The resistance between neighboring chambers may vary between 1MΩ to 10s of MΩ with PBS filled in the chambers with different pressure applied. To realize 100% electrical isolation, normally closed valve was used to isolate chambers and 100% electrical isolation was confirmed with PBS filled inside chambers.

Control channel

Flow channel

Membrane
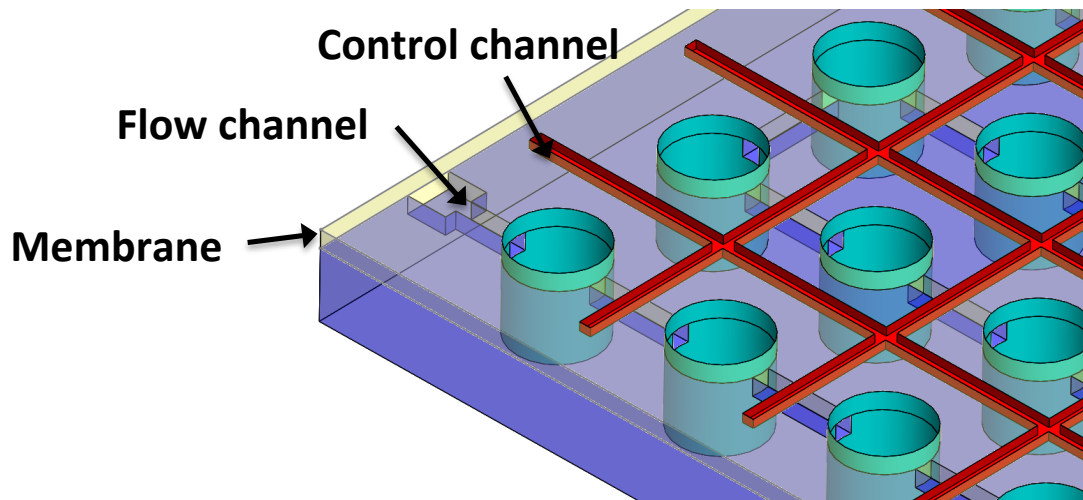
Figure 7.8 Illustration of the microfluidic cathode chamber layer of the 96-well MFC array (8 chambers were shown). The cathode chamber layer is comprised of a flow channel layer on which one flow channel is connecting all 96 cathode chambers to realize catholyte replenishment through a single fluid inlet, a control channel layer that has a all-connecting grid channels to isolate all 96 chambers for power measurement, and a membrane layer to separate the two layers.
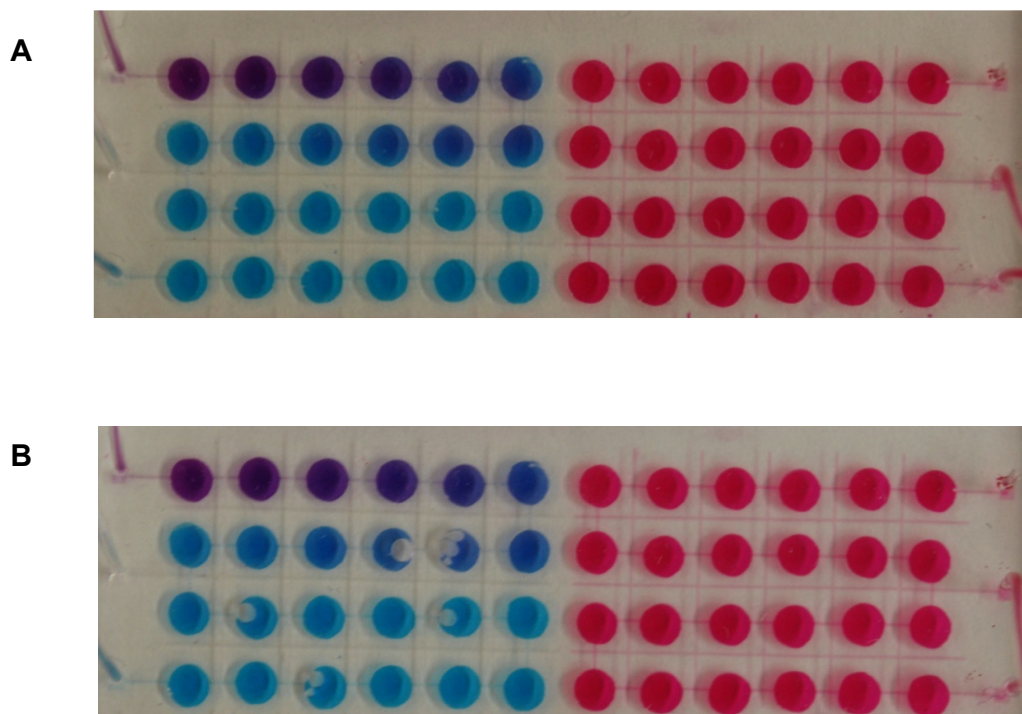
Figure 7.9 Filling the microfluidic-cathode chambers of a 96-well MFC array with color dye. Chambers could be successfully filled without air bubble trapping inside chambers (Left: blue color dye filled; Right: red colored dye filled). A: A small volume of red color dye was then filled into the left chambers to form a color gradient in the first two rows of chambers. Normally opened valves for blue color dye filled chambers were then closed to isolate all chambers, valve controlling the red color dye filled chambers on the right side remained opened. **B:** Image of device from (**A**) after 30 min valve closure, no obvious diffusion was observed in the left side chambers, however, gas bubbles formed inside chambers on the left side, but not inside chambers on the right side, which were not isolated.

7.6   Screening and characterization of electricigens

The fabricated 96-well microfluidic-cathode MFC array equipped with removable anaerobic chambers is shown in **Figure 7.10**. Both oxygen-limited and anaerobic conditions can be tested with the microfabricated MFC array. The assembly of the device is shown in **Figure 7.11**. With the currently integrated catholyte replenishment system, the 96-well MFC array could conduct long-term parallel studies same as the 24-well microfluidic-cathode MFC array but with a much higher throughput (96 vs. 24). The 96-well MFC array could also be integrated with microfluidic anode components to realize anolyte replenishment for long-term anodic parameter studies. The fabricated device need to be characterized and will be used for high throughput screening studies of electricigens.   The developed 96-well microfluidic MFC array will be a versatile platform for long-term high throughput MFC parallel studies.
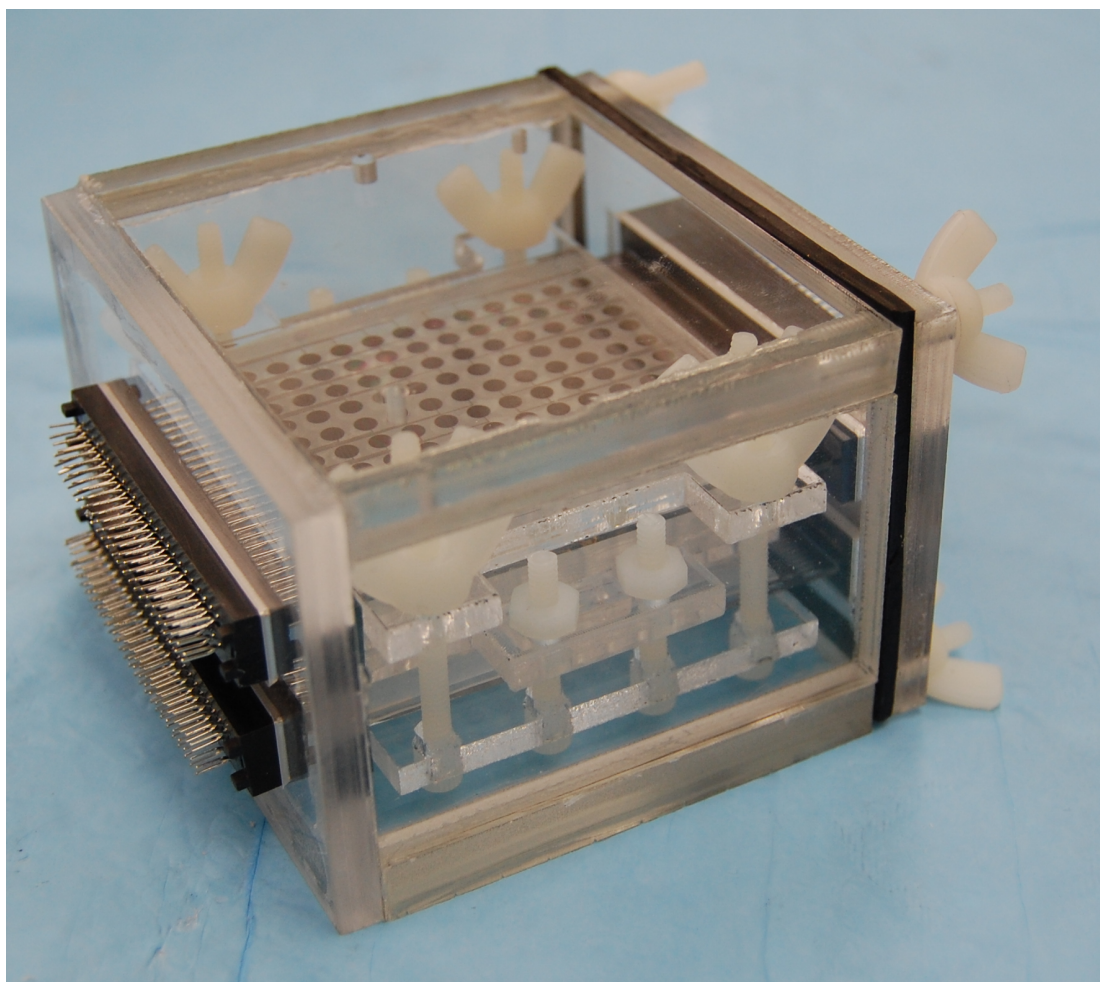
Figure 7.10 Microfabricated 96-well microfluidic-cathode MFC array equipped with anaerobic chambers and data acquisition interfaces.

A Cathode electrode

B Anode electrode layer

C Flow channel layer

D PDMS anode chamber layer1

E Acryl anode chamber layer

F PDMS anode chamber layer2

G Actuation channel layer

H Acryl frame layer

I Final assembly

J Chip in N$_2$ chamber
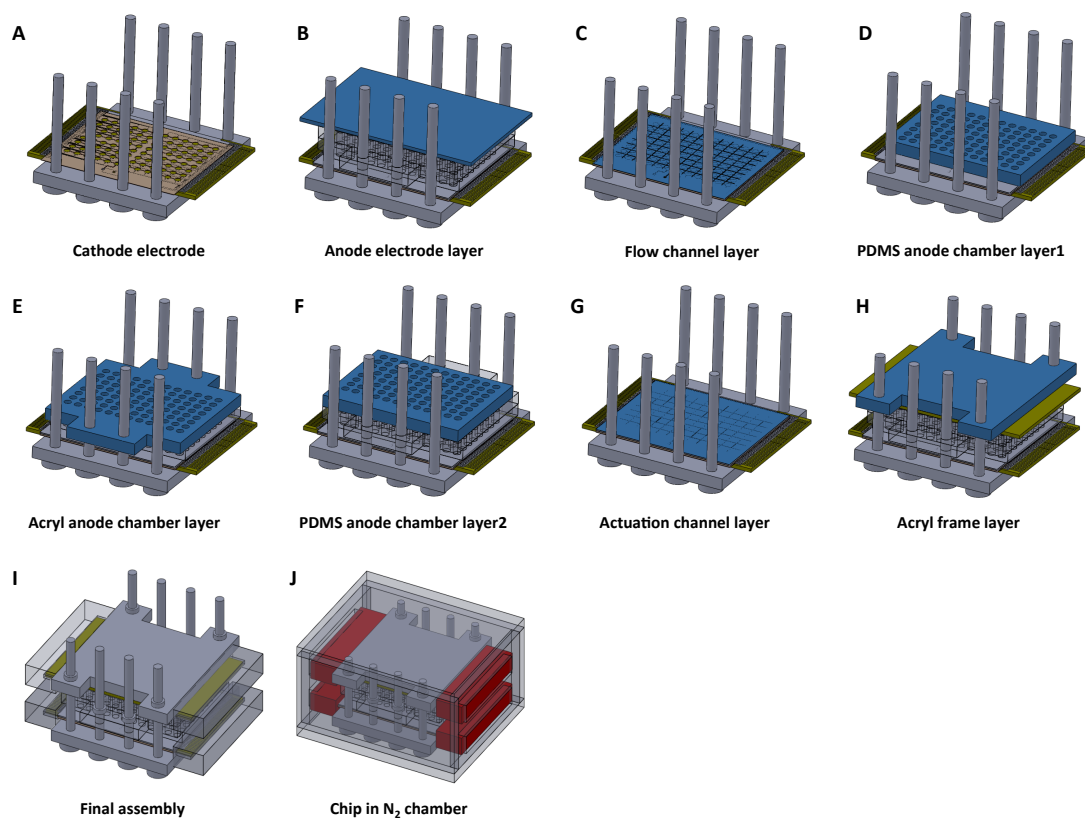
Figure 7.11 A-I: Assembly procedures of the 96-well microfluidic-cathode MFC array and **J:** the 96-well MFC array equipped with a removable nitrogen chamber.

7.7   Conclusions

To further increase the throughput of the MFC array, the 96-well MFC arrays were developed. The microfabricated high throughput screening devices will greatly promote current experimental methods of microbial fuel cells. With 96 miniature MFC units integrated on a 50 x 70 mm^2 format, 96 different parameters could be conducted in parallel, which greatly reduces cost, sample usage, and time for research. Besides, catholyte could be continuously/periodically replenished through the integrated microfluidic controlled cathode chamber layer, allowing long-term study of MFCs. With catholyte replenishment, precise comparison of anodic parameters can be realized by removing cathodic varying factors. Microfluidic anode chamber configuration could also be integrated into the 96-well MFC array. With the anolyte replenishment abilities demonstrated in to previous sections, long-term studies of electrochemical mechanisms of different microbes with different substrates could be conducted. We believe that the 96-well MFC will become a versatile prototype of high-throughput MFC parallel studies.

8. PROJECT REVIEW, FUTURE STUDIES AND CONCLUSIONS

8.1 Project review

The aim of the project is to develop a high throughput screening platform for microbial fuel cell parallel studies. Current MFC technologies are still far from mature that could be practically used. Increasing power generation, reducing plant cost, scaling up MFCs are some of the most important questions to be addressed first. Besides, microbial metabolic mechanisms that contribute to electricity generation are not very well understood and much of current research has focused on only few known model strains or mixed cultures where the microbial population are not well known. Solving all these problems requires massively parallel studies to optimize the working parameters. However, most of the current large batch or miniature MFCs are single unit MFCs that are not suitable for parallel studies.

We have developed a series of 24-well and 96-well MFC arrays as high throughput platforms for various MFC parallel studies, including a 24-well batch-mode MFC array, a 24-well air-cathode MFC array, a 24-well microfluidic-cathode MFC array, a 24-well microfluidic MFC array, and finally a 96-well batch-mode MFC array and a 96-well microfluidic-cathode MFC array. Screening of environmental samples to uncover electrochemical microbes that have superior electricity generation abilities have been performed to demonstrate the functionality of the MFC arrays. The main achievements are elaborated as following:

(1) 24-well batch-mode MFC array: This first MFC array in the world has 24 independent MFC units integrated on a single chip, where 24 different studies could be conducted in parallel. This robust system showed highly reproducible result from unit to unit, day to day, and chip to chip. Here, Au electrode was selected as the anode material and the performances, such as biofilm formation and power generation, were also characterized. The system was utilized for environmental screening and several environmental species were uncovered with higher power generation abilities, with one species 7Ca (*Shewanella* sp. Hac353) showing 230% higher power output than the *Shewanella oneidensis* MR-1.

(2) 24-well air-cathode MFC array: Different from the first MFC array that used ferricyanide as catholyte, we developed an MFC array using oxygen in the air as electron acceptor. The air-cathode MFC array could also conduct 24 parallel studies on the anode side and the performances were also characterized. It is sustainable and more suitable for long-term MFC studies. Through environmental isolates screening, the air-cathode MFC array showed consistent results with that from the ferricyanide 24-well MFC array. Power generations from several environmental species were well characterized.

(3) 24-well microfluidic-cathode MFC array: Comparing performances of the first two MFC array, ferricyanide MFC array is more suitable for parallel studies due to better unit to unit repeatability. However, ferricyanide as catholyte will be gradually depleted due to the limited cathode chamber volume, and thus not suitable for long-term parallel studies. The 24-well microfluidic-cathode MFC

array integrated a microfluidic channel that is connecting all cathode chambers to realize periodic/continuous catholyte replenishment. This design successfully solved the catholyte depletion issue, and at the same time, anodic parameters could be compared more precisely without influences from factors on the cathode side. In this study, MFCs with and without catholyte replenishment were compared in terms of maximum power outputs and lifetime (improved by 362% and 700% respectively with *Shewanella oneidensis* MR-1). Parallel studies with 7Ca （*Shewanella* sp. Hac353) and *Shewanella oneidensis* MR-1 showed that the microfluidic-cathode MFC array could not only be as efficient as the batch-mode MFC array, but also have long-term operation abilities and higher power outputs.

(4) 24-well microfluidic MFC array: This MFC array is upgraded from the microfluidic-cathode MFC array by integrating microfluidic controllable anode chambers into the system. The microfluidic anode chambers have 4 isolated microfluidic channels with each connecting to 6 anode chambers, such that 24 different anodic conditions could be tested simultaneously. This further extended the application of the MFC arrays, making it suitable for long-term anodic parameter studies such as substrate test for microbial metabolism studies. The device has been used for substrate screening with different microbial species, and power generations of different combinations were analyzed.

(5) 96-well batch-mode MFC array: To further increase the throughput of the MFC array, we fabricated a 96-well batch-mode MFC array. Similar design as

the 24-well batch-mode MFC array was used. Power generation with *Shewanella oneidensis* MR-1 loaded in the anode chambers showed that the power density was about 10 times lower than the 24-well MFC array. The performance of the device need to be further improved to decrease internal resistance and increase power outputs for parallel screening studies.

(6) 96-well microfluidic-cathode MFC array: To decrease internal resistance and provide catholyte replenishment capability to the 96-well MFC array, we designed and fabricated a 96-well microfluidic-cathode MFC array. The microfluidic cathode was characterized for fluid isolation and electrical isolation. Complete electrical isolation was achieved with the normally closed valve design. Besides, to decrease internal resistance and realize automatic catholyte loading, the thickness of the cathode chamber was decreased from 2 mm to several hundreds of micrometers. The functionality of the device will be further extended by integrating microfluidic anode such that the full capability of microfluidic control over both anolyte and catholyte replenishment could be realized.

8.2   Future studies

We have successfully developed several platforms of MFC arrays with different functionalities and utilized the arrays for environmental microbe screening. Following are a few suggestions for the future studies with the MFC arrays.

8.2.1 Device design and system operation

Device design and system operation need to be further improved in the following aspects:

(1) The microfluidic MFC array with microfluidic anode chambers need to be further improved to eliminate cross-contamination issue that may happen after several days of operation. Two strategies could be tested: first, separate main flow channel flush and substrate inlets. Second, increase membrane robustness.

(2) LabView^{TM} program could be designed to realize automatic control and data analysis, including solenoid valve control, data acquisition, substrate and catholyte replenishment control to eliminate manual labor.

(3) Ninety six-well device characterization and microfluidic anode chamber integration. The microfluidic cathode of the 96-well MFC array has been well characterized, and the design principle could be used for the design of the microfluidic anode layer. However, periodic anolyte replenishment have to be implemented if using the similar design as the microfluidic anode shown in the 24-well microfluidic MFC array, and the thickness of anode chambers need to be increased compared to the several hundreds micrometer thick cathode chamber layer. If continuous flow anode chamber needs to be integrated, separation of outflow channels is required to prevent cross contamination.

(4) The current platforms are all based on stacking multiple functional layers (anode electrode, anode chamber, PEM, cathode chamber, cathode electrode). It will be very hard to further increase the throughput beyond 96-well MFCs.

Breakthroughs could be made if all the functional compartments could be integrated on a single layer. However, PEM may not be applicable in this design.

8.2.2 Biological studies

Biological studies utilizing the developed MFC arrays could be further investigated as follows:

(1) Environmental samples from different locations have been screened with the developed MFC arrays. So far no super microbes that can generate more than 10 times higher power than *Shewanella oneidensis* MR-1 have been uncovered. Most of the tested samples are below 10x range compared to *Shewanella*. It is highly possible that the naturally occurring metabolism of microbes for electron transfer is inherently low. It is interesting to use MFC as a tool for microbiology studies of electricigens, such as electron transfer mechanism studies.

(2) Substrate screenings with the microfluidic MFC array with anolyte replenishment need to be further studied. Current results show that microbes with different substrates have different power outputs. Future work will need to further analyze the columbic efficiencies of different substrates. The MFC array could be also used as a tool for electricity generation mechanism analysis.

8.3 Conclusions

The development of microbial fuel cell arrays as high throughput screening platforms for MFC parallel studies will generate great impacts in the microbial fuel cell field. The

arrays have integrated 24 or 96 miniature MFC units on a single device that are capable of conducting 24 or 96 parallel studies simultaneously. Multi-functionality of the developed MFC array makes it suitable for versatile MFC studies. The batch-mode MFC array is suitable for short-term parallel studies with high reproducibility. Long-term operation of the MFC array is also achievable through catholyte replenishment with the microfluidic-cathode MFC array, and both lifetime and power generation could be greatly improved. Long-term anodic parameter parallel studies are also available with the microfluidic MFC array that has microfluidic control over both catholyte replenishment and anolyte replenishment. With the 96-well MFC array, the throughput of parallel studies is greatly improved. Anaerobic chambers could also be equipped to conduct studies requiring strict anaerobic environment. The microfabricated MFC array system has the capacity to conduct most of the conventional MFC parallel studies to improve the current MFC technologies and to contribute to the next generations MFCs for practical use.

REFERENCES

1.   N. S. Lewis and D. G. Nocera, *Proc. Nat. Acad. Sci., U.S.A.*, 2006, **103**, 15729-15735.

2.   British Petroleum, *BP Statistical Review of World Energy June 2011,* http://www.bp.com/assets/bp_internet/globalbp/globalbp_uk_english/reports_and_publications/statistical_energy_review_2011/STAGING/local_assets/pdf/statistical_review_of_world_energy_full_report_2011.pdf, Accessed August 17, 2011, 2011.

3.   B. E. Logan, *Microbial Fuel Cells*, John Wiley & Sons, Inc., Hoboken, NJ, 2007.

4.   U.S. Environmental Protection Agency, *Inventory of U.S. Greenhouse Gas Emissions and Sinks: 1990-2009,* http://www.epa.gov/climatechange/emissions/downloads11/US-GHG-Inventory-2011-Complete_Report.pdf Accessed August,17 2011.

5.   I. Dincer, *Renew. Sust. Energ. Rev.*, 2000, **4**, 157-175.

6.   R. Gross, M. Leach and A. Bauen, *Environ. Int.*, 2003, **29**, 105-122.

7.   B. E. Centre, *What Is Biomass?* http://www.biomassenergycentre.org.uk/portal/page?_pageid=76,15049&_dad=portal&_schema=portal, Accessed August, 17 2011.

8.   M. C. Potter, *Proc. R. Soc. Lond. B,* 1911, **84**, 260-276.

9.   R. M. Allen and H. P. Bennetto, *Appli. Biochem.Biotechnol.*, 1993, **39**, 27-40.

10.   B. H. Kim, H. J. Kim, M. S. Hyun and D. H. Park, *J. Microbiol. Biotechnol.*, 1999, **9**, 127-131.

11.   H. J. Kim, M. S. Hyun, I. S. Chang and B. H. Kim, *J. Microbiol. Biotechnol.*, 1999, **9**, 365-367.

12.   S. K. Chaudhuri and D. R. Lovley, *Nat. Biotechnol.*, 2003, **21**, 1229-1232.

13.   I. A. Ieropoulos, J. Greenman, C. Melhuish and J. Hart, *Enzyme Microb. Technol.*, 2005, **37**, 238-245.

14.   D. R. Lovley, *Curr. Opin. Biotechnol.*, 2008, **19**, 564-571.

15. V. G. Debabov, *Microbiology*, 2008, **77**, 123-131.

16. D. R. Lovley, *Nat. Rev. Micro.*, 2006, **4**, 497-508.

17. Z. Du, H. Li and T. Gu, *Biotechnol. Adv.*, **25**, 464-482.

18. A. Shantaram, H. Beyenal, R. R. A. Veluchamy and Z. Lewandowski, *Environ. Sci. Technol.*, 2005, **39**, 5037-5042.

19. C. Donovan, A. Dewan, D. Heo and H. Beyenal, *Environ. Sci. Technol.*, 2008, **42**, 8591-8596.

20. L. M. Tender, S. A. Gray, E. Groveman, D. A. Lowy, P. Kauffman, J. Melhado, R. C. Tyce, D. Flynn, R. Petrecca and J. Dobarro, *J. Power Sources*, 2008, **179**, 571-575.

21. J. C. Biffinger, J. N. Byrd, B. L. Dudley and B. R. Ringeisen, *Biosens. Bioelectron.*, 2008, **23**, 820-826.

22. K. Rabaey and J. Keller, *Water Sci. Technol.*, 2008, **57**, 655-659.

23. S. Wilkinson, *Auton. Robot.*, 2000, **9**, 99-111.

24. F. Davis and S. P. J. Higson, *Biosens. Bioelectron.*, 2007, **22**, 1224-1235.

25. D. Xing, Y. Zuo, S. Cheng, J. M. Regan and B. E. Logan, *Environ. Sci. Technol.*, 2008, **42**, 4146-4151.

26. S.-Y. Teh, R. Lin, L.-H. Hung and A. P. Lee, *Lab Chip*, 2008, **8**, 198-220.

27. V. Neburchilov, J. Martin, H. Wang and J. Zhang, *J. Power Sources*, 2007, **169**, 221-238.

28. P. Lens and L. H. Pol, *Environmental Technologies to Treat Sulfur Pollution: Principles and Engineering*, IWA Publishing, London, 2000.

29. F. Zhao, N. Rahunen, J. R. Varcoe, A. Chandra, C. Avignone-Rossa, A. E. Thumser and R. C. T. Slade, *Environ. Sci. Technol.*, 2008, **42**, 4971-4976.

30. K. Rabaey, K. Van de Sompel, L. Maignien, N. Boon, P. Aelterman, P. Clauwaert, L. De Schamphelaire, H. T. Pham, J. Vermeulen, M. Verhaege, P. Lens and W. Verstraete, *Environ. Sci. Technol.*, 2006, **40**, 5218-5224.

31. H. Liu and B. E. Logan, *Environ. Sci. Technol.*, 2004, **38**, 4040-4046.

32. B. Min, J. Kim, S. Oh, J. M. Regan and B. E. Logan, *Water Res.*, 2005, **39**, 4961-4968.

33. J. R. Kim, B. Min and B. E. Logan, *Appl. Microbiol. Biotechnol.*, 2005, **68**, 23-30.

34. K. Byung Hong, C. In Seop and G. M. Gadd, *Appl. Microbiol. Biotechnol.*, 2007, **76**, 485-494.

35. A. Dewan, H. Beyenal and Z. Lewandowski, *Environ. Sci. Technol.*, 2008, **42**, 7643-7648.

36. B. E. Logan, *Environ. Sci. Technol.*, 2004, **38**, 160A-167A.

37. P. M. Grant, *Nature*, 2003, **424**, 129-130.

38. H.-S. Lee, M. B. Salerno and B. E. Rittmann, *Environ. Sci. Technol.*, 2008, **42**, 2401-2407.

39. D. B. Levin, L. Pitt and M. Love, *Int. J Hydrogen Energy*, 2004, **29**, 173-185.

40. J. Woodward, M. Orr, K. Cordray and E. Greenbaum, *Nature*, 2000, **405**, 1014.

41. K. Rabaey, L. Angenent, U. Schroder and J. Keller, *Bioelectrochemical Systems*, IWA Publishing, London, UK, 2010.

42. J. D. Wall, C. S. Harwood and A. Demain, *Bioenergy*, ASM Press, Washington, DC, 2008.

43. B. E. Logan, D. Call, S. Cheng, H. V. M. Hamelers, T. H. J. A. Sleutels, A. W. Jeremiasse and R. A. Rozendal, *Environ. Sci. Technol.*, 2008, **42**, 8630-8640.

44. H. Liu, S. Grot and B. E. Logan, *Environ. Sci. Technol.*, 2005, **39**, 4317-4320.

45. R. A. Rozendal, H. V. M. Hamelers, G. J. W. Euverink, S. J. Metz and C. J. N. Buisman, *Int. J. Hydrogen Energy*, 2006, **31**, 1632-1640.

46. S. Cheng and B. E. Logan, *PNAS*, 2007, **104**, 18871-18873.

47. H. Hu, Y. Fan and H. Liu, *Water Res.*, 2008, **42**, 4172-4178.

48. D. Call and B. E. Logan, *Environ. Sci. Technol.*, 2008, **42**, 3401-3406.

49.   P. A. Selembo, J. M. Perez, W. A. Lloyd and B. E. Logan, *Int. J. Hydrogen Energy*, 2009, **34**, 5373-5381.

50.   G. K. Rader and B. E. Logan, *J. Hydrogen Energy*, 2010, **35**, 8848-8854.

51.   I. S. Chang, H. Moon, J. K. Jang and B. H. Kim, *Biosens. Bioelectron.*, 2005, **20**, 1856-1859.

52.   I. S. Chang, J. K. Jang, G. C. Gil, M. Kim, H. J. Kim, B. W. Cho and B. H. Kim, *Biosens. Bioelectron.*, 2004, **19**, 607-613.

53.   B. H. Kim, I. S. Chang, G. Cheol Gil, H. S. Park and H. J. Kim, *Biotechnol. Lett.*, 2003, **25**, 541-545.

54.   N. E. Stein, K. J. Keesman, H. V. M. Hamelers and G. van Straten, *Biosens. Bioelectron.*, 2011, **26**, 3115-3120.

55.   J. M. Tront, J. D. Fortner, M. Plˆtze, J. B. Hughes and A. M. Puzrin, *Biosens. Bioelectron.*, 2008, **24**, 586-590.

56.   D. Jiang, M. Curtis, E. Troop, K. Scheible, J. McGrath, B. Hu, S. Suib, D. Raymond and B. Li, *Int. J. Hydrogen Energy*, 2011, **36**, 876-884.

57.   L. Zhang, C. Liu, L. Zhuang, W. Li, S. Zhou and J. Zhang, *Biosens. Bioelectron.*, 2009, **24**, 2825-2829.

58.   P. Aelterman, K. Rabaey, H. T. Pham, N. Boon and W. Verstraete, *Environ. Sci. Technol.*, 2006, **40**, 3388-3394.

59.   D. R. Bond and D. R. Lovley, *Appl. Environ. Microbiol.*, 2003, **69**, 1548-1555.

60.   Y. A. Gorby, S. Yanina, J. S. McLean, K. M. Rosso, D. Moyles, A. Dohnalkova, T. J. Beveridge, I. S. Chang, B. H. Kim, K. S. Kim, D. E. Culley, S. B. Reed, M. F. Romine, D. A. Saffarini, E. A. Hill, L. Shi, D. A. Elias, D. W. Kennedy, G. Pinchuk, K. Watanabe, S. Ishii, B. Logan, K. H. Nealson and J. K. Fredrickson, *Proc. Nat. Acad. Sci., U.S.A.*, 2006, **103**, 11358-11363.

61.   G. Reguera, K. P. Nevin, J. S. Nicoll, S. F. Covalla, T. L. Woodard and D. R. Lovley, *Appl. Environ. Microbiol.*, 2006, **72**, 7345-7348.

62.   K. Rabaey, N. Boon, S. D. Siciliano, M. Verhaege and W. Verstraete, *Appl. Environ. Microbiol.*, 2004, **70**, 5373-5382.

63. D.H. Park, M.Laivenieks, M.V. Guettler, M.K. Jain, J.G. Zeikus, *Environ. Microbiol.*, 1999, **65**, 2912-2917

64. K. Rabaey and W. Verstraete, *Trends Biotechnol.*, 2005, **23**, 291-298.

65. G. Reguera, K. D. McCarthy, T. Mehta, J. S. Nicoll, M. T. Tuominen and D. R. Lovley, *Nature*, 2005, **435**, 1098-1101.

66. E. A. Burton, K. A. Simon, S. Hou, D. Ren and Y.-Y. Luk, *Langmuir*, 2009, **25**, 1547-1553.

67. H. Hou, L. Li, Y. Cho, P. de Figueiredo and A. Han, *PLoS ONE*, 2009, **4**, e6570.

68. K. Watanabe, *J. Biosci. Bioeng.*, 2008, **106**, 528-536.

69. A. Bergel, D. Feron and A. Mollica, *Electrochem. Commun.*, 2005, **7**, 900-904.

70. D. R. Bond, D. E. Holmes, L. M. Tender and D. R. Lovley, *Science*, 2002, **295**, 483-485.

71. B. Min, S. Cheng and B. E. Logan, *Water Res.*, 2005, **39**, 1675-1686.

72. S. Oh, B. Min and B. E. Logan, *Environ. Sci. Technol.*, 2004, **38**, 4900-4904.

73. K. Rabaey, G. Lissens, S. D. Siciliano and W. Verstraete, *Biotechnol. Lett.*, 2003, **25**, 1531-1535.

74. B. E. Logan, B. Hamelers, R. Rozendal, U. Schroder, J. Keller, S. Freguia, P. Aelterman, W. Verstraete and K. Rabaey, *Enviro. Sci. Technol.*, 2006, **40**, 5181-5192.

75. S. You, Q. Zhao, J. Zhang, J. Jiang and S. Zhao, *J. Power Sources*, 2006, **162**, 1409-1415.

76. D. A. Lowy, L. M. Tender, J. G. Zeikus, D. H. Park and D. R. Lovley, *Biosens. Bioelectron.*, 2006, **21**, 2058-2063.

77. J. Niessen, U. Schoder, M. Rosenbaum and F. Scholz, *Electrochem. Commun*, 2004, **6**, 571-575.

78. S. R. Crittenden, C. J. Sund and J. J. Sumner, *Langmuir*, 2006, **22**, 9473-9476.

79. C. Jiang, J. M. Elliott, D. J. Cardin and S. C. Tsang, *Langmuir*, 2008, **25**, 534-541.

80.   H. Richter, K. McCarthy, K. P. Nevin, J. P. Johnson, V. M. Rotello and D. R. Lovley, *Langmuir*, 2008, **24**, 4376-4379.

81.   Z. Du, Q. Li, M. Tong, S. Li and H. Li, *Chin. J. Chem. Eng.*, 2008, **16**, 772-777.

82.   Z. Hu, *J. Power Sources*, 2008, **179**, 27-33.

83.   S. Yang, B. Jia and H. Liu, *Bioresour. Technol.*, 2009, **100**, 1197-1202.

84.   E. HaoYu, S. Cheng, K. Scott and B. Logan, *J. Power Sources*, 2007, **171**, 275-281.

85.   A. A.-M. O. Lefebvre, W. K. Ooi, Z. Tang, D. H. C. Chua and H. Y. Ng, *Water Sci. Technol.*, 2008, **57**, 2031-2037.

86.   S.-E. Oh and B. Logan, *Appl. Microbiol. Biotechnol.*, 2006, **70**, 162-169.

87.   H. Liu, R. Ramnarayanan and B. E. Logan, *Environ. Sci. Technol.*, 2004, **38**, 2281-2285.

88.   H. Liu, S. Cheng, L. Huang and B. E. Logan, *J. Power Sources*, 2008, **179**, 274-279.

89.   H. Moon, I. S. Chang, J. K. Jang and B. H. Kim, *Biochem. Eng. J.*, 2005, **27**, 59-65.

90.   H. Moon, I. S. Chang and B. H. Kim, *Bioresour. Technol.*, 2006, **97**, 621-627.

91.   W. C. Lin, M. V. Coppi and D. R. Lovley, *Appl. Environ. Microbiol.*, 2004, **70**, 2525-2528.

92.   J. Jiang and A. Kucernak, *Journal of Electroanalytical Chemistry*, 2004, **567**, 123-137.

93.   Z. He, S. D. Minteer and L. T. Angenent, *Environ. Sci. Technol.*, 2005, **39**, 5262-5267.

94.   N. Wagner, S. D. Minteer and L. T. Angenent, *Environ. Sci. Technol.*, 2006, **40**, 5212-5217.

95.   K. Rabaey, P. Clauwaert, P. Aelterman and W. Verstraete, *Environ. Sci. Technol.*, 2005, **39**, 8077-8082.

96. S. Shin, Y. Choi, S. Na, S. Jung, and S. Kim, *Bull. Korean Chem. Soc.*, 2006, **27**, 281-285.

97. S. E. Oh and B. E. Logan, *J. Power Sources*, 2007, **167**, 11-17.

98. F. Qian and D. E. Morse, *Trends Biotechnol.*, 2011, **29**, 62-69.

99. B. R. Ringeisen, E. Henderson, P. K. Wu, J. Pietron, R. Ray, B. Little, J. C. Biffinger and J. M. Jones-Meehan, *Environ. Sci. Technol.*, 2006, **40**, 2629-2634.

100. Y. Fan, H. Hu and H. Liu, *J. Power Sources*, 2007, **171**, 348-354.

101. H.-Y. Wang, A. Bernarda, C.-Y. Huang, D.-J. Lee and J.-S. Chang, *Bioresour. Technol.*, 2011, **102**, 235-243.

102. F. Qian, Z. He, M. P. Thelen and Y. Li, *Bioresour. Technol.*, 2011, **102**, 5836-5840.

103. Y. Fan, E. Sharbrough and H. Liu, *Environ. Sci. Technol.*, 2008, **42**, 8101-8107.

104. M. Izallalen, R. Mahadevan, A. Burgard, B. Postier, R. Didonato Jr, J. Sun, C. H. Schilling and D. R. Lovley, *Metab. Eng.*, 2008, **10**, 267-275.

105. Y. J. J. Tang, D. Laidlaw, K. Gani and J. D. Keasling, *Biotechnol. Bioeng.*, 2006, **95**, 176-184.

106. G. S. Jadhav and M. M. Ghangrekar, *Bioresour. Technol.*, 2009, **100**, 717-723.

107. B. E. Logan, *Nat. Rev. Micro.*, 2009, **7**, 375-381.

108. B. E. Logan and J. M. Regan, *Trends Microbiol.*, 2006, **14**, 512-518.

109. J. D. Hoheisel, *Nat. Rev. Genet.*, 2006, **7**, 200-210.

110. C. P. B. Siu and M. Chiao, *J. Microelectromech. S.*, 2008, **17**, 1329-1341.

111. J. Biffinger, M. Ribbens, B. Ringeisen, J. Pietron, S. Finkel and K. Nealson, *Biotechnol. Bioeng.*, 2009, **102**, 436-444.

112. D. B. Weibel, W. R. DiLuzio and G. M. Whitesides, *Nat. Rev. Microbiol.*, 2007, **5**, 209-218.

113. Y. N. Xia and G. M. Whitesides, *Annu. Rev. Mater. Sci.*, 1998, **28**, 153-184.

114. J. K. Fredrickson, M. F. Romine, A. S. Beliaev, J. M. Auchtung, M. E. Driscoll, T. S. Gardner, K. H. Nealson, A. L. Osterman, G. Pinchuk, J. L. Reed, D. A. Rodionov, J. L. Rodrigues, D. A. Saffarini, M. H. Serres, A. M. Spormann, I. B. Zhulin and J. M. Tiedje, *Nat. Rev. Microbiol.*, 2008, **6**, 592-603.

115. C. I. Pearce, R. Christie, C. Boothman, H. von Canstein, J. T. Guthrie and J. R. Lloyd, *Biotechnol. Bioeng.*, 2006, **95**, 692-703.

116. B. E. Logan and J. M. Regan, *Environ. Sci. Technol.*, 2006, **40**, 5172-5180.

117. O. Bretschger, A. Obraztsova, C. A. Sturm, I. S. Chang, Y. A. Gorby, S. B. Reed, D. E. Culley, C. L. Reardon, S. Barua, M. F. Romine, J. Zhou, A. S. Beliaev, R. Bouhenni, D. Saffarini, F. Mansfeld, B. H. Kim, J. K. Fredrickson and K. H. Nealson, *Appl. Environ. Microbiol.*, 2007, **73**, 7003-7012.

118. S. i. Ishii, K. Watanabe, S. Yabuki, B. E. Logan and Y. Sekiguchi, *Appl. Environ. Microbiol.*, 2008, **74**, 7348-7355.

119. T. H. Pham, N. Boon, K. De Maeyer, M. Hofte, K. Rabaey and W. Verstraete, *Appl. Microbiol. Biotechnol.*, 2008, **80**, 985-993.

120. T. H. Pham, N. Boon, P. Aelterman, P. Clauwaert, L. De Schamphelaire, L. Vanhaecke, K. De Maeyer, M. Hofte, W. Verstraete and K. Rabaey, *Appl. Microbiol. Biotechnol.*, 2008, **77**, 1119-1129.

121. B. Logan, S. Cheng, V. Watson and G. Estadt, *Environ. Sci. Technol.*, 2007, **41**, 3341-3346.

122. H. Hou, L. Li, P. de Figueiredo and A. Han, *Biosens. Bioelectron.*, 2011, **26**, 2680-2684.

123. F. Qian, Z. He, M. P. Thelen and Y. Li, *Bioresour. Technol.*, 2011, **102**, 5836-5840.

124. F. Qian, M. Baum, Q. Gu and D. E. Morse., *Lab Chip*, 2009, **9**, 3076.

125. Z. Li, Y. Zhang, P. R. LeDuc and K. B. Gregory, *Biotechnol. Bioeng.*, 2011, 2061-2069.

126. A. M. Leach, A. R. Wheeler and R. N. Zare, *Anal. Chem.*, 2003, **75**, 967-972.

127. I. Ieropoulos, J. Winfield and J. Greenman, *Bioresour. Technol.*, 2010, **101**, 3520-3525.

128.   H. Rismani-Yazdi, A. D. Christy, S. M. Carver, Z. Yu, B. A. Dehority and O. H. Tuovinen, *Bioresour. Technol.*, 2011, **102**, 278-283.

129.   K.-J. Chae, M.-J. Choi, J.-W. Lee, K.-Y. Kim and I. S. Kim, *Bioresour. Technol.*, 2009, **100**, 3518-3525.
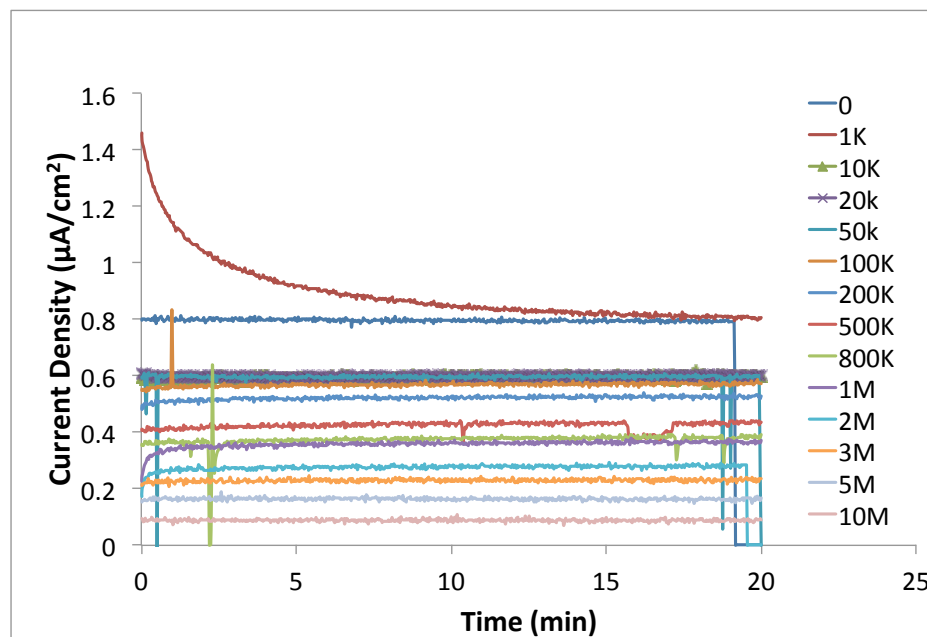
APPENDIX A

FIGURES

Figure A.1 Current change with different external resistances (Unit: Ω) of a 24-well MFC array. Current became stable after 10 min connection, all MFC power measurements in this thesis used 10 min for each resistor connection.
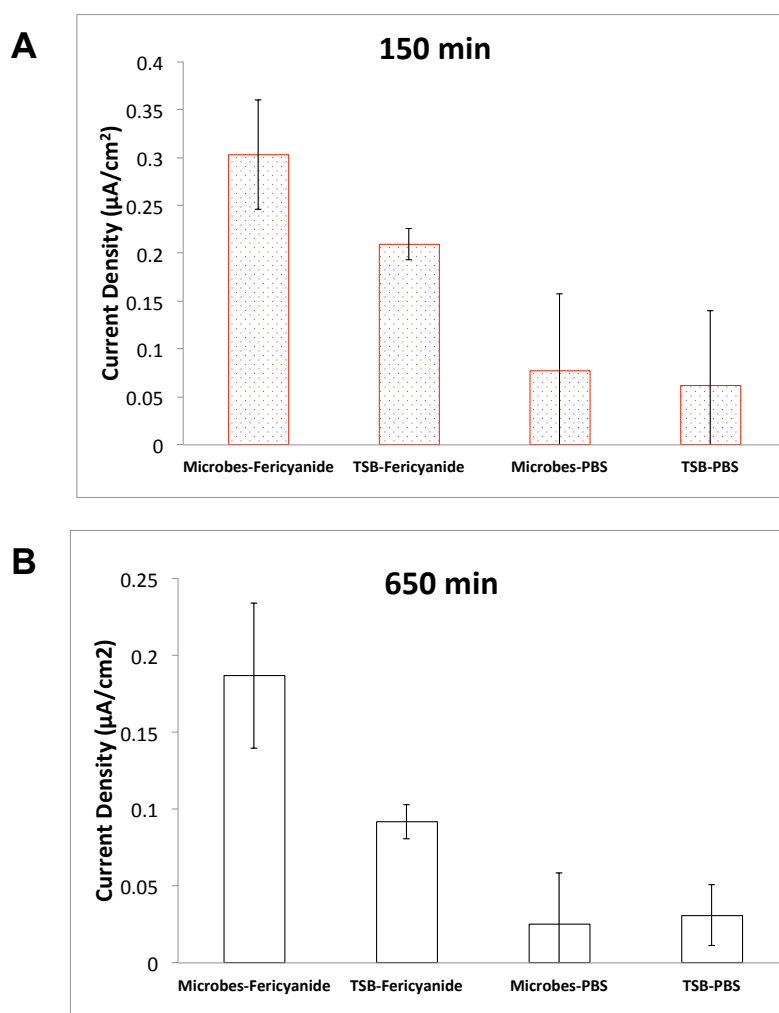
Figure A.2 Current generation comparison with ferricyanide and PBS with catholyte at A: 150 min and B: 650 min after cell loading. 24-well batch-mode MFC array was used with 1 MΩ connected to all units, TSB media was used as negative control (*n = 2-4*). At both 150 min and 650 min, MFC with ferricyanide catholyte generated higher current than PBS catholyte and at 650 min, no dramatic current difference between microbe loaded MFCs and TSB media loaded MFCs with PBS as catholyte.
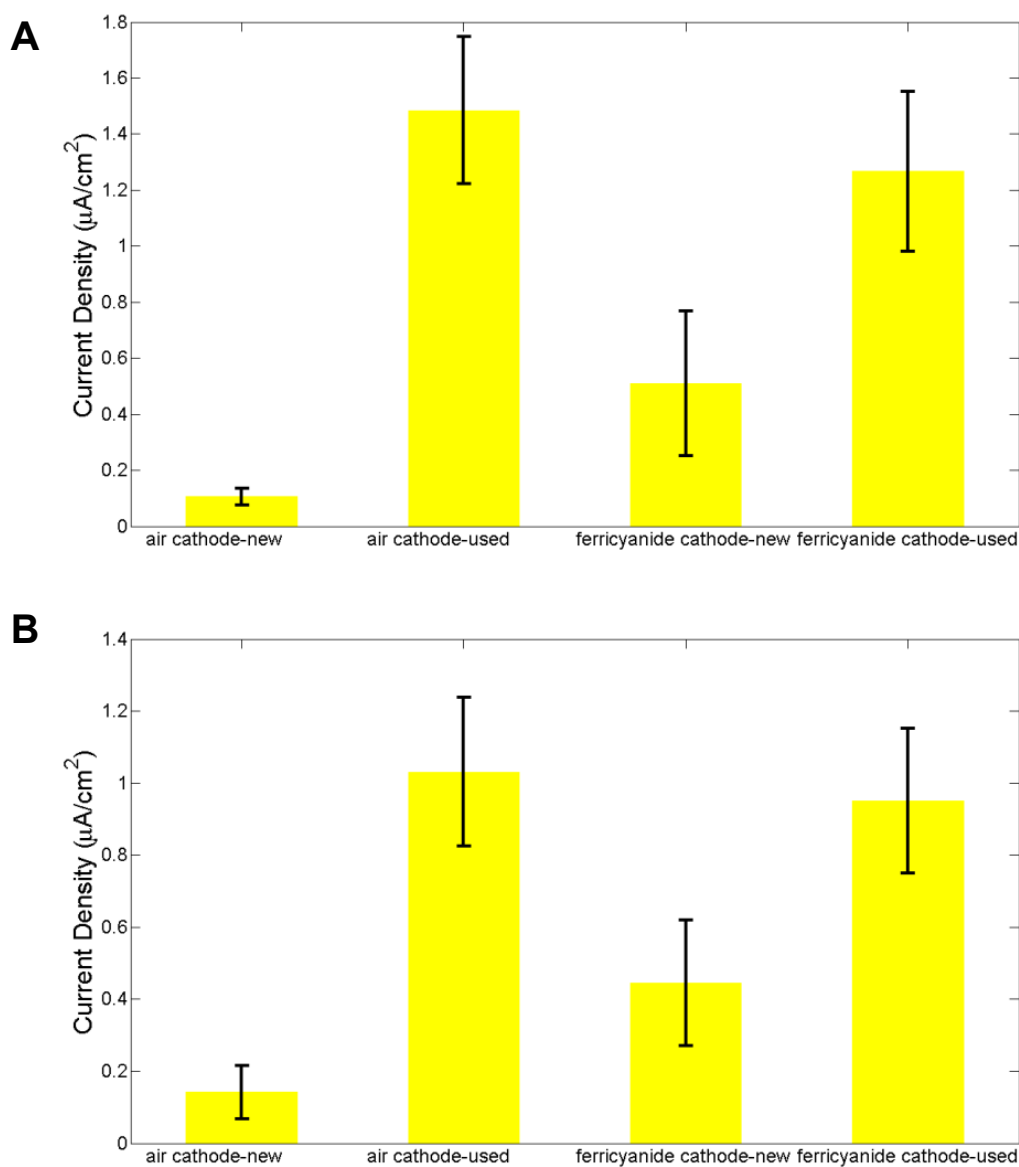
Figure A.3 Current generation comparison of MFC array with new PEM and used PEM. Both air-cathode and ferricyanide-cathode MFC arrays were used for characterization. Current generation at **A:** 1000 min and **B:** 6000 min after cell loading were compared. The results showed that MFCs with used PEM generated higher current. (Used PEM were treated with same protocol for new PEM treatment before reuse)
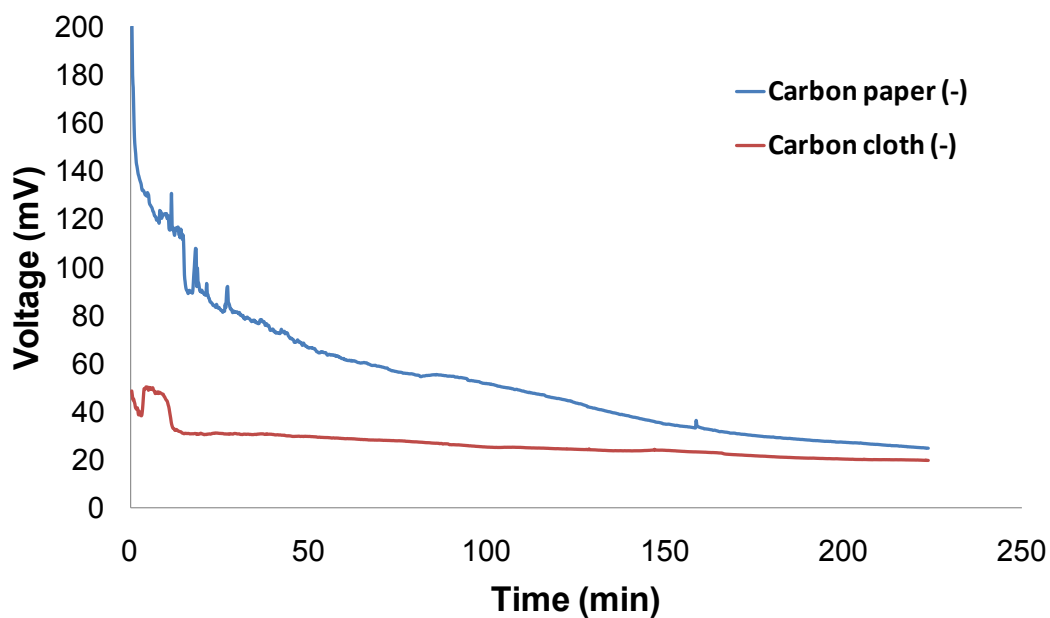
Figure A.4 Comparison of carbon cloth cathode with carbon paper cathode. Result showed that carbon paper generated higher voltage than carbon cloth cathode with 200 KΩ connected.
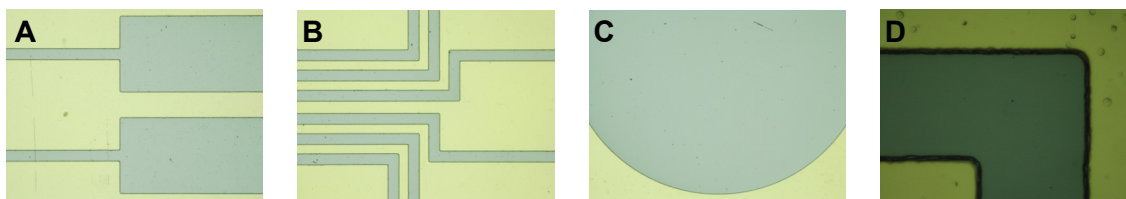
Figure A.5 Microscope images of Pt electrode fabricated with electroplating at A-C: 5X, and D: 50X. (Deposition rate: 12.5 nm/min, thickness: 750 nm)

APPENDIX B

FILM MASKS

24-well MFC array anode/cathode electrode (Clear field mask)
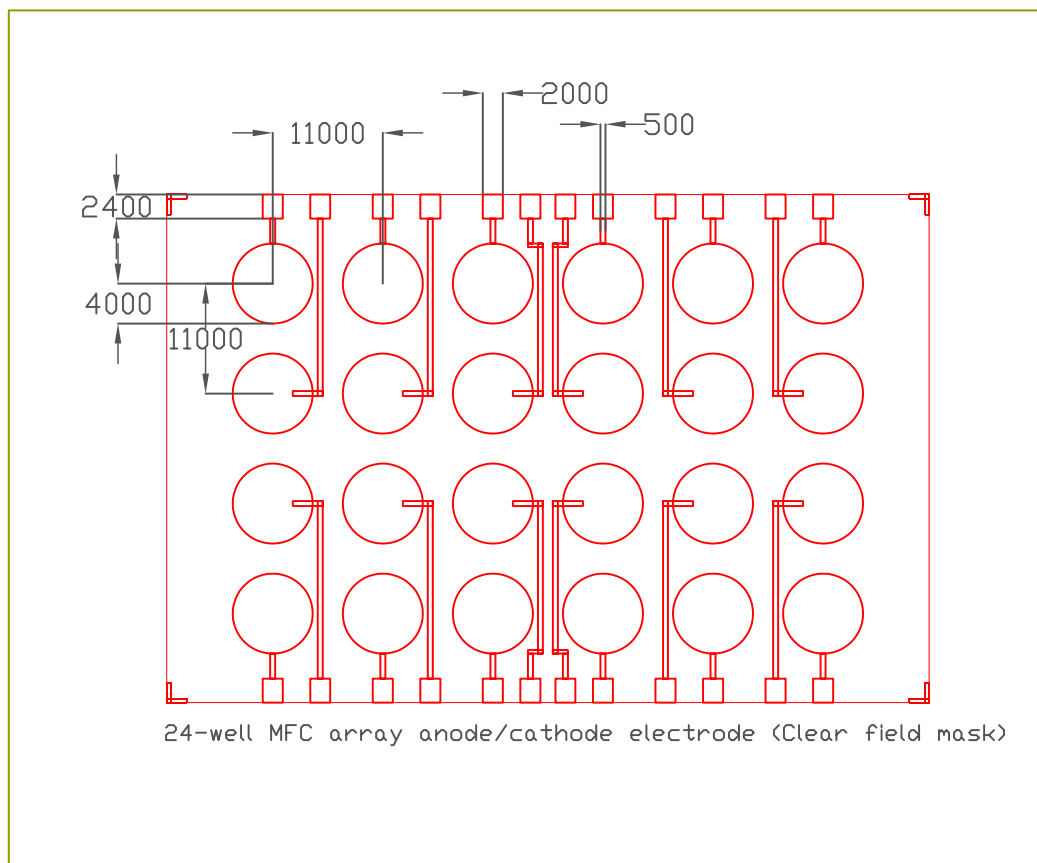
Figure B.1 24-well MFC array electrode (anode and cathode) film mask, clear field.
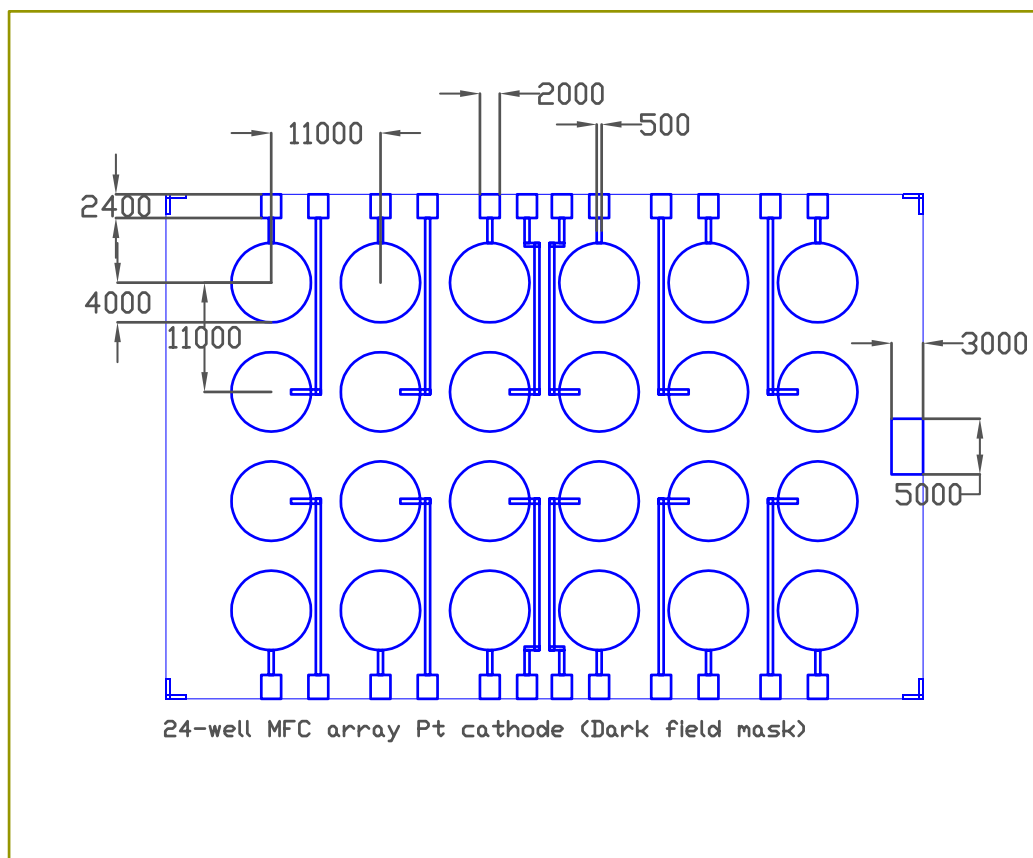
Figure B.2 24-well MFC array Pt cathode film mask, dark field.
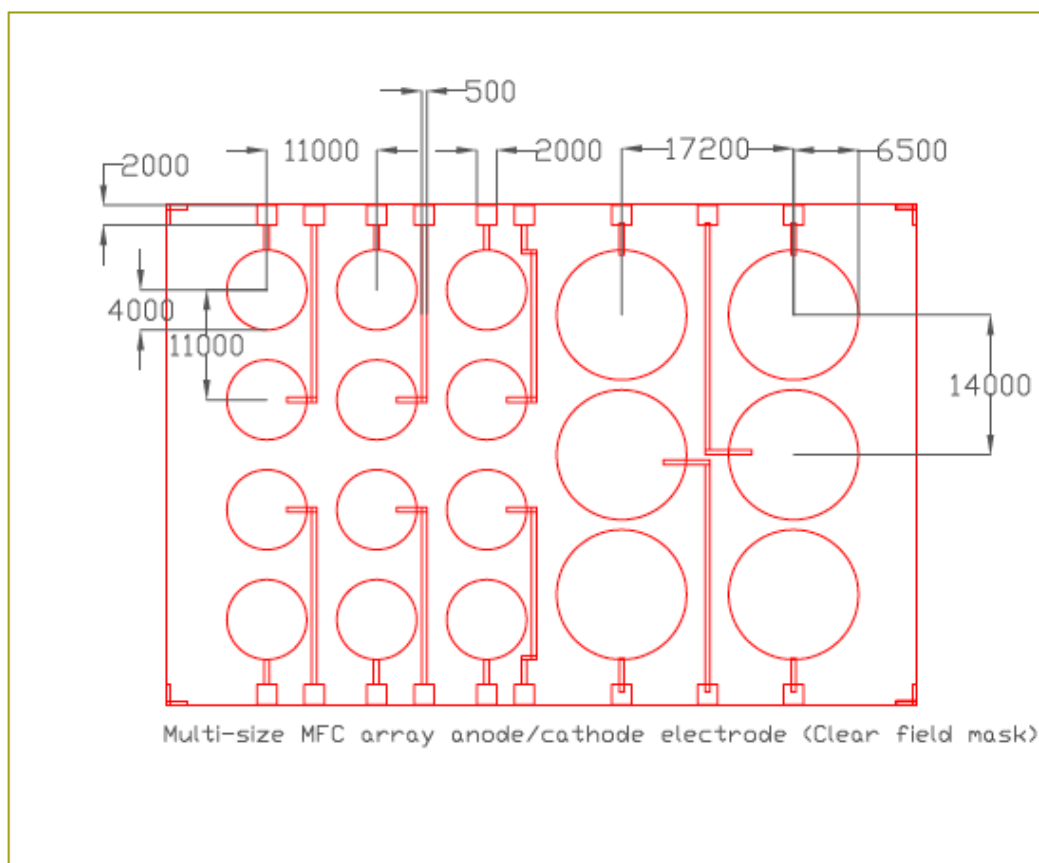
Figure B.3 Multi-well MFC array electrode (anode and cathode) film mask 1, clear field.

24-well MFC array anode/cathode electrode (Clear field mask)
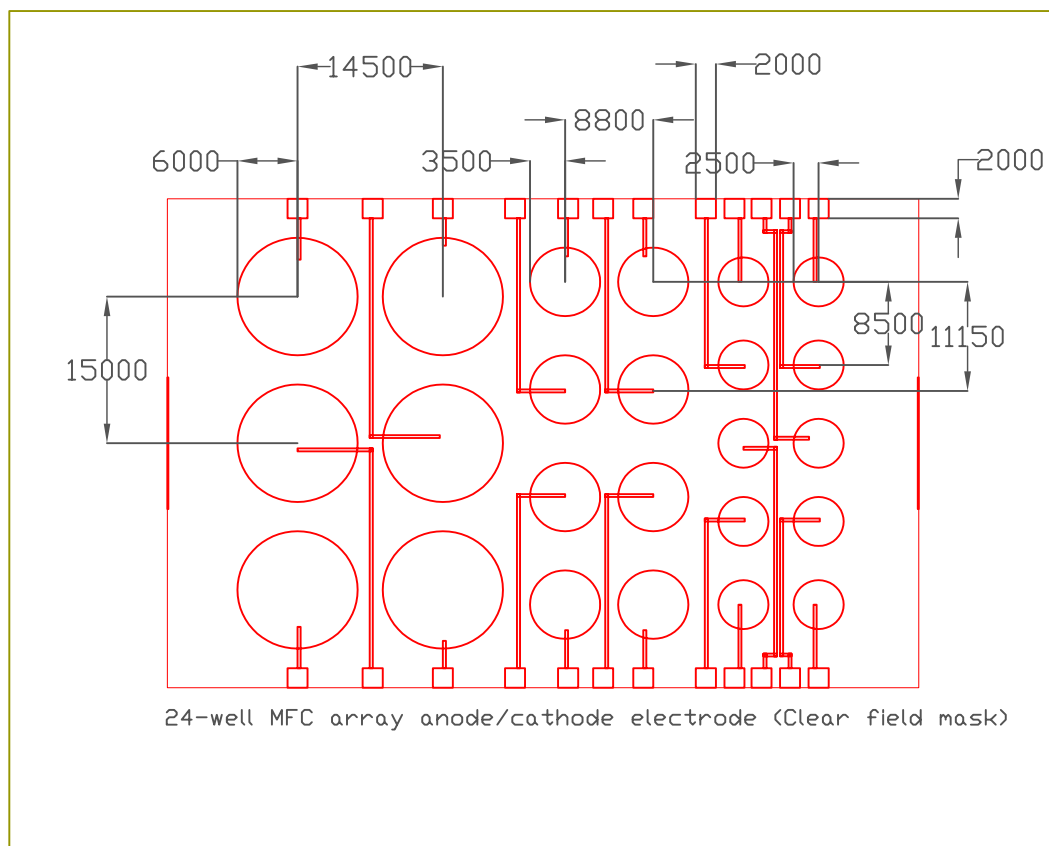
Figure B.4 Multi-well MFC array electrode (anode and cathode) film mask 2, clear field.
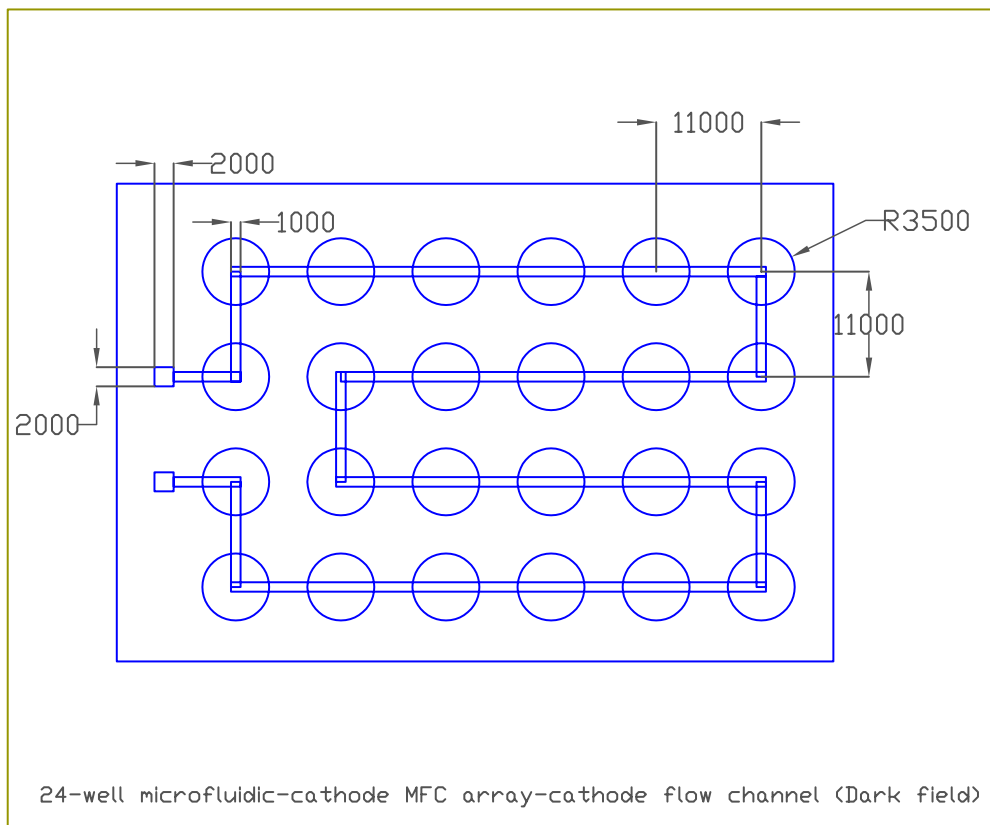
Figure B.5 24-well microfluidic-cathode MFC array cathode flow channel, dark field.
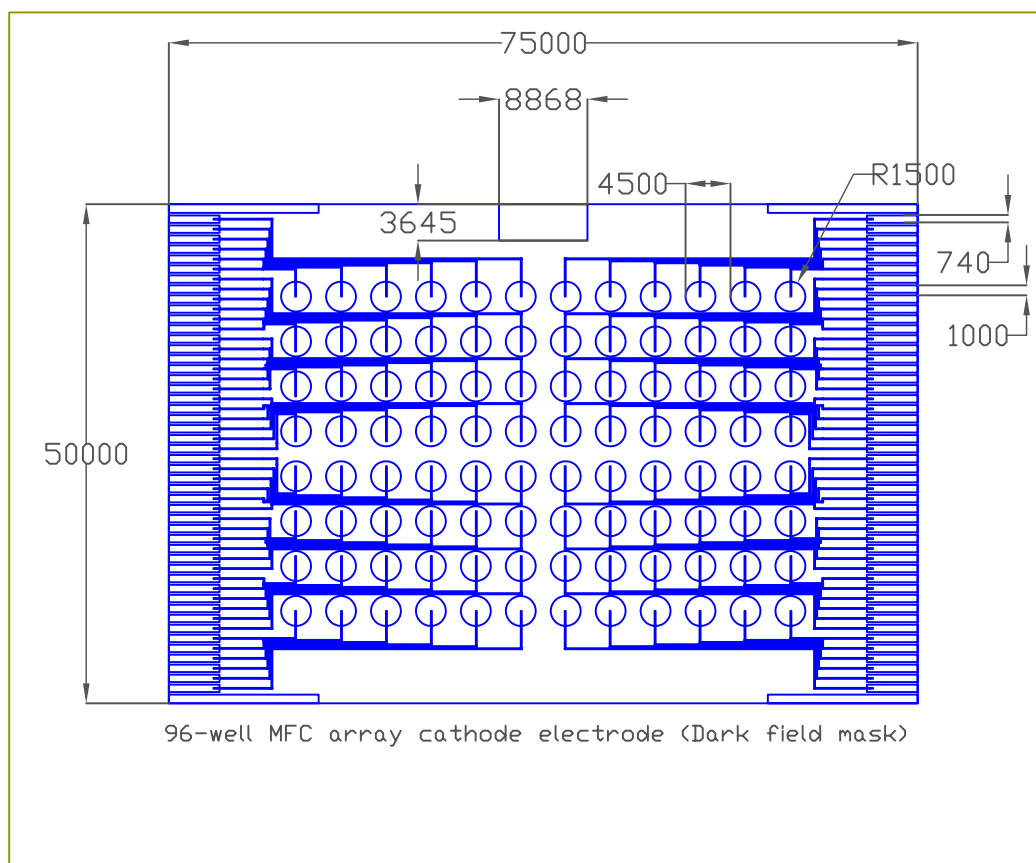
Figure B.6 96-well MFC array Pt cathode electrode film mask, dark field.
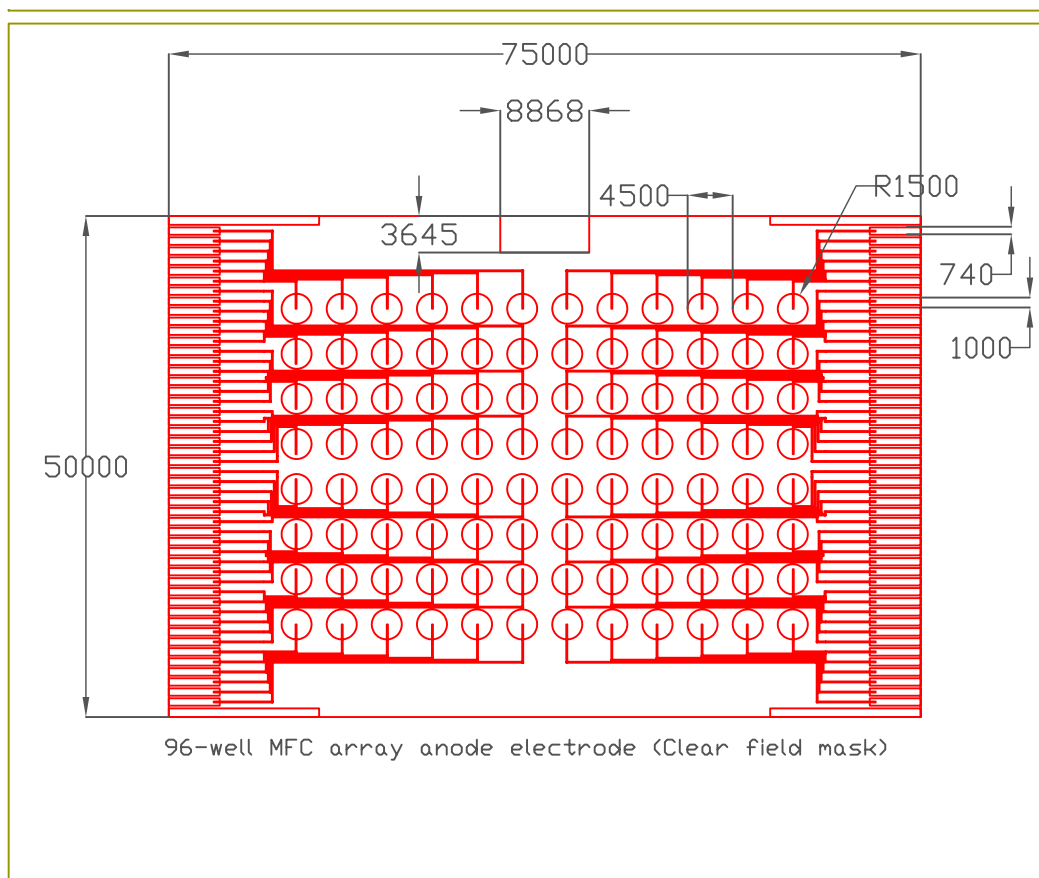
Figure B.7 96-well MFC array anode electrode film mask, clear field.
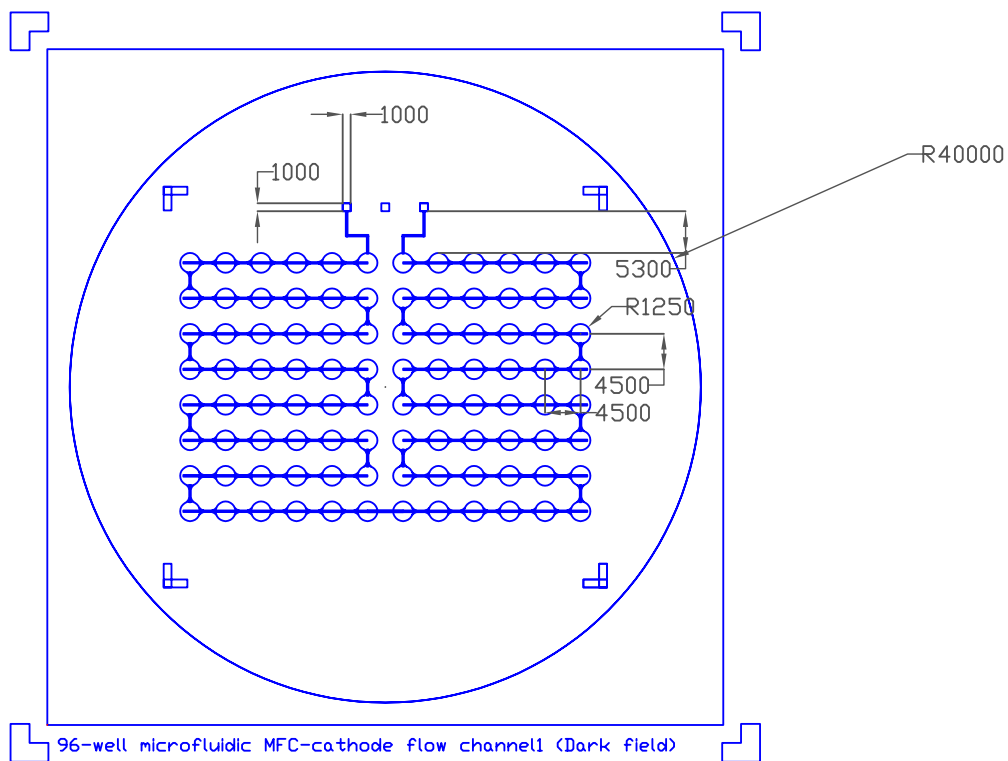
Figure B.8 96-well microfluidic MFC array cathode flow channel (normally-opened valves), design 1, dark field.
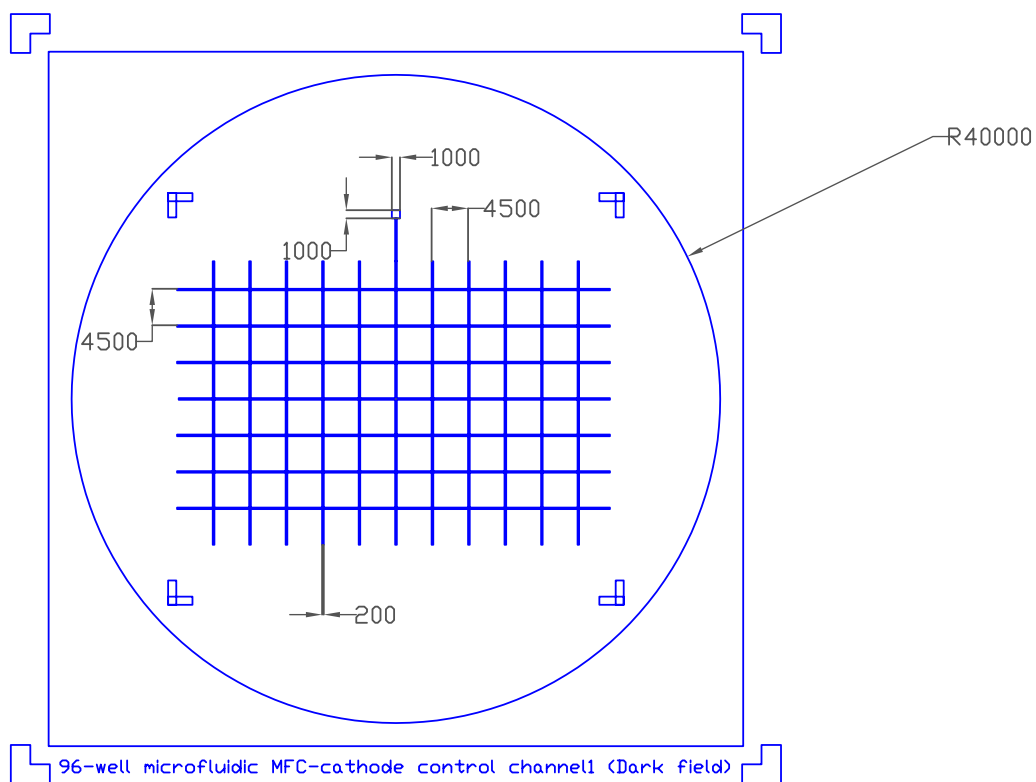
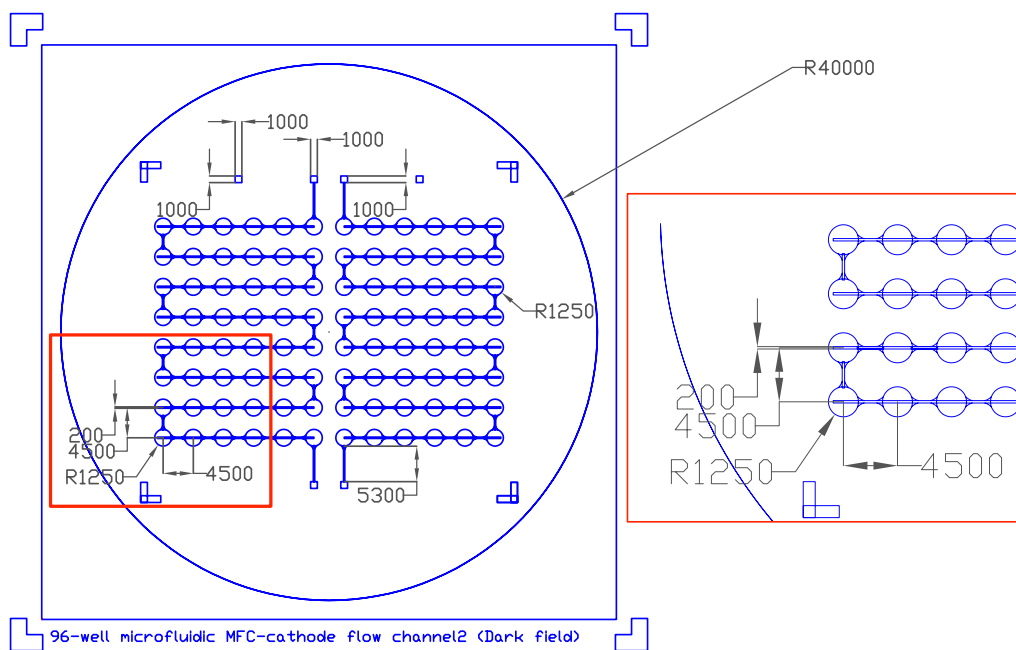**Figure B.9 96-well microfluidic MFC array cathode control channel (normally-opened valves), design 1, dark field.**

Figure B.10 96-well microfluidic MFC array cathode flow channel (normally-opened valves), design 2, dark field. (Right: details of the red rectangular region of the left)
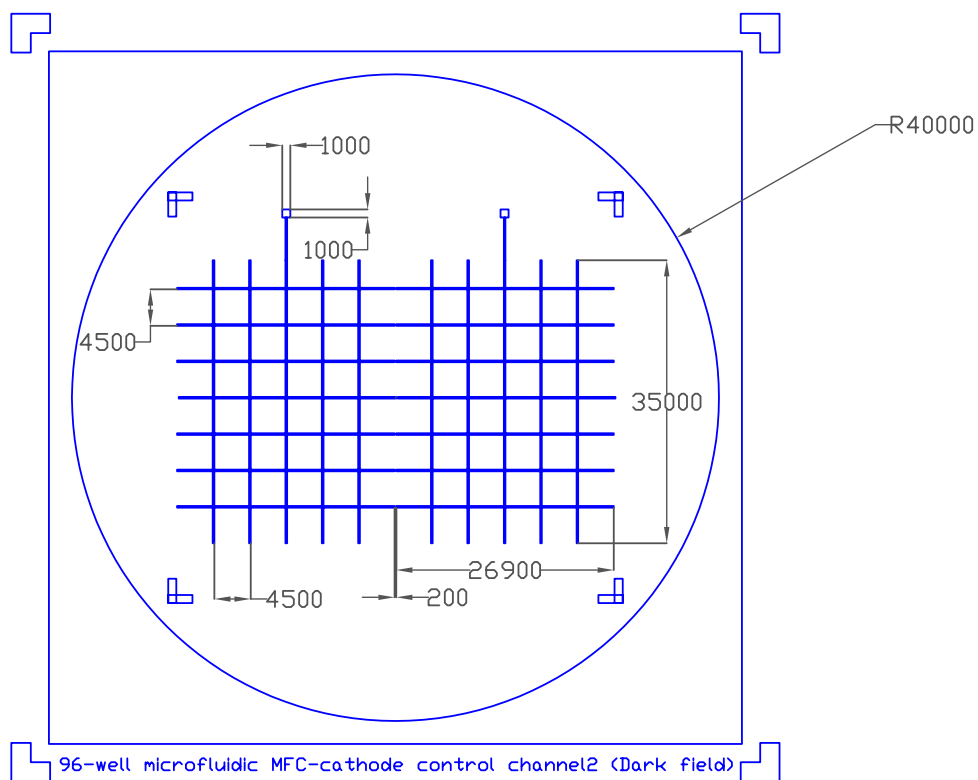
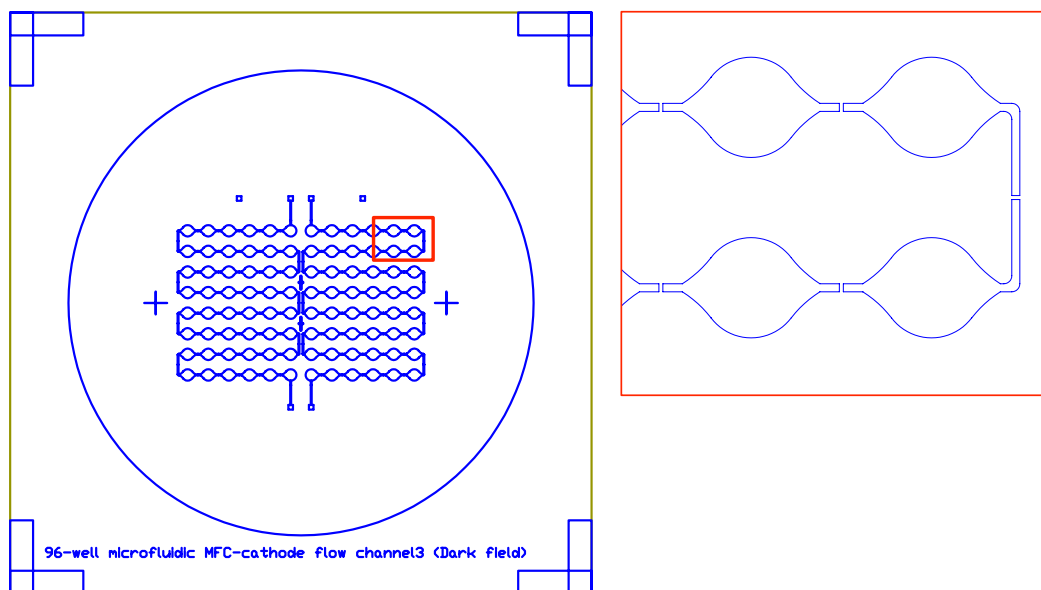**Figure B.11 96-well microfluidic MFC array cathode control channel (normally-opened valves), design 2, dark field.**

96-well microfluidic MFC-cathode flow channel3 (Dark field)

Figure B.12 96-well microfluidic MFC array cathode flow channel (normally-closed valves), design 3, dark field. (Right: details of the red rectangular region of the left)
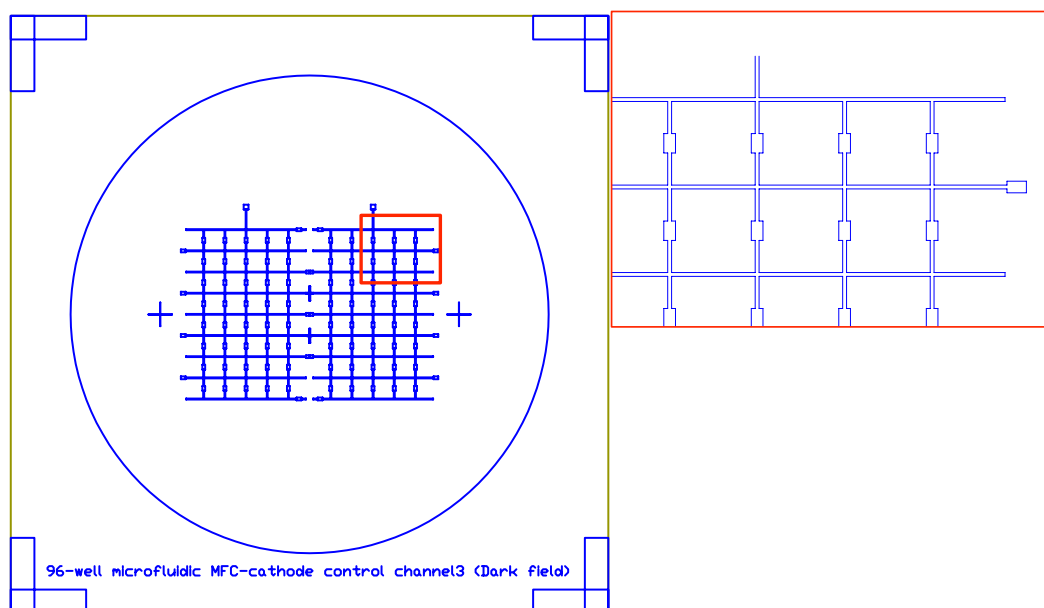
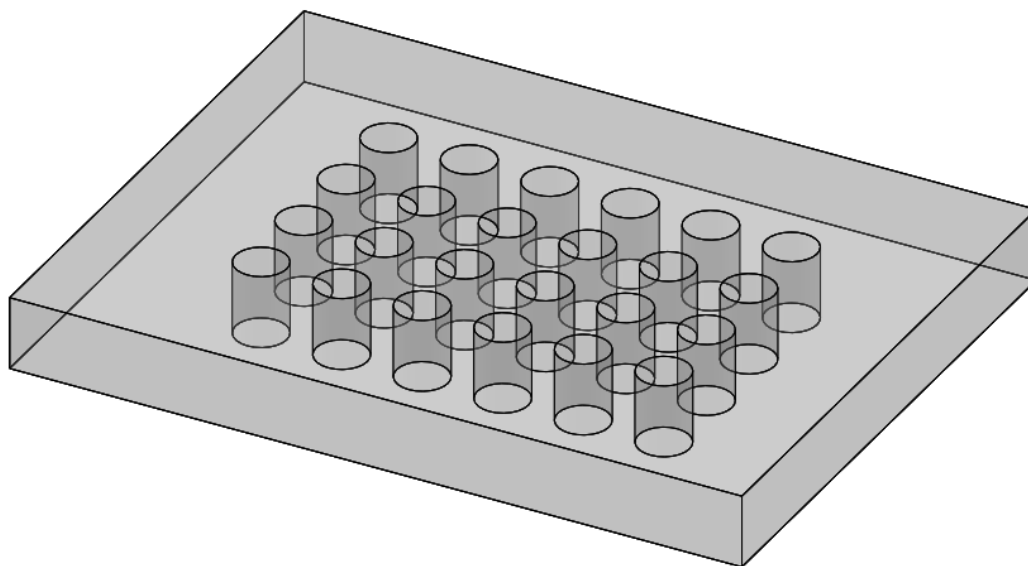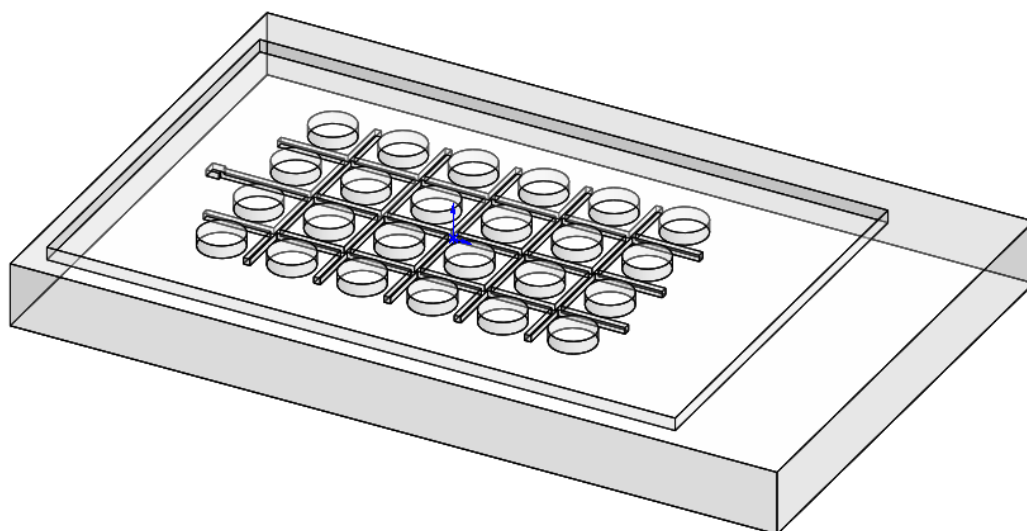96-well microfluidic MFC-cathode control channel3 (Dark field)

Figure B.13 96-well microfluidic MFC array cathode control channel (normally-closed valves), design 3, dark field. (Right: details of the red rectangular region of the left)
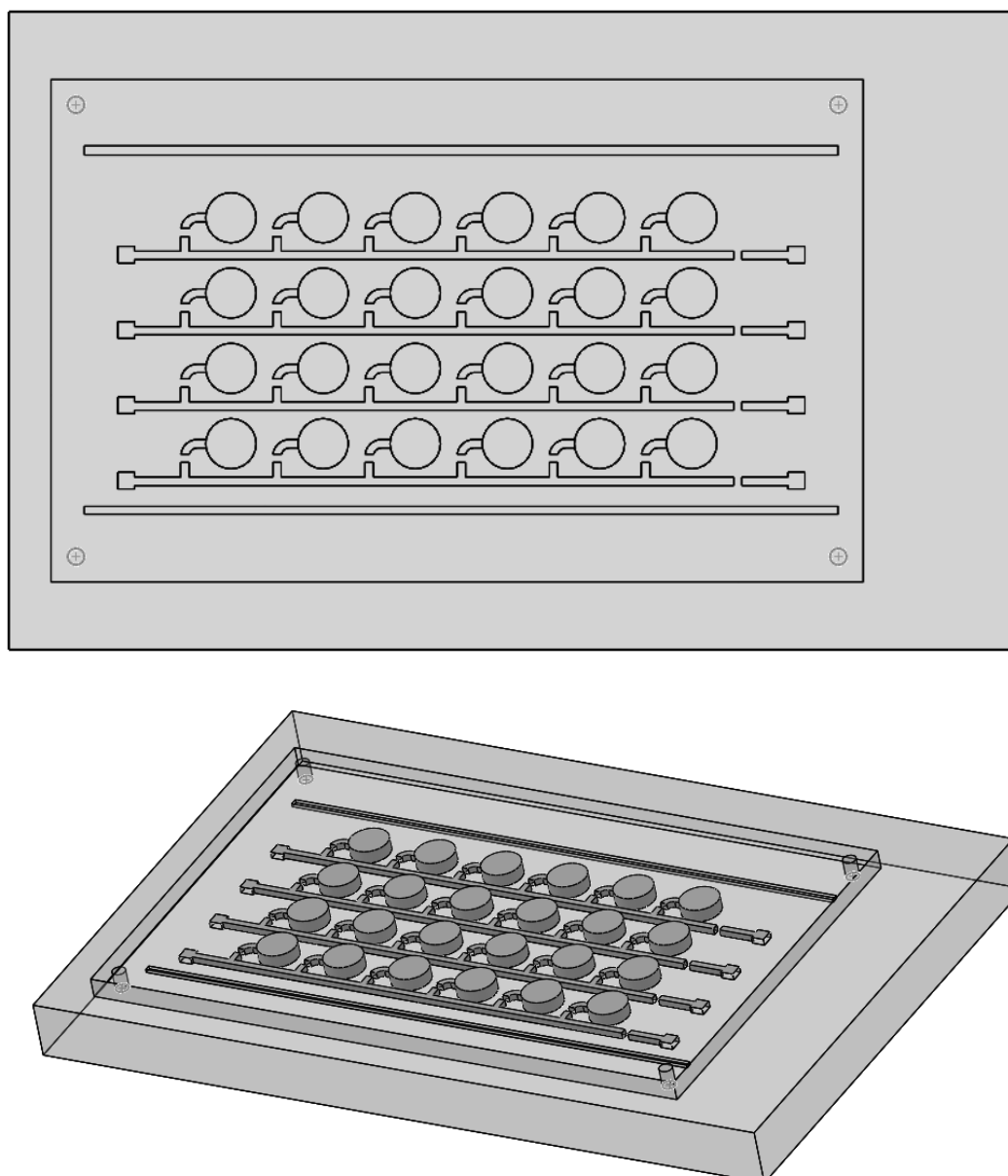
ACRYL MODE DESIGNS

File: 24-well MFC anode chamber.SLDTRP

Figure B.14 Acryl mold for 24-well MFC array PDMS anode chamber fabrication.
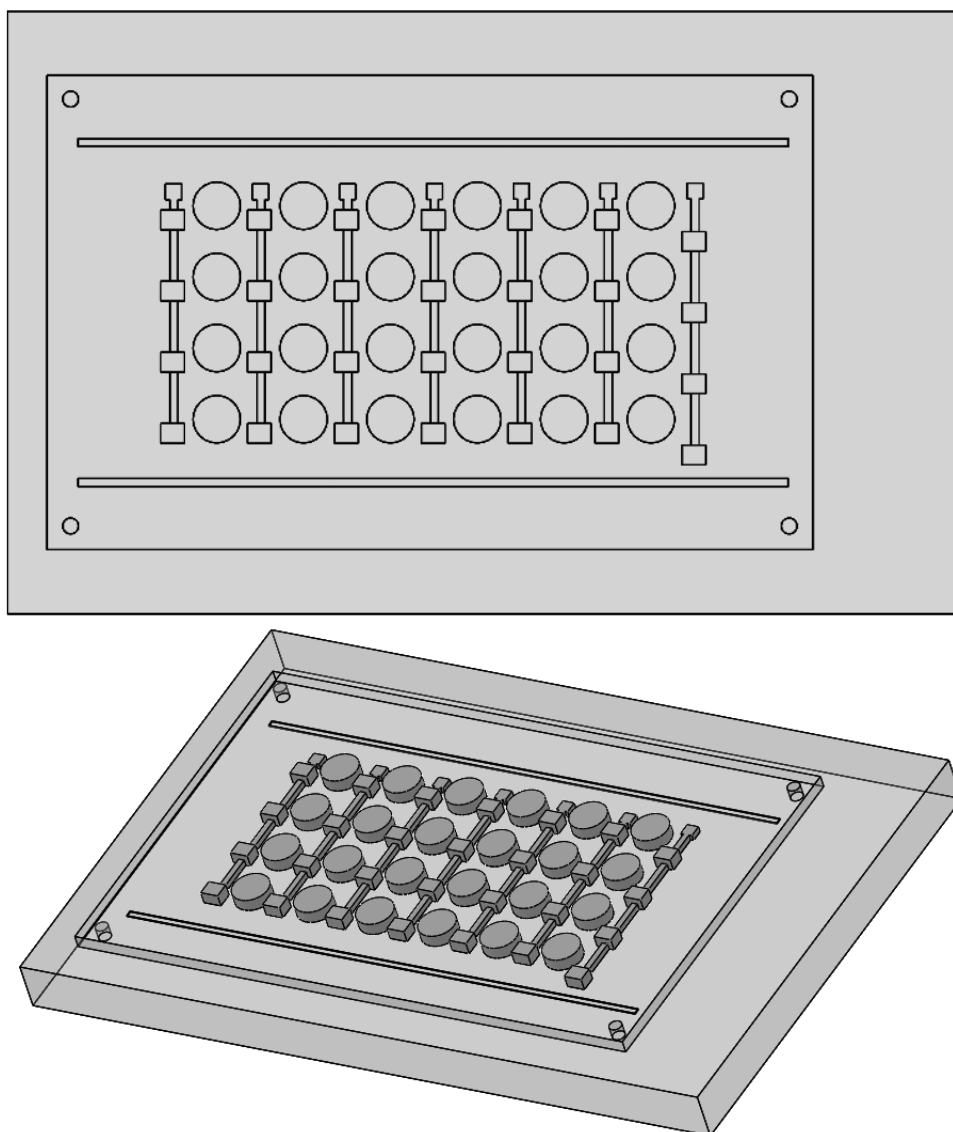
File: 24-well microfluidic-cathode MFC cathode control channel.SLDTRP

Figure B.15 Acryl mold for 24-well microfluidic-cathode MFC array PDMS cathode control channel fabrication.

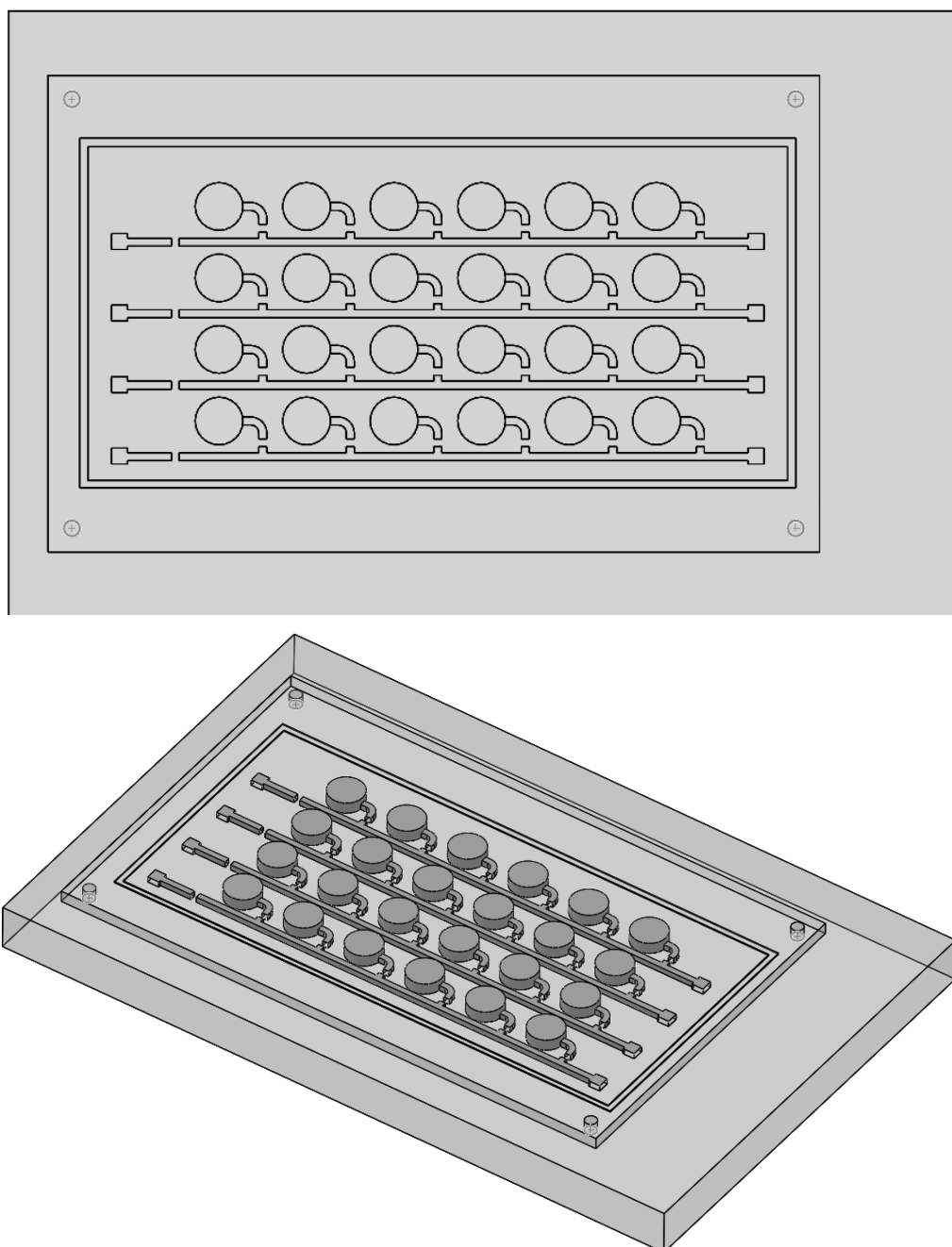File: 24-well microfluidic MFC-inflow channel.SLDTRP

Figure B.16 Acryl mold for 24-well PDMS microfluidic-MFC anode inflow channel fabrication. (Top: top view, bottom: rotated 3D view)

File: 24-well microfluidic MFC-inflow channel control .SLDTRP

Figure B.17 Acryl mold for 24-well PDMS microfluidic-MFC anode inflow channel control fabrication. (Top: top view, bottom: rotated 3D view)

File: 24-well microfluidic MFC-outflow channel.SLDTRP

Figure B.18 Acryl mold for 24-well PDMS microfluidic-MFC anode outflow channel fabrication. (Top: top view, bottom: rotated 3D view)
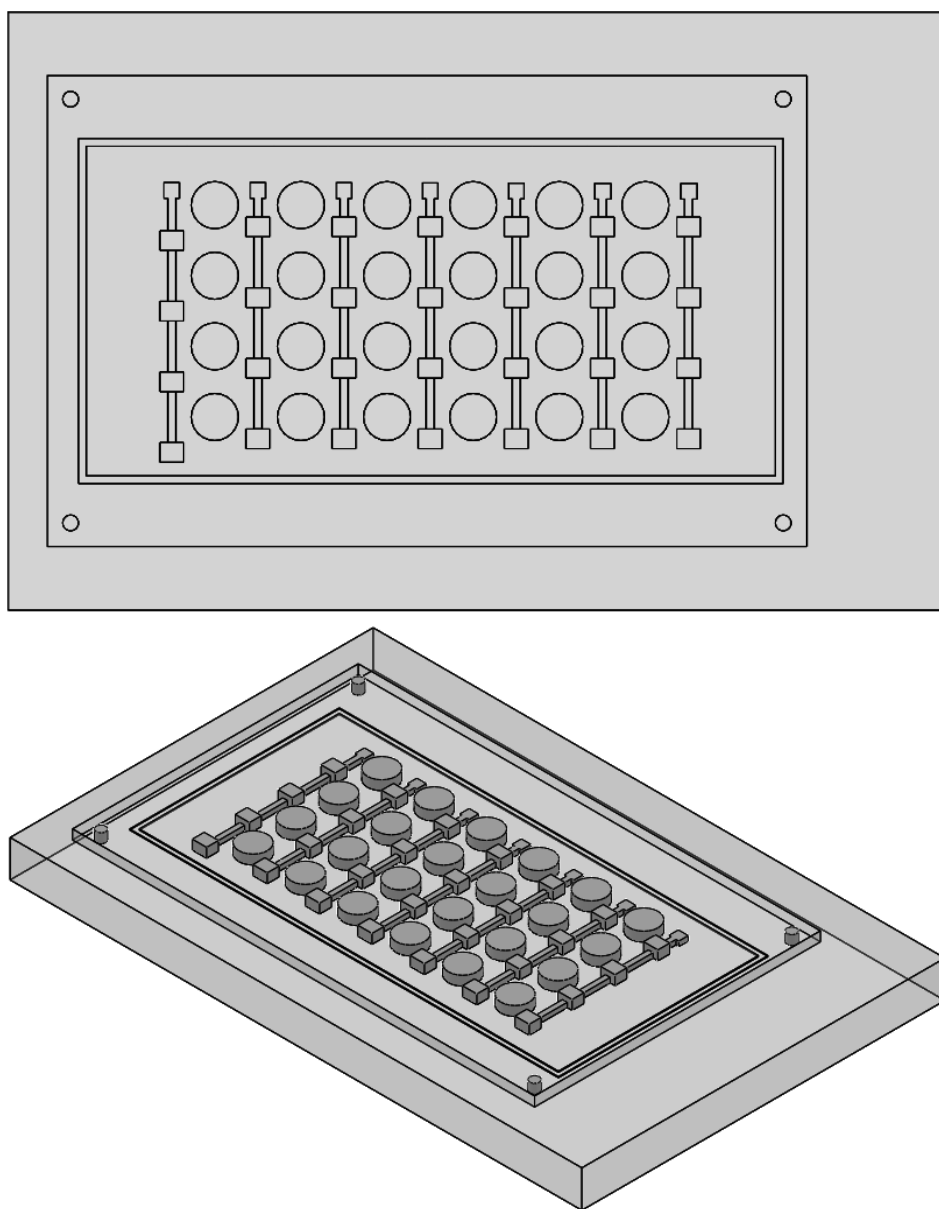
File: 24-well microfluidic MFC-outflow channel control .SLDTRP

Figure B.19 Acryl mold for 24-well PDMS microfluidic-MFC anode outflow channel control fabrication. (Top: top view, bottom: rotated 3D view)

FABRICATION PROTICOLS

Protocol B.1 Piranha cleaning

- Mix concentrated sulfuric acid with hydrogen peroxide in the ratio of 3:1 (Caution: highly corrosive, handle with care)

- Prepare 9 2"x3" glass slides, load glass slides with Teflon wafer holder

- Place glass slides into piranha solution for 15-30 min, agitate if necessary

- Remove glass slides from piranha solution and clean with DI water 3X

- Dry with nitrogen gas

Protocol B.2 MFC array anode electrode fabrication

- Ti/Au deposition on piranha cleaned glass slides (Ti: 200 Å, 2 Å/sec; Au: 3000 Å, 3 Å/sec)

- Electrode patterning through photolithography

  - Spin coating Shipley 1818 on Au deposited glass substrate (10s (acc.) + 30s @ 4000rpm)

  - Soft baking: 10 min @ 95 °C

  - Exposure: 120 mJ (over exposed, to cure edge area)

  - (Optional) Hard baking: 10 min @ 95 °C

  - Developing: 20-40 sec

  - Au etching: 3-5 min

  - Ti etching: mixture of HF to DI water in the ratio of 1:300, for 5 min

  - Remove photoresist mask with acetone, then washed with isopropanol and DI water

Protocol B.3 Cathode electrode fabrication for air-cathode MFC array

- Clean PMMA plate (3" x 3") with isopropanol and DI water, dry with nitrogen

- Electrode patterning with procedures described in **Protocol B.2**

- Drill holes in the center of each electrode pad with laser machine

Protocol B.4 PDMS chamber fabrication for MFC array

- Prepare either photoresist master mold or acryl master mold

- Mix PDMS base with curing agent in the ratio of 1:1 wt.%.

- Degas to remove bubbles

- Pour PDMS on the master mold

- Degas to remove bubbles (optional)

- Cover chamber with cleaned PMMS plate if required to make flat PDMS slab with uniform thickness.

- Cure at 65°C for 30 min - several hours based on the desired thickness

Protocol B.5 96-well microfluidic MFC array PDMS cathode chamber fabrication

- Vapor coating SU-8 master mold with trichlorosilane for 15 min

- Spin coating PDMS on master mold (mix ratio: 1:1 wt.%, spin rate: 5 sec + 25 sec @ 500 rpm)

- Cure at 65 °C for 10 min

Protocol B.6 Pt cathode electroplating

- Prepare Au electrode with photoresist protective patterns

- Connect the cathode of a power source to the Au electrode and the anode to the seed anode

- Start deposition with: Deposition cycle: +0.133A (20ms), -0.133A (10ms) with deposition rate of 12.5 nm/min, temperature: 60 °C

- A final thickness of 750 nm or thicker is required

VITA

Name: Huijie Hou

Address: Department of Electricial and Computer Engineering
                        Texas A&M University
                        TAMU 3128
                        College Station, Texas 77843-3128

Email Address: houhuijie03@gmail.com

Education: B.E., Optical and Electrical Information Engineering,
                        Zhejiang University, China, 2003

                        M.E., Optical Engineering, Zhejiang University, China,
                        2006

                        Ph.D., Electrical Engineering, Texas A&M University,
                        2011